

# Architecture, Dynamics, and Function of the General Stress Response System in *B. subtilis*

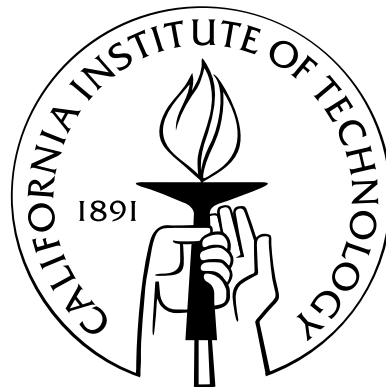
Thesis by

Jonathan W. Young

In Partial Fulfillment of the Requirements

for the Degree of

Doctor of Philosophy



California Institute of Technology

Pasadena, California

2012

(Defended April 12, 2012)

© 2012

Jonathan W. Young

All Rights Reserved

# Acknowledgements

James Locke was a critical contributor to this thesis and essentially served the role of a co-advisor for my PhD. His craft for shaping the story of science, which experiments to pursue, and how best to visualize data were skills he taught me throughout our work, and I am eternally grateful. I wish him the best as he starts his own lab, as he will make an outstanding PI.

I would like to thank Michael Elowitz profusely for many reasons. First, back in 2003 I was an out-of-work college graduate living off his girlfriend's graduate school stipend and struggling to find work. Michael brought me into his new lab, taught me an incredible amount of microscopy, and supported me as I moved onto my MD/PhD program. During my PhD years he has provided incredible ideas for experiments, refined my scientific communication, and given me wonderful opportunities to travel and advance my career.

In no particular order, shout outs go to: Chiraj Dalal, for being an outstanding distraction at any given time. I don't know how many total hours we spent critically thinking about things, not one of them being science. Team Playmakers, for some wonderful memories about D-league flag-football. Joe Levine, Fred Tan, and Sandy Nandagopal, for humor and being a great workout group. Michelle Shah, for 100% positive attitude, 100% of the time. Raj Kulkarni, for his invaluable wisdom with all things medical school. Adam Rosenthal, for his help in analyzing the RNAseq data. Ernie's Al Fresco, for providing fabulous nourishment ( $n_{tunch} \geq 500$ ). And the rest of the Elowitz Lab, for support and advice.

Lastly I thank my amazing, beautiful, and talented wife, Kristina Barkume, for supporting me through these years. She calls me her "long-term investment", and I appreciate her for continuing to believe it so.

# Abstract

Cells exhibit diverse and dynamic responses to stress. However, in many cases it remains unclear what the dynamics are, how they are generated, and why they are beneficial to the cell or organism. To investigate these issues we studied the General Stress Response in *B. subtilis*, a critical, conserved stress signaling pathway, mediated by the alternative sigma factor,  $\sigma^B$ . First, we find that  $\sigma^B$  activates with stochastic, frequency modulated pulses in response to energy stress. We explore the mechanism behind this striking response and find that a small, compact circuit facilitates this behavior. Second, we find that  $\sigma^B$  activates with a single-homogenous pulse of activity exposed to environmental stress, in contrast to energy stress dynamics. We also find that activation is rate-responsive, and show how this property may separate broad and specific regulatory modes. Lastly, we present some preliminary work toward a synthetic sigma factor activation circuit. Combined, these results present a comprehensive study of  $\sigma^B$  activation and generate a platform by which other dynamic stress response systems can be understood.

# Contents

<b>Acknowledgements</b>	<b>iii</b>
<b>Abstract</b>	<b>iv</b>
<b>1 Introduction</b>	<b>3</b>
<b>2 Stochastic Pulse Regulation in Bacterial Stress Response</b>	<b>7</b>
2.1 Supplemental Figures . . . . .	15
2.2 Supplemental Methods . . . . .	28
<b>3 Rate of Environmental Change Determines Stress Response Specificity in Bacteria</b>	<b>43</b>
3.1 Introduction . . . . .	43
3.2 Results . . . . .	45
3.3 Discussion . . . . .	50
3.4 Supplemental Figures . . . . .	53
3.5 Methods . . . . .	57
<b>4 Transplanting a Non-native Sigma Factor Circuit</b>	<b>61</b>
4.1 Introduction . . . . .	61
4.2 Results . . . . .	62
4.3 Conclusions . . . . .	65
4.4 Methods . . . . .	66
<b>5 Conclusions</b>	<b>67</b>
5.1 Future Directions . . . . .	68



# Chapter 1

## Introduction

Signaling systems are a critical organized unit of biology. Defined in basic terms, a signaling system is composed of cellular materials that allow a cell to respond and adapt to changing environmental or intracellular conditions. Systems are composed of the basic building tools of cells, proteins and genes. Proteins sense environmental changes, transduce them into intracellular signals, and respond and change the cellular state. In addition to using proteins, an overwhelming part of cellular response involves changes to gene expression. Cells may activate or repress genes, or a combination of both. Often, this regulation is the key determinant in signaling function. When faced with exposure to antibiotics, bacteria may increase the expression of the antibiotic transporter in an attempt to reduce antibiotic concentrations within the cell (Nikaido, 2009). In contrast, a decrease in pluripotency gene expression may accompany stem-cells exposure to differentiation signals (Loh et al., 2006; Ivanova et al., 2006). These examples serve as a small subset of the total influence of signaling systems. In fact, I argue its near impossible for some cellular response to not rely on some signaling system, as if the response comes ethereally from outside the cell. There may be cell responses we dont understand, but a basic assumption is that some factor, whether it is protein or some other molecule, mediates that response.

Historically, the identification of which signaling system or component was important for a particular function drove biology. The fill-in-the-blank statement, X is necessary for the response of Y to Z, contributed to our library of gene function and signaling systems. Further studies connected genes together along a signaling pathway and led to detailed models showing the relationship between each component. In more recent times, sequence data and bioinformatics have predicted further connec-

tions between genes, allowing the creation of large scale interaction maps that speakers love to show for dramatic effect.

Many of early experiments left large gaps in our understanding of these systems. Conventional genetic methods for studying cell responses, such as mutational and knockout studies, often cannot detect important quantitative relationships within the signaling pathway, such as the strength of interactions. Furthermore, many biologic assays historically have compared cell outputs at static time-points, unable to capture dynamic information. Even when measuring responses over time, common population based assays destroy cells, precluding response data in the same cell over time.

Technological advancements, such as the development of non-destructive in-vivo labeling agents such as fluorescent proteins, have allowed researchers make progress in these arenas (Shimomura et al., 1962; Chalfie et al., 1994). Our lab has used these tools extensively in the past decade and made key contributions in understanding important stress and developmental signaling pathways. This thesis serves to extend this effort, and focuses on critical, general, and quantitative questions facing all pathways. One, what are the dynamic single-cell responses of pathways? Cells act as individuals and analyzing responses at this level may deepen our understand of how a particular pathway operates. Second, how does signaling circuit architecture contribute to these dynamics? We can use a combination of genetic tools, including circuit rewiring to probe how precisely components come together to produce a behavior. Quantitative modeling of circuits can give us predictions, which can then be experimentally tested. Lastly, what function do these dynamics confer to the cell?

Previous studies have addressed some of these questions in diverse systems. In yeast, Cai and Dalal Cai et al. (2008) discovered that a transcription factor, Crz1, responsible for the cellular response to Calcium exposure, translocated to the nucleus from the cytoplasm in bursts. These bursts were frequency modulated (FM), in that Crz1 burst frequency increased as the level of Calcium increased. The authors showed the this type of regulation permitted proportional control over gene expression, something otherwise difficult to achieve in eukaryotic systems. However, the mechanism by which FM could be achieved by this signaling system was still unknown.

Other studies have expanded our understanding of how expression dynamics can occur in single-cells. The process of entry and exit into bacterial competence, a state where the cell uptakes DNA, was



recently characterized and described at the circuit level by Suel et al. Suel et al. (2006). In their system, the master regulator of competence, ComK, was shown to activate excitably, resulting in a pulse of activity. This transient activation was shown, through mathematical modeling and experiments, to result from an interaction of positive and negative feedback loops. Whether other such systems use similar strategies to generate transient activity were open questions.

To further develop our understanding of dynamic gene expression systems, we focused our studies on a critical signaling pathway of *Bacillus subtilis*, which centers around the control of an alternative sigma factor,  $\sigma^B$  (Hecker et al., 2007). Sigma factors are a key subunit of bacterial RNA polymerase, the final piece of a protein complex that allows the polymerase to bind to promoter regions and initiate transcription. Different sigma factors bind distinct promoter consensus sequences and each has a specific group of genes that they are responsible for regulating (Gruber and Gross, 2003). In all bacteria, a house-keeping sigma factor controls the expression of basal metabolic and necessary proteins for cell growth and division. Alternative sigma factors, those outside of the house-keeping sigma factors, are responsible for controlling responses to environmental stress. Each species of bacteria contain different number of alternative sigma factors and it is thought that the diversity of sigmas reflects the diversity of conditions and environment the bacteria experience. For example, obligate intracellular pathogens such as *Mycoplasma genitalium* grow in environments buffered by the host, and only contain a single sigma factor. In contrast, soil bacterium, such as *B. subtilis*, face a variety of quickly changing environmental conditions and must be poised to adapt. At present, researchers have identified at least 14 different sigma factors in *B. subtilis*. This number seems impressive, until one considers *Streptomyces coelicolor*, another soil dwelling organism known to have at least 60 sigma factors!

It seems perplexing that the bacteria would use sigma factors, when it seems like transcription factors, regulatory proteins that also control transcription, could easily supplant the need for this additional layer of regulation. Why couldn't a cell use a transcription factor where a sigma factor is used? This question, seemingly fundamental to how and why sigma factors have developed, remains unasked in the literature.

Part of the answer may lie in the regulation of sigma factors. At any given moment for *B. subtilis*,

many alternative sigma factors wait, dormant inside the cell. They are present at concentrations that would activate gene expression, but are regulated and sequestered by complex means, so accessibility to the RNA polymerase is prevented. For many sigma factors, including  $\sigma^B$ , a unique anti-sigma factor exists and binds to the sigma and prevents transcriptional activation (Osterberg et al., 2011). Under activating conditions, events cause the eventual dissociation of the anti-sigma factor from the sigma factor, which then allows association of RNA polymerase and gene production. The conventional thought about this sequestration mechanism is that it allows release of sigma factor without additional transcription, which may enable rapid responses to environmental insults.

It's worthwhile to ask though, within this sigma/anti-sigma factor framework, whether there are other possible reasons for using sigma factors. Could it be that the cell uses the sigma factor platform to develop novel gene regulatory mechanisms and modes, quickly and easily to suit circumstances? The work in this thesis serves to support this idea. Further chapters will reveal that  $\sigma^B$  uses a simple signaling architecture that yields rich dynamics and interesting outputs to control its large downstream regulon. In Chapter 2, we uncover that  $\sigma^B$  activates under energy stress using pulses of activation, that increase in frequency with increasing stress. The mechanism behind this response, including how the signaling circuit contributes to the response, is discussed at length. In Chapter 3, we explore how  $\sigma^B$  activates under physical stress, and describe how the response magnitude is proportional to the rate increase of stress. Furthermore, we discuss how this type of response allows different collections of genes to be activated, depending on the urgency of the oncoming stress. In total, we give a comprehensive account of how *B. subtilis* differentially responds to multiple types of stress, the role of the  $\sigma^B$  signaling circuit in influencing these responses, and propose why these responses may be advantageous.

## Chapter 2

# Stochastic Pulse Regulation in Bacterial Stress Response

Gene regulatory circuits exhibit significant fluctuations, ('noise'), in their components (Raj and van Oudenaarden, 2008; Rosenfeld et al., 2005)<sup>1</sup>. Noise can play a functional role in some systems (Eldar et al., 2009), generating necessary phenotypic diversity Losick and Desplan (2008), and allowing alternative regulatory strategies (Cai et al., 2008). However, it remains unclear how genetic circuits use noise to control cellular behaviors. Here we show how  $\sigma^B$ , the regulator of general stress response in *B. subtilis* (Hecker et al., 2007; Haldenwang and Losick, 1979; Igoshin et al., 2007), controls its targets using a noise-dependent pulse frequency modulation system (figure 2.1A).

In prokaryotes, alternative sigma factors form a part of the RNA polymerase holoenzyme, directing it to key regulons, which control distinct regulatory programs (Gruber and Gross, 2003).  $\sigma^B$  is found in gram-positive bacteria, and impacts pathogenicity in *Listeria monocytogenes* and *Staphylococcus aureus* (Kazmierczak et al., 2003; Lorenz et al., 2008). In *B. subtilis*,  $\sigma^B$  activates over 150 target genes in response to diverse stresses (Hecker and Volker, 1998; Hecker et al., 2007).  $\sigma^B$  is kept inactive by its anti-sigma factor RsbW, and is activated by the anti-anti-sigma factor RsbV, which can be reversibly phosphorylated (see figure 2.1B-C for regulatory interactions). To analyze  $\sigma^B$  activation dynamics, we constructed reporter strains incorporating a yellow fluorescent reporter (*yfp*) for  $\sigma^B$  activity (figure 2.1B), and used quantitative time-lapse microscopy to follow  $\sigma^B$  activation in individual cells (Locke and Elowitz, 2009). To quantify  $\sigma^B$  activity in movies, we computed the  $P_{sigB}$  promoter activity, defined as the rate of production of YFP (figure 2.5A and supplementary).

---

<sup>1</sup>This chapter is published in its entirety under the same title with authors J.C.W. Locke and J.W. Young as co-first authors, with equal contribution. See bibliography for full citation (Locke et al., 2011).

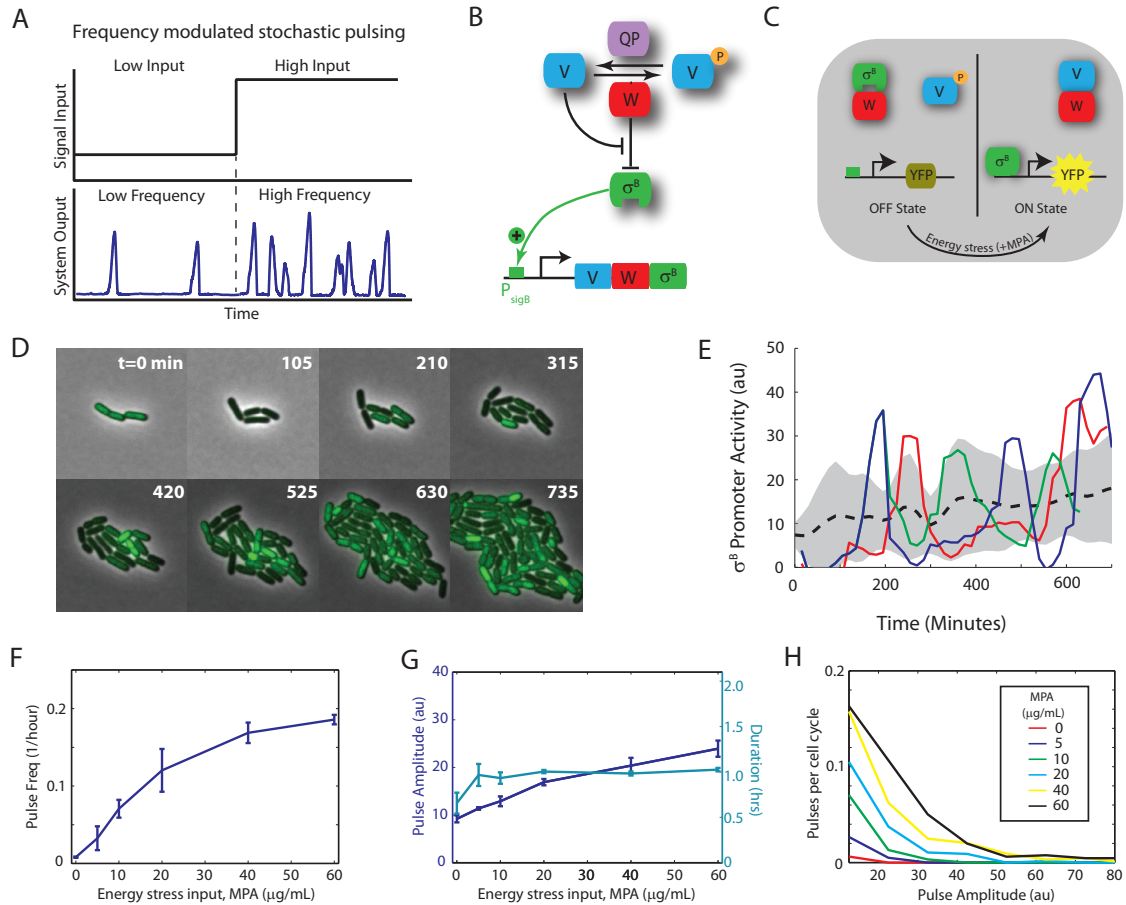


Figure 2.1: Energy stress modulates the frequency of stochastic pulses of  $\sigma^B$  activation. (A) In a Frequency Modulated (FM) system, a low or high constant input signal (black line) results in low or high frequency of stochastic pulses, respectively (blue line). (B)  $\sigma^B$  can be inhibited by anti-sigma factor, RsbW (W, red), which can in turn be inhibited by the anti-anti-sigma factor RsbV (V, blue). Uninhibited  $\sigma^B$  activates its own operon. RsbV phosphorylation is controlled by the RsbQP phosphatase complex (QP, purple) and the RsbW kinase activity. (C) Partner switching controls  $\sigma^B$  activity. When RsbV is phosphorylated (off),  $\sigma^B$  is inactive, bound to RsbW. Under energy stress RsbV is dephosphorylated (on) and binds to RsbW, releasing  $\sigma^B$  to activate endogenous target genes and a yfp reporter (yellow). (D) Filmstrip of  $\sigma^B$  activation at 60  $\mu\text{g/mL}$  MPA. Heterogeneous expression levels of P<sub>sigB</sub>-YFP reflect pulsing activity. (E) Promoter activity of the P<sub>sigB</sub>-YFP reporter pulses in individual lineages (colored solid lines), and its mean and standard deviation across all lineages in 4 movies (dashed line and shaded area, respectively). (F,G) MPA concentration strongly modulates the mean frequency, whilst more weakly modulating the mean amplitude and duration, of pulses. (H) Pulse amplitude histograms for varying levels of MPA. In (F-H), each data point represents statistics from four microcolonies, acquired on two different days.

We first measured the response of  $\sigma^B$  to mycophenolic acid (MPA), an energy stress transduced by RsbQP (figure 2.6) (Zhang and Haldenwang, 2005). Constant MPA led to pulses of  $\sigma^B$  activation in individual cells (figure 2.1C,D and movie S1). These pulses were unsynchronized across the population, sporadic in time, and sustained, continuing throughout the movie ( $\sim 6$  generations) (figure 2.7). Similar behavior was observed with other energy stresses and during growth in liquid culture (figure 2.5, 2.8).

Pulses reflected changes in  $\sigma^B$  activity and not intrinsic variability of the  $P_{sigB}$ -YFP promoter (figure 2.9). Increasing MPA concentration caused a strong increase in pulse frequency, with weaker increases in mean pulse amplitude and duration (figure 2.1E, 2.10), showing that  $\sigma^B$  is regulated predominantly by frequency modulation (FM) in response to energy stress (figure 2.1A). Pulse amplitudes exhibited broad and monotonically increasing variability with increasing MPA, with coefficients of variation ranging from 0.16 to 0.70 (figure 2.1F). Together, these results provoke the question of how FM pulse regulation is implemented by the  $\sigma^B$  regulation circuit.

In principle, pulses could be generated in two qualitatively distinct ways: They could arise through amplification of an inherently stochastic underlying process (Hodgkin1952JP, Suel2006N). Alternatively, they could result from a limit cycle oscillator whose dynamics become erratic due to noise (Elowitz and Leibler, 2000). Systematically reducing cellular noise would distinguish between these possibilities, eliminating pulses in the first case, but making them more regular in the second case.

To modulate the amplitude of noise in cells, we created strains which could be induced to grow into long multi-nucleoid filaments by controlling expression of FtsW, a cell division protein necessary for septation. These cells exhibit similar mean expression levels of cellular components (figure 2.11) but reduced fluctuations (Suel et al., 2007), allowing us to test how reduced noise affects pulse frequency. In time-lapse movies, we observed a systematic decline in pulse frequency in noise-reduced (long) cells across a range of energy stress levels (2.2A, 2.12), which was also consistent with reduced cell-cell variability in  $\sigma^B$  activity in liquid conditions (2.2B). This reduction in pulse frequency did not reflect reduced sensitivity to MPA, which had a similar effect on growth rate in long and short cells (figure 2.12). Together, these results rule out limit cycle models and suggest a noise-dependent mechanism for pulse generation.

How, then, does the  $\sigma^B$  circuit amplify noise to initiate discrete pulses of  $\sigma^B$  activity? To address this question we analyzed the response of  $\sigma^B$  to increased expression of each circuit component. Up-regulation of kinase (RsbW) and phosphatase (RsbQP) expression had much stronger (opposite) effects on  $\sigma^B$  activity compared to up-regulation of RsbV (figure 2.13). This result is interesting because opposing kinase and phosphatase activities can generate sharp, switch-like responses in the phosphorylation of their substrate. An extreme example is zero-order ultrasensitivity where the phos-

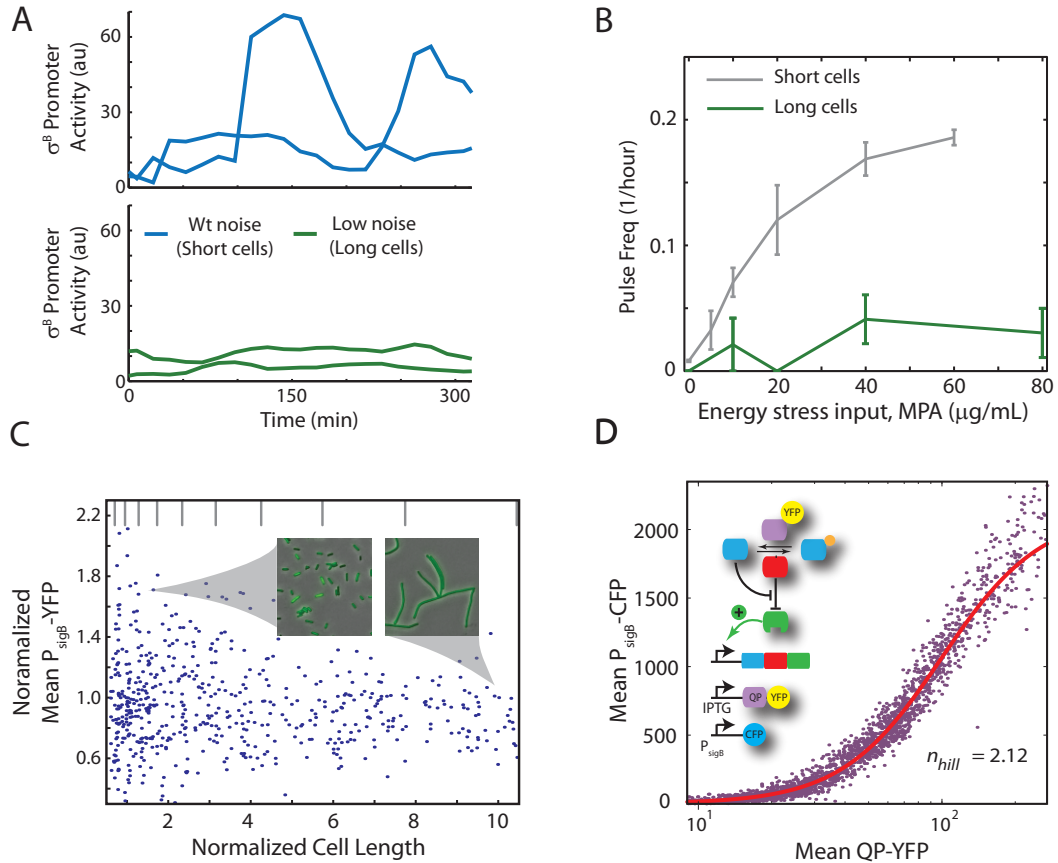


Figure 2.2: Pulsing is noise-dependent and involves an ultrasensitive phospho-switch. (A)  $\sigma^B$  activity traces from two cell lineages, in a conditional *ftsW* strain in which septation was normal (short cells, top) or inhibited (long cells, bottom) at 40  $\mu\text{g/mL}$  MPA. (B) Pulse frequency in long cells (green) is strongly reduced compared to short cells (gray, replotted for comparison from figure 2.5F). Error bars, mean  $\pm$  SEM (C) Static variability in  $P_{sigB}$ -YFP expression decreases with increasing cell length (cf. figure 2.12). Equal number of cells (represented by dots) are plotted in each log-spaced bin (delimited by gray vertical lines). Inset: overlay of phase contrast and  $P_{sigB}$ -YFP expression (green) at different cell lengths. Note greater  $\sigma^B$  variability in short cells. (D)  $\sigma^B$  expression is ultrasensitive to QP phosphatase levels. Each dot represents the mean QP-YFP level and  $P_{sigB}$ -CFP level of one cell, using the strain shown schematically. Red line is a Hill function with Hill coefficient  $n_H = 2.12$  (95% CI,  $n_H = 2.09$ -2.15). See supplementary for strain details.

phatase and kinase operate at saturation (Goldbeter and Koshland, 1981; Melen et al., 2005; Cheng et al., 2009). We found that  $\sigma^B$  activity exhibited an ultrasensitive response to inducible phosphatase concentration (2.2C, 2.14), with an effective Hill coefficient of 2.12 (95% CI,  $n_H=2.09$ -2.15). Similar results were also observed with the RsbTU phosphatase (figure 2.15). Moreover, this ultrasensitivity was not due to the transcriptional feedback loop. It could be observed in an ‘open-loop’ strain, in which operon expression was inducible and independent of  $\sigma^B$  (figure 2.16). In this strain, increasing operon expression led to increasing ultrasensitivity to phosphatase level. These effects could be explained by a minimal mathematical model of the phosphoswitch that does not include the detailed

dynamics of the network. Finally, consistent with this model, ectopic expression of the kinase RsbW shifted the switching point to higher phosphatase expression levels (figure 2.17). This ultrasensitive phospho-switch could activate  $\sigma^B$  in response to fluctuations in the phosphatase/kinase ratio and thereby initiate pulses.

How are  $\sigma^B$  pulses further amplified and subsequently terminated?  $\sigma^B$  activates its own operon (*rsbV-rsbW-sigB*). This feedback loop could increase  $\sigma^B$  activity, due to the activating effects of RsbV and  $\sigma^B$ , or it could repress  $\sigma^B$  activity, due to increased production of RsbW. We hypothesized that the phospho-switch sets a threshold between activating (phosphatase dominant) and repressing (kinase dominant) feedback regimes. As long as phosphatase activity exceeds kinase activity, activation of the operon increases free  $\sigma^B$  (positive feedback). However, this also increases production of RsbW kinase. When kinase activity approaches that of the phosphatase, increased operon expression will cause RsbW levels to cross the threshold, shutting off activation (negative feedback). Thus, autoregulation could result in a ‘mixed’ feedback loop, providing a compact mechanism to first amplify and then terminate a pulse (Ray and Igoshin, 2010).

To test this hypothesis, we constructed an open-loop strain and quantified the change in  $\sigma^B$  activity in response to a step increase in operon expression. In these experiments, we first established a basal level of phosphatase activity in cells and subsequently induced a step, of varying size, in  $\sigma^B$  operon expression (2.3A). We observed a striking transition between two qualitatively different responses: At lower operon induction levels, the system produced a sustained response, while at higher induction levels, it exhibited a pulse (figure 2.3B). These results are consistent with the mixed feedback model: Initially, increased operon induction produces more  $\sigma^B$ , which is active due to the high levels of phosphatase, engaging the positive feedback loop. For lower (sub-threshold) operon induction levels, RsbW levels never exceed phosphatase levels, so the system remains on indefinitely (2.3A, dashed). In contrast, at higher induction levels (supra-threshold), RsbW activity eventually crosses the threshold set by the phosphatase, and thereby shuts the system off, resulting in a pulse (2.3A, solid). Indeed, RsbW dominated other operon components at steady-state, suppressing  $\sigma^B$  activity in a dose-dependent fashion (figure 2.13). In this mechanism, pulse amplitude should be roughly proportional to the difference between the phosphatase level and the kinase level immediately

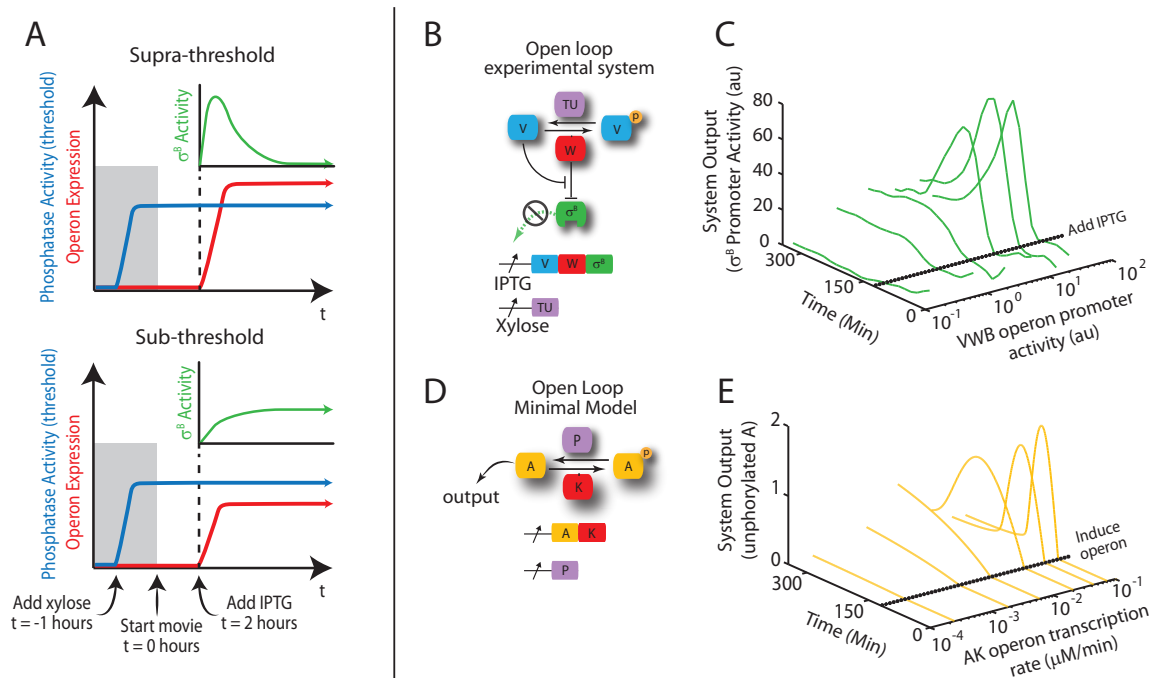


Figure 2.3: A mixed transcriptional feedback loop amplifies and terminates pulses. (A) Schematic diagram of supra- and sub-threshold protocols. Prior to time-lapse acquisition (gray shaded region), phosphatase is induced to a constant level by addition of xylose (see strain diagram in B). After the start of acquisition, IPTG is added to induce *rsbVWB* to levels that exceed (top) or do not exceed (bottom) the level of phosphatase. This results in pulsed (top) or sustained (bottom)  $\sigma^B$  activity dynamics. (B) An ‘Open-loop’ strain allows independent control of  $\sigma^B$  operon and phosphatase (RsbTU, to avoid energy stress inputs) expression by IPTG and xylose, respectively. (C)  $\sigma^B$  promoter activity exhibits a transition between sub- and supra-threshold behaviors. Each trace shows the mean  $P_{sigB}$  promoter activity (YFP production rate) averaged over 4 colonies. The promoter activity of the IPTG-inducible  $\sigma^B$  operon (x-axis) was estimated using a separate strain containing a similar IPTG-inducible *yfp* reporter. Two repeat movies showed similar behaviors. (D) A minimal mathematical model of the open-loop  $\sigma^B$  network. In this model, an unphosphorylated activator, A, directly activates target genes (see supplementary modeling section). (E) The minimal model reproduces the main features of the experimental data (C).

after the initiating fluctuation, as confirmed experimentally (figure 2.18). A minimal mathematical model of the circuit exhibited qualitatively similar behavior (figure 2.3C). This mechanism for pulse initiation, amplification, and termination is summarized in 2.4A,B.

These results provoke a final question: how can the cell modulate the frequency of pulses in this system? Systematic changes in the activity of either kinase or phosphatase could modulate the likelihood of threshold-crossing events, and thereby control pulse frequency. We first examined the distribution of RsbQP expression levels, using a  $P_{rsbQP}$ -rsbQP-YFP protein fusion that complements an RsbQP null mutant (figure 2.19). In response to 40  $\mu\text{g}/\text{mL}$  MPA, we observed a  $\sim 3$ -fold increase in mean RsbQP-YFP levels, and a  $\sim 6$ -fold increase in mean  $\sigma^B$  activity (figure 2.20A-B). At the



single-cell level, RsbQP-YFP expression mapped to  $\sigma^B$  activity (figure 2.20C), closely following the (independently determined) ultrasensitive response function (2.2C). These results suggest that stress increases  $\sigma^B$  pulse frequency by increasing the distribution of RsbQP expression levels, and thereby increasing the frequency with which RsbQP fluctuations cross the threshold set by RsbW (2.4C). Note that these results do not rule out the complementary possibility, suggested previously (Alper et al., 1994), that some energy stresses may activate  $\sigma^B$  by reducing kinase activity.

To show that this mechanism is indeed sufficient to enable frequency modulation, we rewired the endogenous circuit, replacing RsbQP with an inducible, constitutively active RsbTU phosphatase complex that unaffected by energy stress (2.4D, inset). The rewired system exhibited stochastic pulsing in response to RsbTU expression (figure 2.21, 2.22 and movie S2). Furthermore, we observed an increased frequency of pulsing in response to increased RsbTU phosphatase expression (2.4E), with weaker effects on pulse amplitude and duration (figure 2.24). These results, qualitatively similar to those observed in wild-type cells under energy stress, also match an extended mathematical model that includes the wild-type transcriptional feedback (gray dashed lines in 2.4E-F, figure 2.23, figure 2.24 and supplementary text). Thus, modulation of phosphatase expression is sufficient to recapitulate FM pulsing, and no special property of the RsbQP phosphatase is required.

FM pulsing can be implemented by a strikingly simple circuit of three genes (*rsbW*, *rsbV*, *sigB*), with input from a phosphatase complex. This system provides a fundamental signal processing capability to bacterial cells, enabling them to convert steady “DC” inputs into pulsatile, predominantly “AC” outputs. Noise plays a key functional role in this signal processing system (Eldar et al., 2009). The  $\sigma^B$  circuit conserves its core architecture in diverse bacteria (Hecker et al., 2007), and other alternative sigma factors similarly feature both post-translational regulation by anti-sigma factors and autoregulatory feedback. Thus, related stochastic pulse modulation schemes are likely employed more generally in bacteria (Gruber and Gross, 2003). The relatively slow timescale of  $\sigma^B$  pulses (figure 2.1E) could confer advantages in responding to unpredictable environments and maintaining a broad, but dynamic, distribution of states in the population, through bet-hedging (Acar et al., 2005; Kussell and Leibler, 2005). Given the negative effect of  $\sigma^B$  activation on growth rate in some conditions, even under energy stress (Schweder et al., 1999), these results suggest that cells balance the benefits

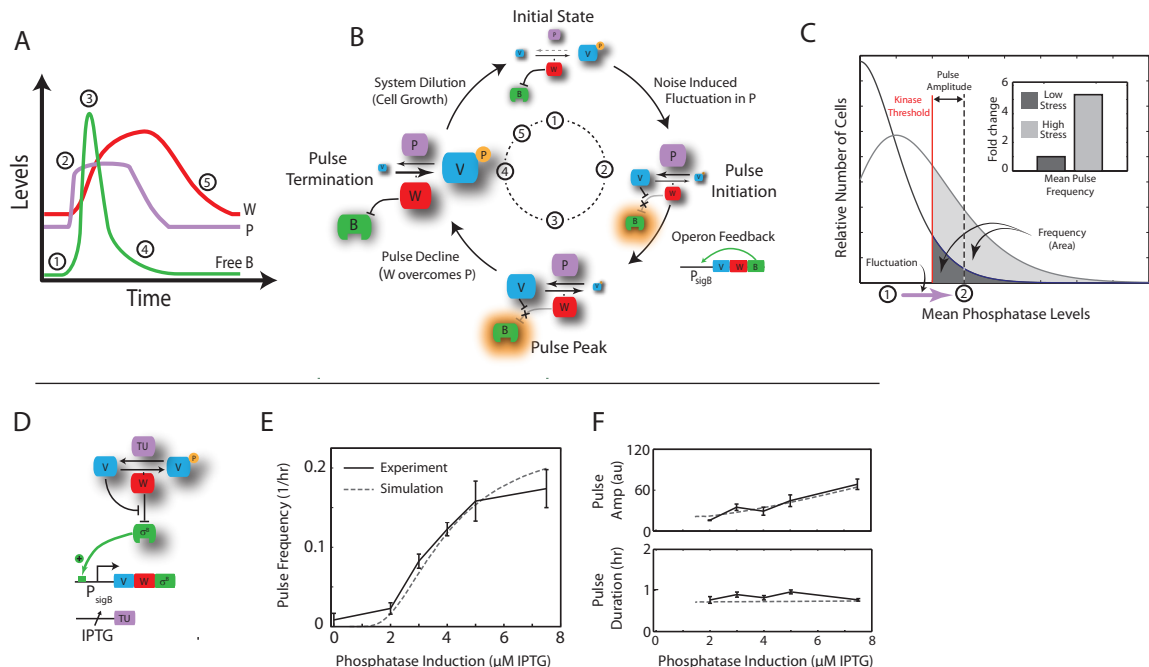


Figure 2.4: Mechanism of FM pulse control. (A) Schematic time-course of phosphatase RsbQP (denoted P, purple), free  $\sigma^B$  (B, green), and kinase W (red) during a pulse cycle. (B) Stages of pulse generation. The relative concentration of each component is indicated schematically by size (compare to A). Circled numbers indicate specific stages: (1) Initial state: system components are present at low levels, and RsbV is mostly phosphorylated since kinase activities exceed phosphatase activities. A threshold-crossing upward fluctuation in RsbQP level can dephosphorylate  $V^P$ , leading to pulse initiation. (2) Initiation: Activation of  $\sigma^B$  (indicated by glowing halo) leads to up-regulation of operon components. (3) Pulse peak:  $\sigma^B$  activity peaks just before RsbW kinase activity exceeds phosphatase activity. (4) Termination: Re-phosphorylation of RsbV shuts the system off. (5) Dilution: Component levels reset to the original state. (C) Threshold-crossing fluctuations enable FM. Fluctuations in phosphatase level (purple arrow from state 1 to 2) can cross the Kinase threshold (red line) to initiate pulses. Pulse amplitude is determined by the difference between phosphatase and kinase activities after the fluctuation (distance between dashed gray and solid red lines) and pulse frequency is determined by the fraction of the phosphatase distribution above the threshold (shaded areas), which differ for low and high stress (dark and light gray, respectively). (D) In the re-wired input strain, the energy stress phosphatase RsbQP is replaced by an IPTG-inducible, constitutively active RsbTU phosphatase (supplementary). (E) In this strain, pulse frequency increases with phosphatase induction, while amplitude and duration are more weakly affected (F). These results are consistent with the corresponding model, hand-fit to these data (gray dashed lines). Each data point represents statistics from two colonies. Two repeat datasets showed similar trends. Due to the small number of pulses at 0  $\mu\text{M}$  IPTG, these data are omitted from (F).

and costs of  $\sigma^B$  activation dynamically. It will be interesting to see whether other dynamic encoding schemes are similarly implemented by relatively simple circuit modules.

## 2.1 Supplemental Figures

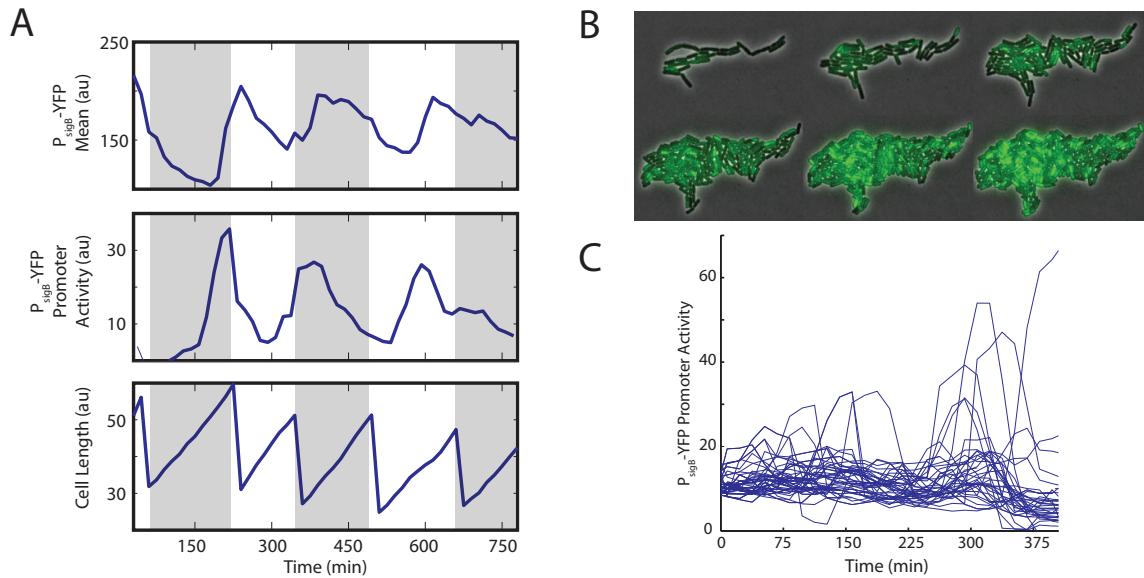


Figure 2.5:  $\sigma^B$  activity pulses under energy stress. (A) Example of cell lineage trace from a P<sub>sigB</sub>-YFP reporter strain (JJB240, see strain list) exposed to 60  $\mu\text{g}/\text{mL}$  MPA showing promoter activity (middle) calculated from the mean fluorescence (top) and the cell length (bottom). Alternating light/dark regions represent different cell cycles. (B-C) Cells also pulse under energy stress due to nutrient limitation / stationary phase. (B) Film strip of a time-lapse movie strain JJB240 grown on a LB/20 conditioned media pad mimicking stationary phase. Cells were grown to OD 1.8 and the resulting conditioned media was filtered from cells and made into low-melt agarose pads. Cells were then imaged on these conditioned pads (as described in supplementary methods). Colony images start from 450 min after the start of time-lapse to illustrate  $\sigma^B$  pulsing activity. (C) Cell lineage traces showing P<sub>sigB</sub>-YFP promoter activity from movie described in (B), where  $t=0$  min corresponds to the beginning of the filmstrip. For clarity, every 8th cell trace is shown.

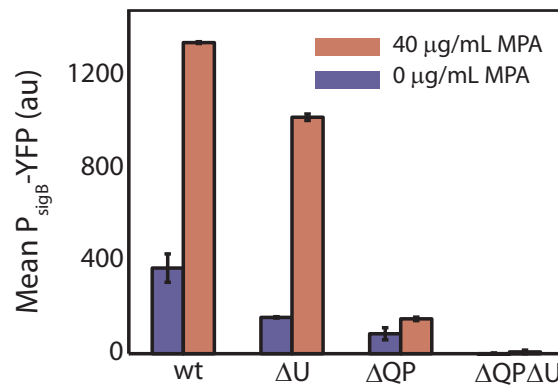


Figure 2.6: MPA induces  $\sigma^B$  activation through the RsbQP phosphatase. Wild-type (JJB213) and rsbU (JJB240) strains, where the environmental stress phosphatase is deleted, strongly activate  $\sigma^B$  upon MPA exposure, in contrast to rsbQP and rsbQPrsbU strains without the RsbQP phosphatase (JJB629 and JJB461 respectively). Cells were grown in SMM and exposed to  $\pm 40$   $\mu\text{g}$  MPA for 150 minutes as described in supplemental methods. RsbU is the phosphatase that mediates environmental stress (see supplemental for full description of the  $\sigma^B$  network).

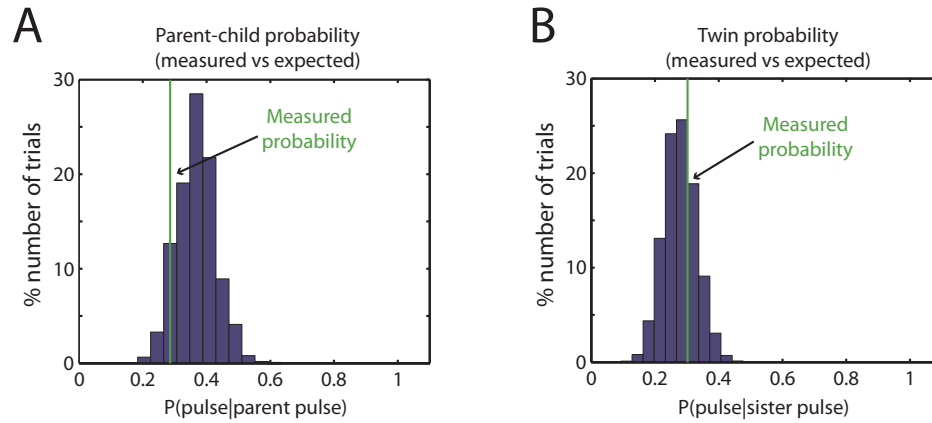


Figure 2.7: Pulse characteristics indicate  $\sigma^B$  pulses are stochastic. (A) The probability of pulses in generation  $n+1$  is independent of the presence of pulses in generation  $n$ . The frequency of instances where a parent and subsequent child pulsed (green line) was compared to a bootstrapped model (histogram) where parent/child pulses were randomized. (B) Pulse probability is nearly independent of the presence of pulses in sister cells. Green line indicates measured probability and can be compared to expected probabilities in a bootstrap model where sister cell pulses are randomized. For further descriptions of statistical methods, see Supplemental Methods.

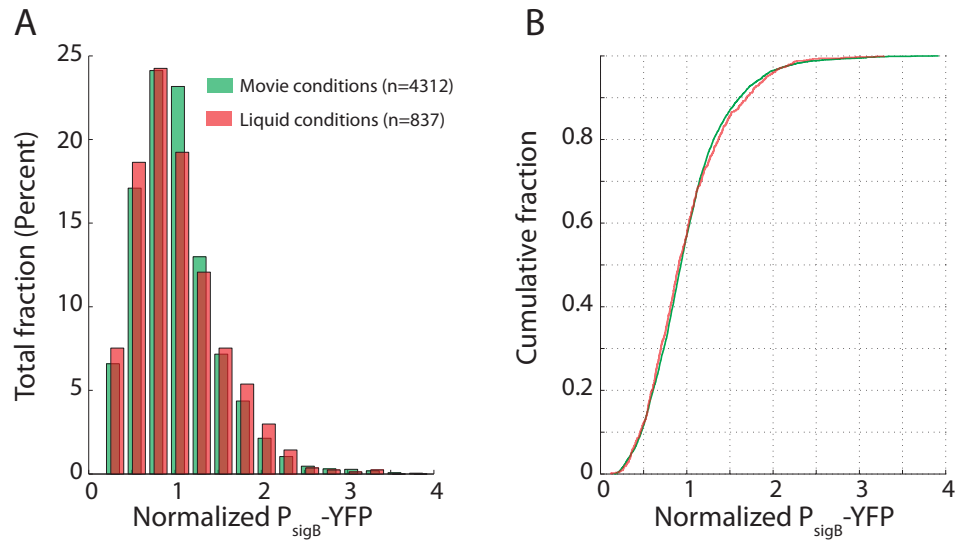


Figure 2.8:  $\sigma^B$  activity distributions exhibit similar variability in movies and liquid culture. (A) Mean single-cell  $P_{sigB-YFP}$  levels (shown in green) from strain JJB240 were extracted from individual frames of four time-lapse movies under 40  $\mu\text{g}/\text{mL}$  MPA (from figure 2.1). Mean single-cell data were also acquired in liquid conditions after exposing cells to 40  $\mu\text{g}/\text{mL}$  MPA in SMM (shown in orange). Data were corrected for autofluorescence using images of a strain containing no reporter construct (JJB176 (see strain list)) and mean normalized. (B) Cumulative distribution plots of movie and snapshot data shown in (A). A KS test showed that the differences between the distributions are not significant ( $p = 0.46$ ).

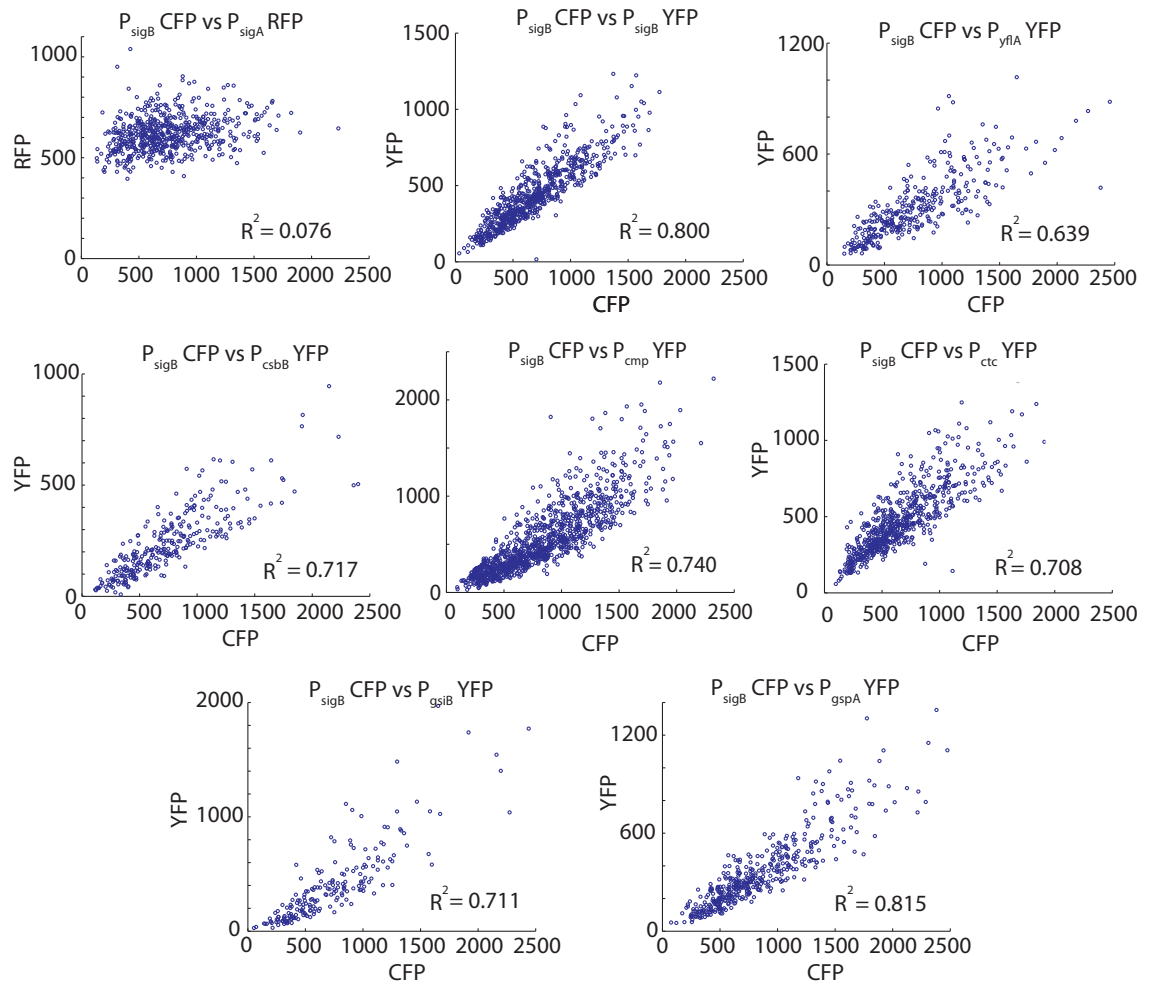


Figure 2.9:  $\sigma^B$  target genes are highly correlated at the single cell level. An independent YFP transcriptional reporter of  $\sigma^B$  activity was integrated into the *sacA* locus of an *amyE::P\_{sigB}*-3Xcfp *ppsB::P\_{sigA}*-mCherry reporter strain (JJB556-JJB572). Snapshots of gene expression were taken after growth in SMM liquid culture under 40  $\mu\text{g}/\text{mL}$  MPA energy stress for 90 min. (Top left)  $P_{sigA}$ -mCherry vs  $P_{sigB}$ -3XCFP. In this control, no correlation is observed between  $\sigma^B$  and a constitutive  $\sigma^A$  promoter. (B) (Top middle)  $P_{sigB}$ -YFP vs  $P_{sigB}$ -CFP. In this ‘intrinsic noise’ strain, YFP and CFP are values are highly correlated (high correlation coefficient ( $R^2$ )) showing that the variation in expression at the  $P_{sigB}$  promoter is due to global changes in  $\sigma^B$  activity. (Other plots) Different  $\sigma^B$  targets are also highly correlated with the  $P_{sigB}$  promoter.

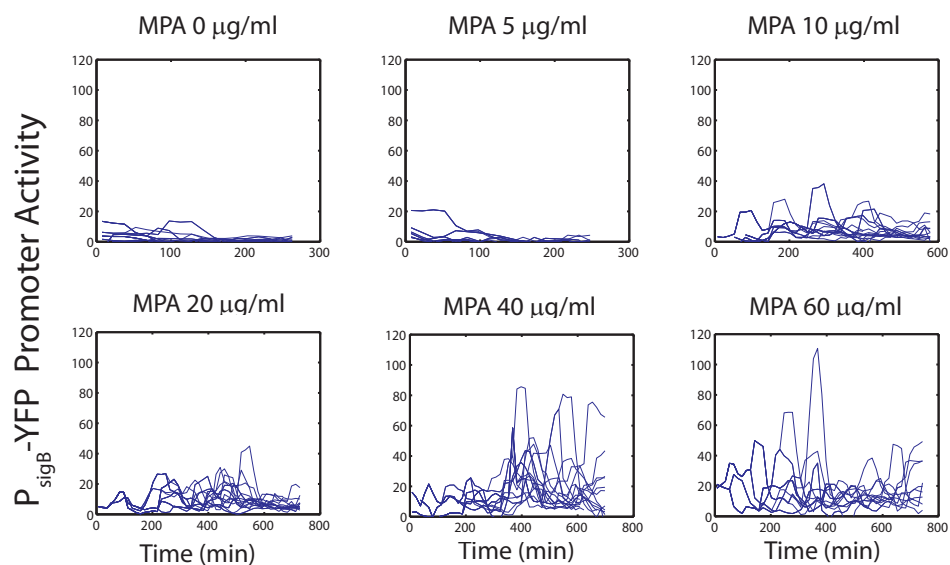


Figure 2.10:  $P_{sigB}$ -YFP promoter activity traces of individual cell lineages from movies acquired at various MPA concentrations. Cell lineage promoter activity traces of single movies from each MPA exposure. Pulse analysis of multiple movies comprise the data found in 2.1D-H in the main text. Every 8th cell trace is shown for clarity. For full time-lapse microscopy methods, see supplementary.

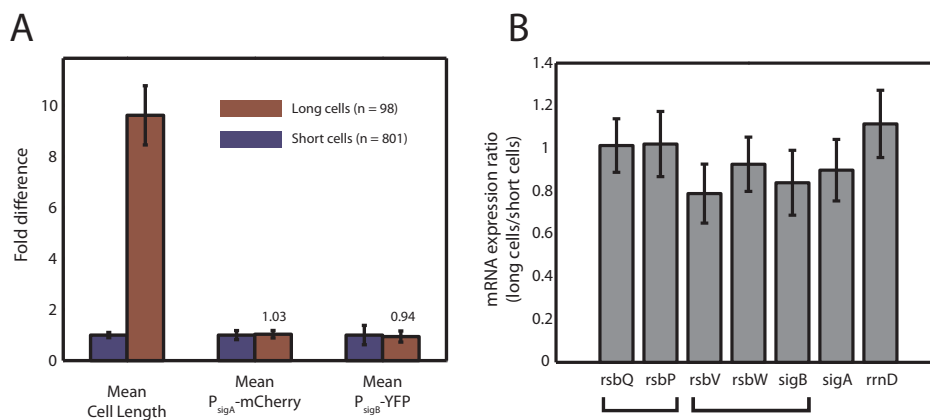


Figure 2.11: RNA expression is consistent with fluorescent cell measurements in filamented cells. (A) Using strain JJB712, long filamented cells (red bars) show similar mean expression of  $P_{sigA}$ -mCherry and  $P_{sigB}$ -YFP compared to wild-type cells (blue bars, each normalized to 1), despite 10-fold longer mean cell length. Standard deviations are shown on bar plots (red bars are ratios to the wild-type values). (B) Histograms showing mRNA expression ratio of selected genes in long cells versus short cells, relative to mCherry expression, whose expression per cell volume was found to be constant (see A). Housekeeping and  $\sigma^B$  network components are expressed similarly in short cells versus long cells. Each measurement reflects data from three separate days, with three independent biological replicates. Standard deviations are shown on bar plots. Brackets show genes expressed from the same operon.

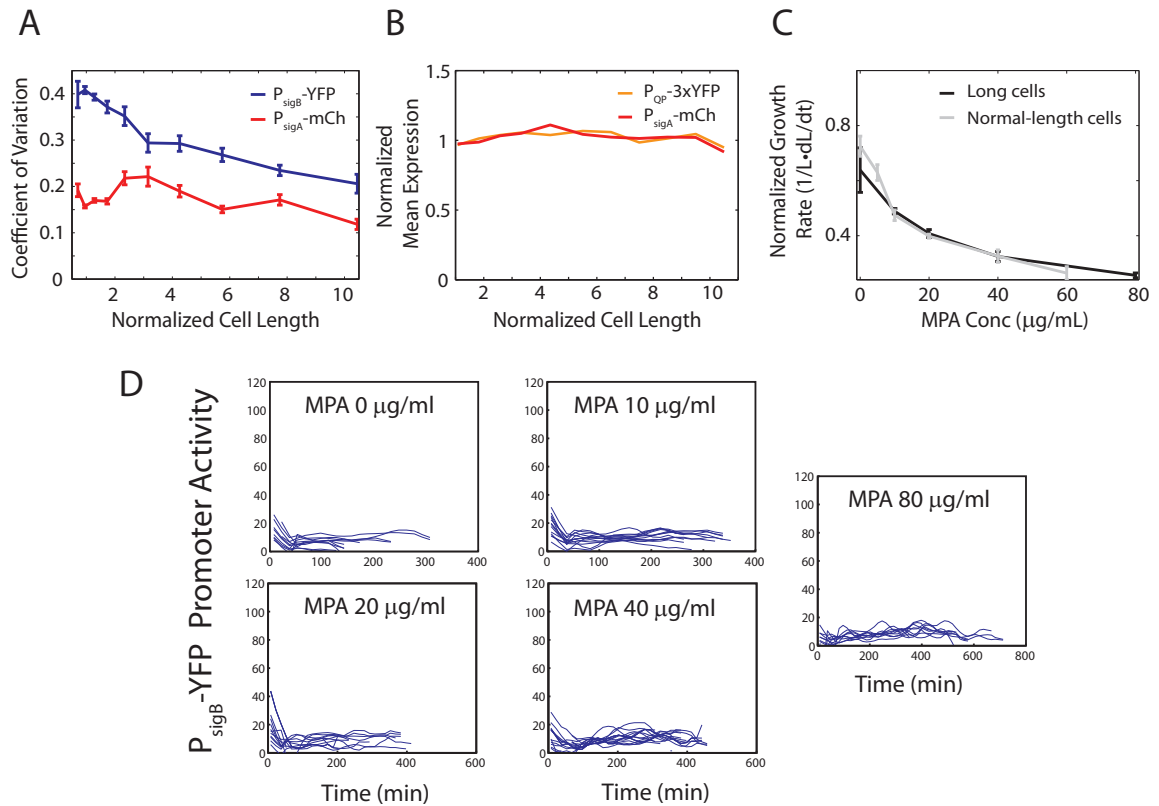


Figure 2.12: Reduced noise lowers  $P_{sigB}$ -YFP variability and reduces pulsing without changing QP phosphatase levels. (A) Plot of coefficient of variation of  $P_{sigB}$ -YFP activity (blue trace) or constitutive  $P_{sigA}$ -mCherry reporter (red trace) versus normalized cell length in conditional *ftsW* filament strain (JJB712). At longer cell lengths  $\sigma^B$ -YFP variability becomes comparable to that of the constitutive  $\sigma^A$  reporter due to a reduction in pulse frequency. (B) A reporter of phosphatase expression (orange trace) shows that mean phosphatase levels do not decrease with increasing cell lengths, similar to that of a constitutive control (red trace). Mean expression was normalized to the overall mean expression across all cell lengths for each reporter. (C) The physiological effect of MPA on growth rate is similar between long cells (black) and normal length cells (grey). (D) Filament cell lineage promoter activity traces of single movies from each MPA exposure. Pulses in this strain are reduced compared to normal length cells (figure 2.10). Scale for the y-axis is set for comparison with data in figure 2.10.

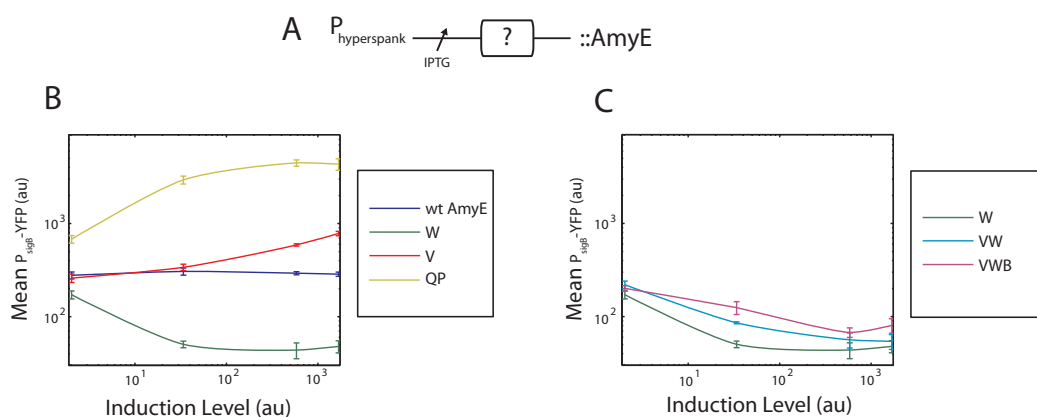


Figure 2.13: Ectopic expression of  $\sigma^B$  circuit components reveals sensitivity to phosphatase and kinase levels. (A) Diagram of genetic construct (for more details, see strain list). Each gene or gene combination (indicated by “X”) was placed under the control of  $P_{hyperspank}$ , a strong IPTG-inducible promoter and integrated into the *amyE* locus. (B) Overexpression of RsbW, RsbV, RsbQP reveal that  $\sigma^B$  activity is most sensitive to kinase and phosphatase levels. Static snapshots of  $\sigma^B$  activity were taken 90 min after induction with various concentrations of IPTG. (C) RsbW exhibits a dominant negative effect over other operon components. Expression of fractional operon constructs containing RsbW alone, RsbVW, or RsbVWB were chromosomally integrated into the  $\sigma^B$ -YFP reporter strain. Despite the positive effects of RsbV and  $\sigma^B$  itself, inducing full operon RsbVWB repressed the system to almost the same level as expressing RsbW alone. In (B) and (C), induction level was measured by taking the mean expression of  $P_{hyperspank}$ -yfp (JJB432) at the same IPTG inducing concentrations.

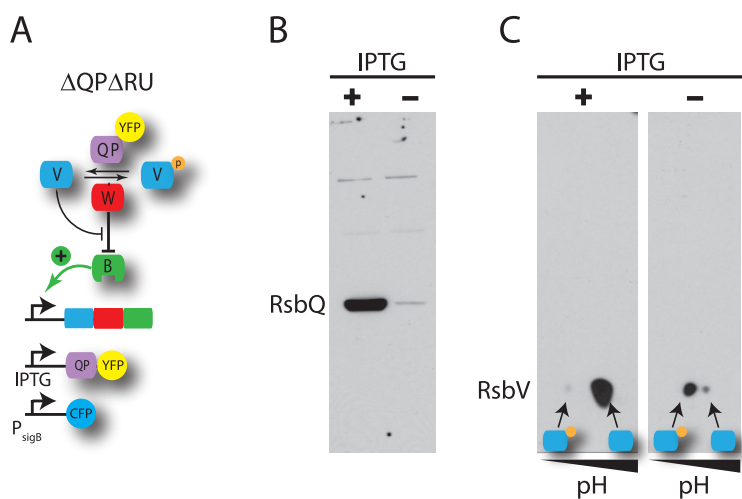


Figure 2.14: Upregulation of phosphatase QP-yfp increases phosphatase activity on RsbV substrate. (A) Strain JJB737 was grown in LB and phosphatase QP-yfp was induced with 1 mM IPTG for 45 minutes. Cell lysates were extracted and used for western blotting. (B) Strong induction of the phosphatase RsbQ protein occurs with IPTG. 100  $\mu$ g of cell lysate was loaded from each IPTG condition and blotted for the presence of RsbQ. The small amount of RsbQ present in the ‘no IPTG’ condition likely results from leakiness from the inducible promoter. (C) 2D Isoelectric/SDS electrophoresis was performed on cell lysates to separate the phosphorylated versus unphosphorylated forms of RsbV. Induction of ectopic phosphatase by IPTG switched RsbV from a predominately phosphorylated state (right) to a state where RsbV was almost exclusively unphosphorylated (left).



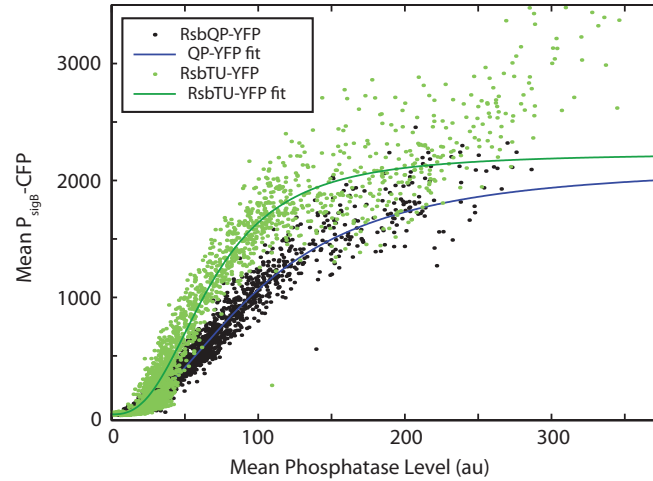


Figure 2.15:  $\sigma^B$  Activity is ultrasensitive to phosphatase expression. The *yfp* gene was fused to the C-terminus end of the *rsbQP* or *rsbTU* operon in the absence of other RsbV phosphatases. Dots represent individual cells where QP-*yfp* (black) or TU-*yfp* (green) was expressed to different levels and  $\sigma^B$  activity was measured using a  $P_{sigB}$ -CFP reporter via microscope snapshots. Hill fit (green and blue solid lines) estimate the Hill coefficient as 2.12 (95% CI,  $n_H=2.09-2.15$ ) for QP-*yfp* and 2.62 (95% CI,  $n_H=2.54-2.69$ ) for TU-*yfp*. Data for QP-*yfp* here is shown in 2.2D and is repeated for comparison to TU-*yfp*.

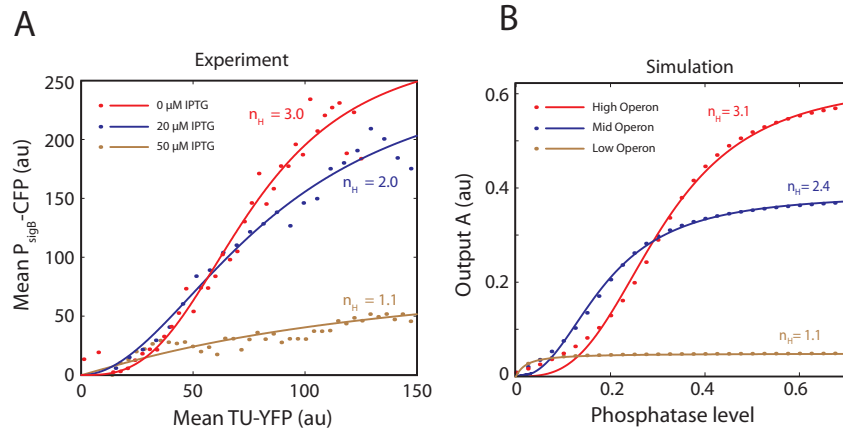


Figure 2.16: Ultrasensitivity is preserved in an open-loop system and increases with increasing operon expression. A strain expressing a xylose inducible phosphatase fused to *yfp* was integrated in a background where the  $\sigma^B$  operon was controlled by an IPTG inducible promoter (JJB749). Cells were spotted on SMM agarose pads with various IPTG concentrations (0, 20, 50 mM) to induce the operon to different basal levels. After 2.5 hours of equilibration, xylose (0.5, 1, 2, 4%) was added the different levels of IPTG to create a grid of conditions. After 1.5 hours of phosphatase induction, snapshots were taken. (A) Experimental data. Data were grouped according to IPTG concentration and sensitivity to phosphatase concentration was measured. Cells with similar phosphatase expression, as measured by *yfp*, were binned together and a Hill function was fit to each IPTG concentration. The Hill coefficient is shown for each IPTG (operon level). (B) The open-loop simulation, (network diagram depicted in 2.3D), shows that, like the experimental data, phosphatase sensitivity increases with increasing basal operon expression.

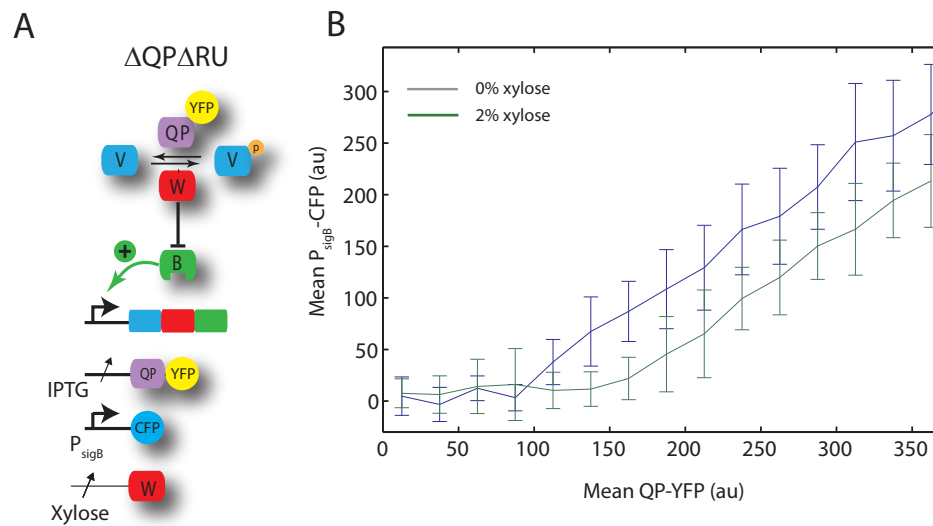


Figure 2.17: Balance between kinase and phosphatase sets threshold for  $\sigma^B$  activation. A) Strain JJB819 allows inducible control of both the kinase RsbW and phosphatase QP-YFP. In this experiment, first additional RsbW was induced by adding 2% Xylose. 2h later QP-YFP was then induced to varying levels by adding IPTG. 2h later snapshots of the resulting sigB expression were taken. B) Upregulation of RsbW shifts the threshold for  $\sigma^B$  activation to higher levels of phosphatase. Cells with upregulated RsbW (2% Xylose, green line), require more QP-YFP expression to activate  $\sigma^B$  compared to uninduced cells (0% Xylose, blue line).

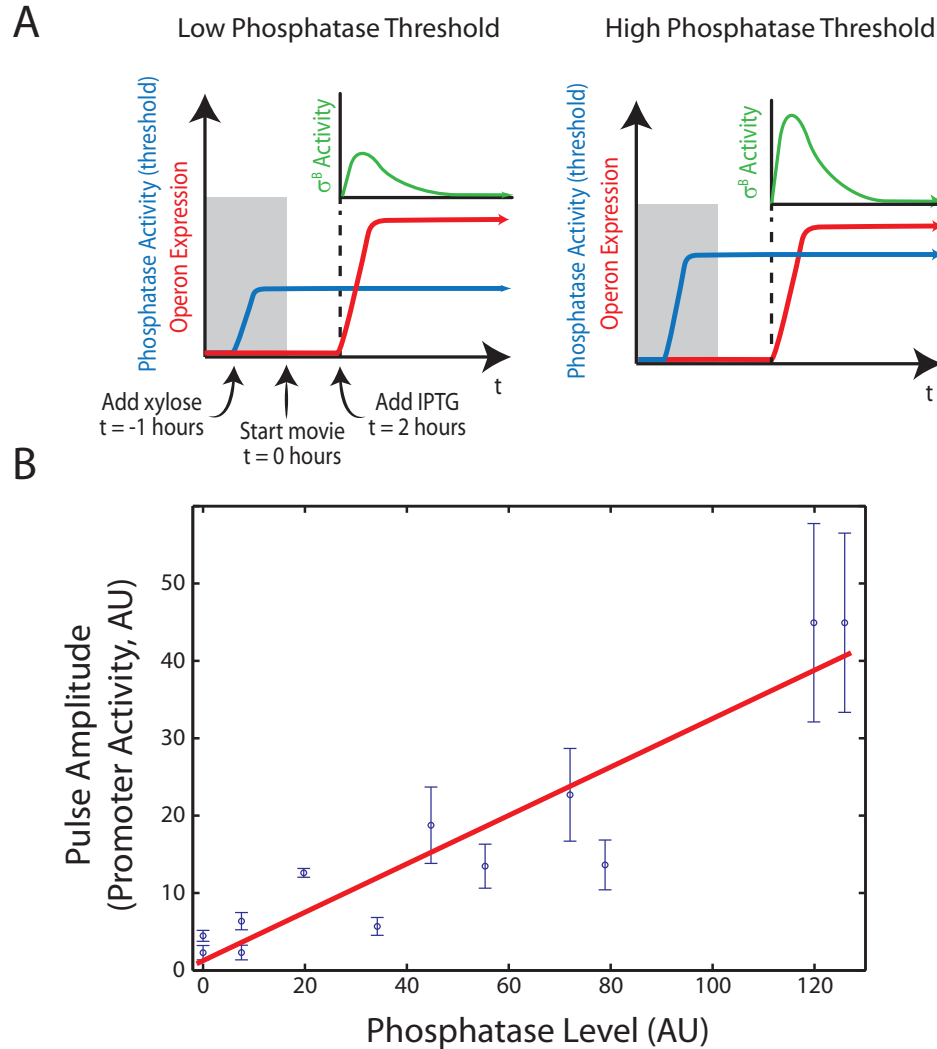


Figure 2.18: Pulse amplitude is proportional to phosphatase threshold. (A) Schematic of experimental protocol (modified from 2.3, see open loop experiment description in Supplemental Methods). In order to test whether  $\sigma^B$  pulse amplitude increases with higher phosphatase threshold level, we preinduced the phosphatase RsbTU in strain JJB578 by adding xylose to varying levels (0%, 0.2%, 0.4%, 0.6%, 1.0%, 2.0% Xylose). After phosphatase had reached steady state levels, we then fully induced the  $\sigma^B$  operon (1 mM IPTG) and measured the resulting  $P_{sigB}$ -YFP activity via timelapse. (B) Pulse amplitude is proportional to the phosphatase threshold. Phosphatase level is estimated from the fluorescence values of a  $P_{sweet}$ -YFP reporter induced to the same level of xylose as the open loop strain.  $\sigma^B$  promoter activity is calculated from the mean fluorescence across the colony. Pulse amplitude for each data point represents an average amplitude from at least 3 movies on the same day, with error bars represent SEM. Two days of data are shown. Red line is unweighted linear fit ( $R^2 = 0.86$ ).

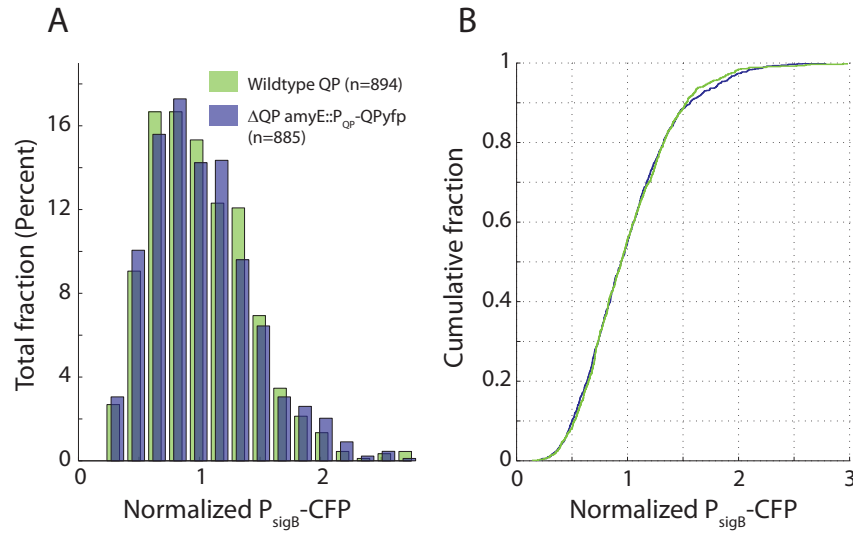


Figure 2.19: Expression of QP-yfp complements a QP deletion. (A) Expression of the phosphatase fusion protein QP-yfp from its endogenous promoter in the *amyE* locus (JJB739) produces similar mean-normalized  $\sigma^B$  activity distributions compared to wild-type QP (JJB781) upon treatment with 40  $\mu$ g/mL MPA (blue and green respectively). MPA led to a fold  $\sigma^B$  activation in JJB739 similar to wildtype QP (5.0 versus 7.1). (B) Cumulative distribution plots of the data shown in (A). A KS test showed that the differences between the distributions are not significant ( $p = 0.94$ ).

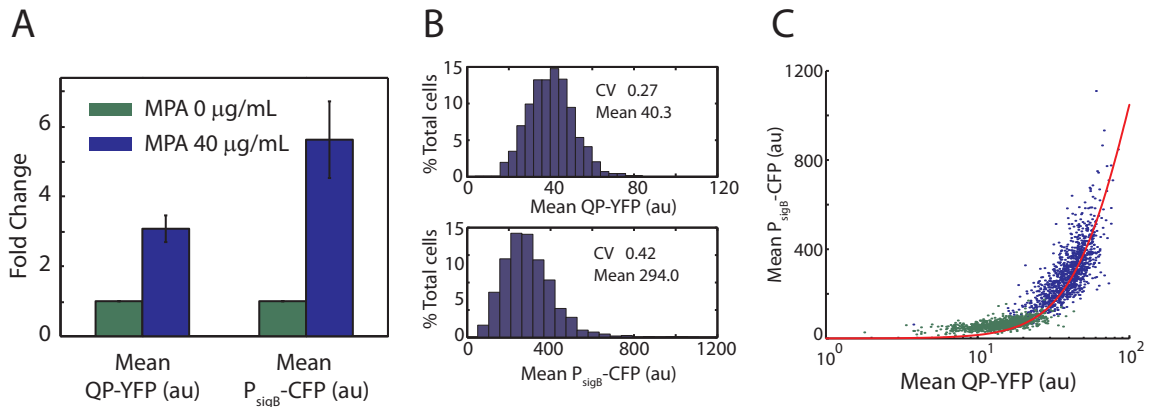


Figure 2.20: Pulse initiation is due to variability in phosphatase levels. (A) Under energy stress, the fold change in mean  $\sigma^B$  activity is greater than the change in phosphatase QP levels. Strain JJB739 was grown in SMM and exposed to 0 or 40  $\mu$ g/ml MPA for 180 minutes. The fold change measurement used non-stressed cells (green) as a reference, and was calculated for the stressed condition (blue) using two experiments. Standard error is shown on bar plots. (B) Histograms showing greater variation (measured by CV) of P<sub>sigB</sub>-CFP (bottom) compared to RsbQP-YFP levels (top). (C) Scatter plot of RsbQP-YFP vs P<sub>sigB</sub>-CFP from the same data as found in (B). Solid red line represents the Hill function fit representing relationship between the overexpression of QP-YFP and P<sub>sigB</sub>-CFP as found in figure 2.15 and figure 2.2D). Strong correlation between wild-type RsbQP-YFP and this fit suggests that pulses are initiated by fluctuations in phosphatase levels.

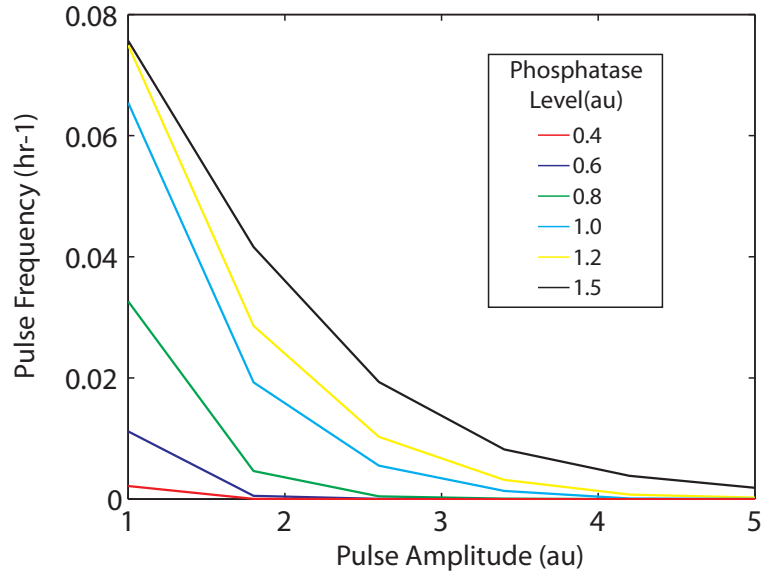


Figure 2.21: Closed-loop model recapitulates broad pulse amplitude distributions with monotonic decreasing frequency. Pulse statistics were collected from 250 repeats of a 20000 minute numerical simulation, at each phosphatase level. Simulated curves agree with experimental results (compare to figure 2.1H).

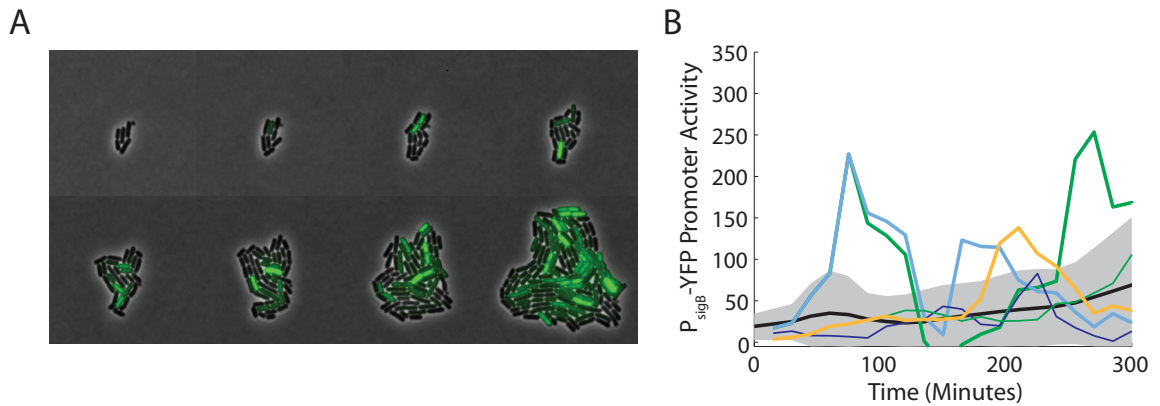


Figure 2.22:  $\sigma^B$ -YFP pulses can be induced by expression of constitutive phosphatase. (A) Film strip of time-lapse movie of  $P_{sigB}$ -YFP activity for phosphatase induction strain (JJB643), induced with 7.5 mM IPTG. (B) Individual lineage traces (colored lines) showing promoter activity of the  $P_{sigB}$ -YFP reporter for phosphatase induction strain. The grey shaded area shows the standard deviation of promoter activity across 2 movies at each timepoint, while the black line is the average promoter activity.

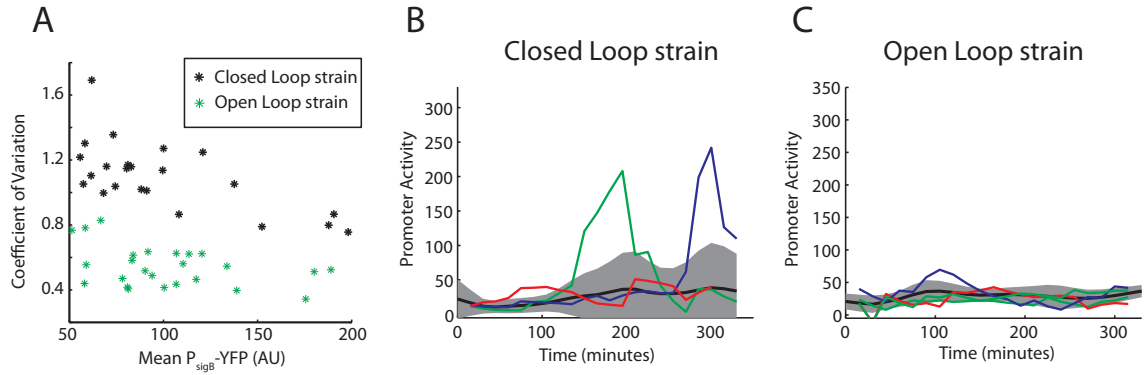


Figure 2.23: Effects of feedback on pulsing in the rewired input strain. (A) Variability in  $\sigma^B$  activity is much reduced in the open loop strain, compared to the closed loop strain. Movies of the open loop strain (strain JJB578) were acquired using the following protocol. First the  $\sigma^B$  operon was induced with 10 mM IPTG, and then 90 min. later the phosphatase RsbTU was induced with varying concentrations of xylose (0, 0.2, 0.4, 0.6, 1.0, 2.0%). The mean  $\sigma^B$  level across the entire movie was extracted, and the coefficient of variation (CV) calculated (green stars). Similarly, we computed mean  $\sigma^B$  levels and CV from the closed loop strain movies (black stars, see also 2.4). The open loop strain (mean CV = 0.5) is much less variable than the closed loop strain (mean CV = 1.1), suggesting a reduction in pulsing. B-C) Individual lineage traces (colored lines) from a closed (B) and open (C) loop strain with the same mean  $\sigma^B$  promoter activity. The grey shaded area shows the standard deviation of promoter activity across each timepoint of the movie, while the black line is the mean promoter activity.

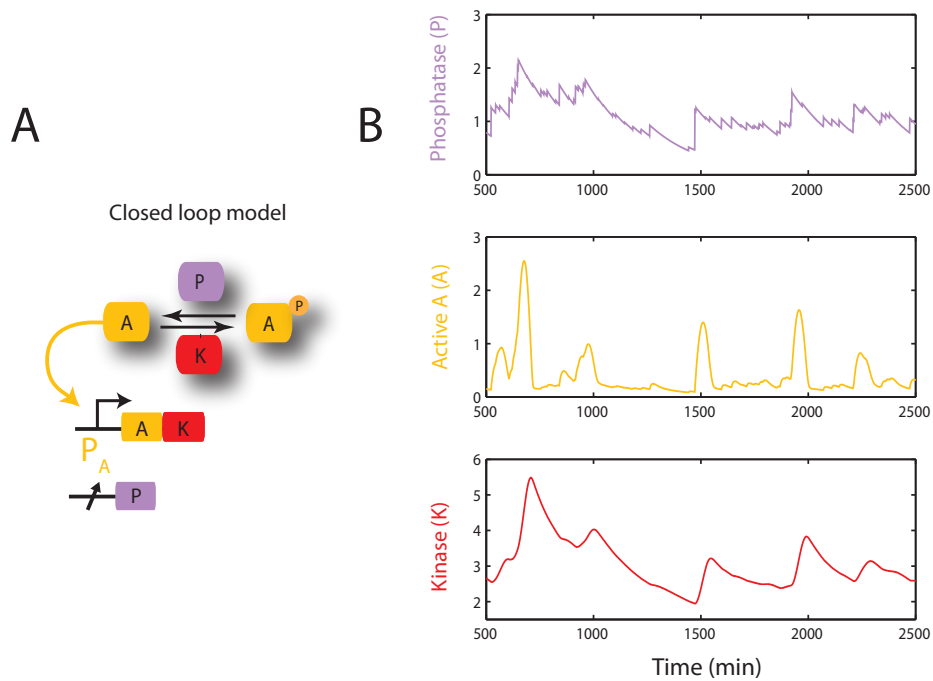


Figure 2.24: Closed-loop model shows pulsing behavior with noisy phosphatase levels. A minimal closed-loop model of the  $\sigma^B$  system (see supplementary methods), where the inducible phosphatase levels fluctuate through time, gives rise to  $\sigma^B$  pulses and frequency, amplitude, and duration responses that are similar to the closed loop strain (see 2.4D-F). (A) Closed-loop model where the output of the system autoregulates the operon. The phosphatase is controlled from an inducible promoter. (B) Simulation results of the closed-loop system. The phosphatase levels (shown in purple) fluctuate according to a gamma distributed Ornstein-Uhlenbeck process, which result in pulses of active A (shown in yellow). Kinase levels (K, red) are upregulated by Active A and shut off pulses.

## 2.2 Supplemental Methods

**Plasmid construction.** All plasmids were cloned using *E. coli* strain Dh5 $\alpha$  and a combination of standard molecular cloning techniques and non-ligase dependent cloning using Clontech In-Fusion Advantage PCR Cloning kits. Plasmid constructs were integrated into *B. subtilis* chromosomal regions via double crossover using standard techniques. The following list provides a description of each plasmid constructed, with details on integration position/cassette and selection marker given at the beginning. Note that all plasmids below replicate in *E. coli* but not in *B. subtilis*.

### Plasmid list

1. *ppsb::P<sub>trpE</sub>-mCherry Erm<sup>R</sup>* - This plasmid was used to provide uniform expression of mCherry from a  $\sigma_A$ -dependent promoter, enabling automatic image segmentation (cell identification) in time-lapse movie analysis. A minimal  $\sigma_A$  promoter was used from the *trpE* gene and cloned into a vector with *ppsb* homology regions. The original integration vector was a gift from A. Eldar (Eldar et al., 2009). For some strains, the selection marker was subsequently changed, in *B. subtilis*, to either KanR or PhleoR.
2. *sacA::P<sub>sigB</sub>-yfp Cm<sup>R</sup>* - The promoter immediately upstream of *RsbV*, containing a well-characterized  $\sigma^B$  promoter, was cloned into the EcoRI/BamHI sites of AEC127 (Eldar et al., 2009), yielding a Venus (YFP) reporter for  $\sigma^B$  activity.
3. *amyE::P<sub>hyperspank</sub>-X Spect<sup>R</sup>* - Where X = *rsbW*, *rsbV*, *rsbQP*, *rsbVW*, *rsbVWB*, *yfp*. The coding region of each single gene or combination, along with a 5' transcriptional terminator, was cloned behind the *P<sub>hyperspank</sub>* IPTG-inducible promoter in plasmid pDR-111 (gift of D. Rudner, Harvard).
4. *amyE::P<sub>spac</sub>-Y Spect<sup>R</sup>* - Where Y = *rsbQP-yfp*, *rsbTU-yfp*, *yfp*. The *P<sub>spac</sub>* promoter is also controlled by IPTG, but promoter leakiness (basal expression) is less than *P<sub>hyperspank</sub>* (D. Rudner, Harvard). This reduced leakiness allowed modulation of low levels of phosphatase.
5. *amyE::P<sub>sweet</sub>-TU Spect<sup>R</sup>*. The *rsbTU* coding region was cloned into pdr160 (gift of D. Rudner, Harvard). *P<sub>sweet</sub>* is induced by xylose. Although full activation is not achieved in the presence of



glucose, the absence of maximal expression did not adversely affect results under our conditions.

6. *amyE::P<sub>sweet</sub>-yfp Spect<sup>R</sup>*. Originally pdr160 (a kind gift of D. Rudner). The yfp gene was cloned into this plasmid in order to compare expression levels between the different inducible promoters.
7. *amyE::3xCFP Spect<sup>R</sup>*. We constructed an integration plasmid based on pDL30 in which 3 separate copies of cfp, each with its own RBS were constructed with a multiple cloning site preceding the first cfp.
8. *amyE::P<sub>sigB</sub>-3xCFP Spect<sup>R</sup>*. This alternative  $\sigma^B$  reporter, containing three tandem copies of the CFP fluorescent protein gene, was used in combination with yfp reporters of different genes.
9. *sacA::cfp Cm<sup>R</sup>* - An integration vector where cfp replaced the yfp gene from AEC127.
10. *sacA::P<sub>sigB</sub>-cfp Cm<sup>R</sup>* - The same upstream promoter of RsbV (as in plasmid (2) above) was cloned into plasmid (9), providing a CFP reporter for  $\sigma^B$  activity integrated in the *sacA* locus.
11. *amyE::P<sub>QP</sub>-QP-yfp Spect<sup>R</sup>* - A derivative of the original plasmid (3), where *P<sub>hyperspank</sub>* was removed and replaced with the QP gene along with the upstream coding region of this operon.
12. *sacA::X-yfp Cm<sup>R</sup>* - Where X = *P<sub>yfla</sub>*, *P<sub>yfhN</sub>*, *P<sub>cmp</sub>*, *P<sub>ctc</sub>*, *P<sub>gsib</sub>*, *P<sub>csbB</sub>*, *P<sub>gspA</sub>*. The promoters immediately upstream of various target genes of  $\sigma^B$ , were cloned into the EcoRI/BamHI sites of AEC127 (Eldar et al., 2009), yielding Venus (YFP) reporters for each of these downstream targets of  $\sigma^B$ .
13. *thrC::P<sub>sweet</sub>-RsbW Erm<sup>R</sup>* - We constructed an integration plasmid where the xylose repressor and the promoter responsive to xylR (*P<sub>sweet</sub>*) from pdr160 (see above) was subcloned into pDG1664 (or ECE117 from the BGSC). The gene RsbW was then subcloned into this plasmid.

**B. *subtilis* strains.** Strains used were in the PB2 genetic background, except where noted. Antibiotic resistance was switched using a previously described antibiotic switching vector system (Steinmetz and Richter, 1994). Deletions were made by replacing genes of interest with a selection marker via a linear DNA fragment homologous to the region of interest. Many starting strains/genomic DNA were kind gifts of C.W. Price (see references below). Under construction procedure, the ‘ $\rightarrow$ ’ symbol indicates an

integration event from plasmid or genomic DNA into the strain after the arrow. For example, in strain JJB730, the construction procedure is listed as “JJB461 (selection on Tet)→JJB635 (selection on Erm)→JJB176,” meaning, “the genomic DNA of JJB635 was prepared and transformed into JJB176 with selection on Erm; This strain was then transformed with the genomic DNA of JJB461, with selection on Tet.”

#	Strain name	Genotype	Construction Procedure	Used in figure
1	PB2	<i>trp2C</i> (this genotype omitted in derived strains, below)		
2	JJB174	PB2; <i>ppsbs::P<sub>trpE</sub>-mCh neo<sup>R</sup></i>	Plasmid (1) above → PY79 → PB2. Antibiotic cassette switched from Erm <sup>R</sup> to Neo <sup>R</sup>	
3	JJB176	PB2; <i>ppsbs::P<sub>trpE</sub>-mCh Phleo<sup>R</sup></i>	Plasmid (1) above → PY79 → PB2. Antibiotic cassette switched from Erm <sup>R</sup> to Phleo <sup>R</sup>	Negative control for snapshots
4	JJB213	JJB176; <i>sacA::P<sub>sigB</sub>-yfp Cm<sup>R</sup></i>	Plasmid (2) above → JJB176	
5	JJB240	JJB174; <i>delRsbU</i>	Plasmid (2) above → JJB174 → PB494 [3]	1D-H, S(1-4), S6
6	JJB256	JJB213; <i>sigB::Spect<sup>R</sup></i>	BGSC1A790 → JJB213	
7	JJB332	JJB240; <i>amyE::P<sub>hyperspank</sub>-rsbV Spect<sup>R</sup></i>	Plasmid (3, RsbV) above → JJB240	S9
8	JJB334	JJB240; <i>amyE::P<sub>hyperspank</sub>-rsbW Spect<sup>R</sup></i>	Plasmid (3, RsbW) above → JJB240	S9
9	JJB367	JJB240; <i>amyE::P<sub>sigB</sub>-3Xcfp Spect<sup>R</sup></i>	Plasmid(8) → JJB240	
10	JJB413	JJB240; <i>amyE::P<sub>hyperspank</sub>-rsbQP Spect<sup>R</sup></i>	Plasmid (3, RsbQP) above → JJB240	S9
11	JJB415	JJB240; <i>amyE::P<sub>hyperspank</sub>-rsbVW Spect<sup>R</sup></i>	Plasmid (3, RsbVW) above → JJB240	S9
12	JJB423	JJB240; <i>amyE::P<sub>hyperspank</sub>-rsbVWB Spect<sup>R</sup></i>	Plasmid (3, RsbVWB) above → JJB240	S9
13	JJB432	JJB176; <i>amyE::P<sub>hyperspank</sub>-yfp Spect<sup>R</sup></i>	Plasmid (3, yfp) above → JJB176	S9 (induction level)
14	JJB434	JJB176; <i>amyE::P<sub>spac</sub>-yfp spect<sup>R</sup></i>	Plasmid (4, yfp) above → JJB176	
15	JJB461	JJB240; <i>rsbQP::Tet<sup>R</sup></i>	<i>ΔrsbQP Tet<sup>R</sup></i> recombination at the <i>rsbQP</i> locus → JJB240	S2
16	JJB467	JJB461; <i>rsbU::Tet<sup>R</sup>; P<sub>spac</sub>-rsbVWBX Erm<sup>R</sup></i>	JJB469 → JJB461 (with Erm <sup>R</sup> selection)	
17	JJB469	JJB176; <i>rsbU::Tet<sup>R</sup>; P<sub>spac</sub>-rsbVWBX Erm<sup>R</sup></i>	<i>ΔrsbU Tet<sup>R</sup></i> recombination at the <i>RsbU</i> locus → PB212 [4] → JJB176	
18	JJB503	JJB176; <i>amyE::P<sub>sweet</sub>-yfp Spect<sup>R</sup></i>	Plasmid(6) above → JJB176	
19	JJB578	JJB467; <i>amyE::P<sub>sweet</sub>-TU Spect<sup>R</sup></i>	Plasmid(6) above → JJB467	3B-C, S14, S19
20	JJB556	JJB367; <i>sacA::P<sub>yflA</sub>-yfp Cm<sup>R</sup></i>	Plasmid(12, <i>P<sub>yflA</sub>-yfp</i> ) → JJB556	S5
21	JJB559	JJB367; <i>sacA::P<sub>yflN</sub>-yfp Cm<sup>R</sup></i>	Plasmid(12, <i>P<sub>yflN</sub>-yfp</i> ) → JJB556	S5
22	JJB564	JJB367; <i>sacA::P<sub>ctc</sub>-yfp Cm<sup>R</sup></i>	Plasmid(12, <i>P<sub>ctc</sub>-yfp</i> ) → JJB556	S5
23	JJB563	JJB367; <i>sacA::P<sub>gsiB</sub>-yfp Cm<sup>R</sup></i>	Plasmid(12, <i>P<sub>gsiB</sub>-yfp</i> ) → JJB556	S5
24	JJB565	JJB367; <i>sacA::P<sub>gsiA</sub>-yfp Cm<sup>R</sup></i>	Plasmid(12, <i>P<sub>gsiA</sub>-yfp</i> ) → JJB556	S5
25	JJB572	JJB367; <i>sacA::P<sub>sigB</sub>-yfp Cm<sup>R</sup></i>	Plasmid(12, <i>P<sub>sigB</sub>-yfp</i> ) → JJB556	S5
26	JJB629	JJB213; <i>rsbQP::Tet<sup>R</sup></i>	JJB461 → JJB213 (with Tet <sup>R</sup> selection)	S2
27	JJB635	JJB176; <i>RsbR-U::Erm<sup>R</sup></i>	<i>ΔrsbRU Erm<sup>R</sup></i> recombination at the <i>rsbRU</i> locus	
28	JJB637	JJB635; <i>rsbQP::Tet<sup>R</sup></i>	JJB461 → JJB635 (with Tet <sup>R</sup> selection)	
29	JJB643	JJB637; <i>amyE::P<sub>spac</sub>-rsbTU Spect<sup>R</sup></i>	Plasmid (4, RsbTU) above → JJB637	4D-F, S18, S19
30	JJB675	PY79; <i>amyE::P<sub>spank</sub>-ftsW Spect<sup>R</sup>; ftsW::Tet<sup>R</sup>; ppsbs::P<sub>trpE</sub>-mCh Neo<sup>R</sup></i>	JJB174 → sub-strain of Fili-SOG from Suel [5]	
31	JJB676	JJB675; <i>sacA::P<sub>sigB</sub>-yfp Cm<sup>R</sup></i>	Plasmid (2) above → JJB675	
32	JJB712	JJB676; <i>rsbR-U::Erm<sup>R</sup></i>	JJB635(selection on Erm) → JJB676	2A-C, S7, S8
33	JJB730	JJB176; <i>rsbR-U::Erm<sup>R</sup>; rsbQP::Tet<sup>R</sup></i>	JJB461 (selection on Tet) → JJB635 (selection on Erm) → JJB176	
34	JJB733	JJB730; <i>sacA::P<sub>sigB</sub>-cfp Cm<sup>R</sup></i>	Plasmid(10) above → JJB730	
35	JJB736	JJB733; <i>amyE::P<sub>spac</sub>-rsbTU-yfp Spect<sup>R</sup></i>	Plasmid(4, TU-yfp) → JJB733	S11
36	JJB737	JJB733; <i>amyE::P<sub>spac</sub>-rsbQP-yfp Spect<sup>R</sup></i>	Plasmid(4, QP-yfp) → JJB733	2D, S11
37	JJB739	JJB733; <i>amyE::P<sub>rsbQP</sub>-rsbQP-yfp Spect<sup>R</sup></i>	Plasmid(11) → JJB733	S15, S16
38	JJB746	JJB710; <i>rsbQP::Tet<sup>R</sup>; sacA::P<sub>sigB</sub>-cfp Cm<sup>R</sup></i>	JJB461 (selection on Tet) → Plasmid(10) above → JJB176	
39	JJB749	JJB746; <i>P<sub>sweet</sub>-rsbTU-yfp Spect<sup>R</sup>; RsbU::Tet<sup>R</sup>; P<sub>spac</sub>-rsbVWBX Erm<sup>R</sup></i>	Plasmid(4, TU-yfp) → JJB469 (selection on Erm) → JJB746	S12
40	JJB780	JJB174; <i>P<sub>spac</sub>-rsbQP-yfp; sacA::P<sub>sigB</sub>-cfp Cm<sup>R</sup>; delRsbU</i>	Plasmid(4, QP-yfp) → <i>sacA::P<sub>sigB</sub>-cfp Cm<sup>R</sup></i> → JJB176 → PB494 [3]	
41	JJB781	JJB176; <i>sacA::P<sub>sigB</sub>-cfp Cm<sup>R</sup>; rsbR-U::Erm<sup>R</sup></i>	JJB635(selection on Erm) → Plasmid(10) → JJB176	S15
42	JJB819	JJB780; <i>P<sub>sweet</sub>-rsbW Erm<sup>R</sup>; rsbQP::Tet<sup>R</sup></i>	JJB461 (selection on Tet) → plasmid(13) → JJB780	S13

**Microscopy.** All data were acquired using a CoolSnap HQ2 attached to a Nikon inverted TI-E microscope, equipped with the Nikon Perfect Focus System (PFS) hardware autofocus module. Molecular Devices commercial software (Metamorph 7.5.6.0) controlled microscope, camera, motorized stage (ASI instruments), and epifluorescent and brightfield shutters (Sutter Instruments). Epi-illumination was provided by a 300 W Xenon light source (LamdbaLS, Sutter instruments) connected via a liquid

light guide into the illuminator of the scope. Phase contrast illumination was provided by a halogen bulb to allow verification of cell focus and cell shape. Temperature control was achieved using an enclosed microscope chamber (Nikon) attached to a temperature sensitive heat exchanger set to 37°C. All experiments used a Phase 100x Plan Apo (NA 1.4) objective, except for experiments involving filamentous cells, which used a 60x Plan Apo (NA 1.4) objective. Chroma filter sets used were as follows: #41027 (mCh), #41028 (YFP), and #31044v2 (CFP).

**Sample Preparation.** Between days, relative lamp intensity levels were monitored by taking an image of fluorescent beads and measuring their mean intensity. Exposure times were then adjusted to keep per exposure light levels constant between experiments. For snapshots, cells were spotted on 1.5% low melt agarose in PBS and imaged. Images were then analyzed via custom MATLAB software, where mean cell intensities were background corrected using strain JJB176, which has mCherry expression for segmentation, but lacks YFP or CFP expression. For most time-lapse movies (unless otherwise specified), larger 1.5% low melt agarose pads were prepared by pipetting 1 mL of media/agarose solution and allowed to solidify between two 22 x 22mm coverglass (no. 1). A 6 mm biopsy punch cut the larger pad into smaller uniform sized pads, to which 2.25  $\mu$ L of culture diluted to OD 0.01 was pipetted. This protocol tended to give consistent and well-separated densities on the pad, ideal for time-lapse conditions. Prepared pads were then enclosed in coverglass bottom dishes (Willco #HBSst-5040) and sealed with parafilm or grease to prevent evaporation.

## Growth Conditions

**Media.** SMM is derived from Spizizen's minimal media (Spizizen, 1958), which uses 0.5% glucose as the carbon source and tryptophan (50  $\mu$ g/mL) as an amino-acid supplement. Mycophenolic acid (MPA) was dissolved in DMSO and diluted 1000 fold into working concentrations in liquid and pad conditions. IPTG and xylose were dissolved in H<sub>2</sub>O and diluted 1000 fold and 12.5 fold respectively into working concentrations. Concentrations of 0.1% DMSO were not found to affect cell growth or  $\sigma^B$  activity.

Mycophenolic Acid (MPA) experiments (figures 2.1, 2.5-2.10, 2.20)

*Liquid snapshots:* Cells were grown from glycerol stocks in SMM to mid-log (OD 0.3-0.8), then diluted back into SMM to an OD of 0.01. After regrowing to OD 0.1 at 37°C, the culture volume was split and varying concentrations of MPA (MP Biomedicals cat #194172), dissolved in 1000 fold DMSO concentrate, were added to separate cultures. After 2 hours of MPA exposure, cells were imaged as described above.

*Time-lapse microscopy:* Protocol was similar to liquid snapshot protocol above, except when cells regrew to OD 0.1, cells were then spotted on SMM 1.5% low melt agarose pads containing various concentrations of MPA. MPA pads were prepared by taking 1 mL of the SMM/agarose mixture and adding it to 1  $\mu$ L of various MPA stock concentrations. After allowing cells to equilibrate after 2-3 hours, time-lapse acquisition was started.

#### Closed-loop sensitivity measurements (figure 2.2C and 2.15)

Cells were prepared similarly to previous experiments. Upon regrowth to OD 0.1 in SMM, culture volume was split and varying levels of IPTG (0, 10, 20, 30, 40, 50, 1000  $\mu$ M) were added to separate cultures. After 90 minutes of growth, cells were spotted on PBS 1.5% agarose pads and imaged. MATLAB software was used to generate the composite scatter plot (figure 2.2C), and fit it to a standard Hill function equation.

#### Open-loop experiment (figure 2.3)

Upon regrowth to OD 0.1 in SMM, cells were spotted on SMM pads. Xylose was pipetted on the tops (non-cell side) of the 6mm pads to give a saturating concentration of xylose (2%). Time-lapse acquisition was started  $\sim$ 1 hour after exposure to xylose. After microcolonies reached the size of  $\sim$ 8 cells ( $\sim$ 2h), the lid to the Willco dish was removed and varying levels of IPTG (0, 6, 15, 30, 60, 1000  $\mu$ M) were pipetted on to separate pads. Time-lapse acquisition was then continued.

#### Closed-loop experiment (figure 2.4)

Upon regrowth to OD 0.1 in SMM, cells were spotted on SMM pads. Various levels of IPTG were added to the pads (0, 2, 3, 4, 5, 7.5  $\mu$ M IPTG). After allowing cells to equilibrate after  $\sim$ 1 hours, time-lapse acquisition was started.

**Quantitative PCR (figure 2.11).** Strain JJB712 was grown in triplicate to mid-log from glycerol stocks in SMM minimal media + 1 mM IPTG in order to maintain FtsW expression. Cells were then diluted back into SMM + 1 mM IPTG to an OD of 0.01. After regrowth to OD 0.1, cells were washed with several exchanges of SMM without IPTG, and the resulting cultures was re-diluted to OD 0.025 with either 0 or 1000  $\mu$ M IPTG. Cells were allowed to grow to an OD of 0.25 before harvesting. RNA from 1 mL of culture was extracted using the Qiagen RNeasy Protect Bacteria Mini Kit(#74524), using 5 mg/mL lysozyme for cell lysis.

0.5  $\mu$ g of RNA was reverse transcribed using the Biorad iScript One-Step RT-PCR Kit for Probes. Quantitative PCR was performed on a BioRad CFX96 Real Time System using 1/1000th of the cDNA reaction, single gene qPCR primer/probe mixtures from IDT (see table below), and BioRad SsoFast Probes Supermix, in a final volume of 20  $\mu$ L. Each gene for each biological replicate was analyzed in triplicate and averaged to obtain the C(t) value for each gene.

Gene expression was measured relative to mCherry, whose mean fluorescence per cell was measured to be consistent between long and short cells (see figure 2.11A). An additional housekeeping gene (*rrnD*) was also included for comparison and yielded qualitatively similar results. To compute the ratio of long cell to short cell gene expression, each long cell biological replicate (9 total across three days) was compared to the mean short cell expression for each day. These 9 points were averaged and error was calculated for each gene and plotted (see figure 2.11B).

**Immunoblot Analysis (figure 2.14).** Strain JJB737 was grown at 37°C in LB to OD600 of 0.2. The culture was divided into two equal volumes, and exposed to either 0 or 1 mM IPTG. After 30 minutes of further growth, cells were pelleted by centrifugation at 3,000 x g for 10 minutes at 25°C. Proteins were extracted by detergent lysis, using Thermo Scientific Y-PER Yeast Protein Extraction Reagent (Product No. 78991) according to the manufacturer's instructions. To prevent degradation of proteins, protease inhibitors (Thermo Scientific Halt Protease Inhibitor Cocktail, EDTA-Free, Product No. 87785) were added to the samples. Total protein concentrations were determined by a BCA Protein Assay (Thermo Scientific Pierce BCA Protein Assay Kit, Product No. 23227).

*Immunoblotting of RsbQ:* Samples (100  $\mu$ g) of total proteins were resolved on NuPAGE Novex 4-12% Bis-Tris Gels (Invitrogen, Product No. NP0335BOX) with MES SDS running buffer at 150

Table 2.1: Quantitative PCR primer/probe sequences

Gene	Forward Primer	Reverse Primer	Probe
mCherry	CAG GTT TCT TGG CTT TGT ACG	AAA AGA CGA TGG GTT GGG AG	<b>HEX</b> - AT GTA TCC GGA AGA TGG TGC GCT G
rrnD	GCC CTT TGT TCT GTC CAT TG	ACC CTT GAT CTT AGT TGC CAG	<b>HEX</b> - CG TCA TCC CCA CCT TCC TCC G
rsbQ	AAG AAC ATC CTG GGC ATA GC	GTT CGG GAC ATT CAG ATT TGC	<b>FAM</b> - CG CGC ATA TG ACC TGA ATC GTT ACC A
rsbP	TGC CGT GCT ATA TCA ATC TCG	TCT CAG CCC CGT TAA AGT TAT G	<b>FAM</b> - TG TGA AGG TG CCG GTC CAA TTC
rsbV	CCT TCA AGC CTG TAA TGT CAA AC	TGC CTG AAA GAT GTC AGC TAC	<b>FAM</b> - AA ACG CCC A A TCC GGT ACT GTC C
rsbW	CAT TAA ATA TAG ACC GAG CCC TCC	TTA GAG GTT ATT GTG GCG GAT G	<b>FAM</b> - TG ATC AAC TG TGT GCG AAG GTG TGT
sigB	TCT GAA AGG ACA TGA AGC ACG	AAG CCT TAT CCG TTG ACC AC	<b>FAM</b> - AG GAC GGA TA TGA GCG GGT CAA C
sigA	AGA TCA AGG AAC AGC ATA CCG	GAA ATC GCC TAC GCT CAA AAG	<b>FAM</b> - AG TAT CGC AA AAC GGT ATG TCG GAC G

V constant for 1 hour. After performing electrophoresis, proteins were transferred to nitrocellulose membranes (0.2  $\mu$ m) by dry blotting using an iBlot Gel Transfer Device (Invitrogen, Product No. IB1001). The blotted membranes were soaked in freshly prepared blocking reagent, which comprised of TBST (20 mM Tris base, 137 mM sodium chloride, 0.1% (v/v) Tween 20, pH 7.6), 5% nonfat dry milk, and 2% BSA, for 1 hour at room temperature with constant agitation. The blots were then incubated in a 1:10000 dilution of anti-RsbQ in fresh blocking solution for 2 h with agitation. The RsbQ polyclonal antibody was a gift of CW Price (Brody et al., 2001). After washing in TBST 3 times for 10 min each time, the blots were incubated with a 1:2000 dilution of the secondary antibody (ECL Rabbit IgG, HRP-Linked Whole Ab from donkey, Product No. NA934-100UL) in fresh blocking solution for 1 hour. The blots were then washed in TBST 3 times for 5 min each time, followed by a 30 minutes final wash. SuperSignal West Pico Chemiluminescent Substrate (Thermo Scientific, Product No. 34077) was used for horseradish peroxidase detection according to the manufacturer's instructions. Protein bands were visualized on a VersaDoc gel imaging system (Bio-Rad Laboratories).

Immunoblotting of RsbV and RsbV<sup>P</sup>: Proteins extracts were processed with Pierce Detergent Removal Spin Columns followed by Zeba Desalt Spin Columns (Thermo Scientific, Product No. 87778 and 89889) according to the manufacturer's instructions. 200  $\mu$ g of total proteins were separated by two-dimensional electrophoresis according to the carrier ampholine method of isoelectric focusing

(O'Farrell, 1975; Burgess-Cassler et al., 1989) by Kendrick Labs, Inc. (Madison, WI) as follows: Isoelectric focusing was carried out in a glass tube of inner diameter 2.3 mm using 2% pH 3.5-10 mix4L Servalytes, (Serva, Heidelberg, Germany) for 9600 volt-hrs. One  $\mu\text{g}$  of an IEF internal standard, tropomyosin, was added to the sample. This protein migrates as a doublet with lower polypeptide spot of MW 33,000 and pI 5.2. The enclosed tube gel pH gradient plot for this set of Servalytes was determined with a surface pH electrode.

After equilibration for 10 min in Buffer 'O' (10% glycerol, 50 mM dithiothreitol, 2.3% SDS and 0.0625 M tris, pH 6.8), each tube gel was sealed to the top of a stacking gel that overlaid a 10% acrylamide slab gel (0.75 mm thick). SDS slab gel electrophoresis was carried out for about 4 hrs at 15 mA/gel. After slab gel electrophoresis, the gel was placed in transfer buffer (10mM Caps, pH 11.0, 10% methanol) and transblotted onto a PVDF membrane overnight at 200 mA and approximately 100 volts/ two gels.

The PVDF membranes were destained with 100% methanol, rinsed with TBST and blocked as described above. The membranes were incubated overnight at 4°C in a 1:50 dilution of anti-RsbV in fresh blocking solution with constant agitation. The RsbV monoclonal antibody was a gift of WG Haldenwang (described in Dufour and Haldenwang (1994)). The secondary antibody was used at a 1:2000 dilution (ECL Mouse IgG, HRP-Linked Whole Ab from sheep, Product No. NXA931). SuperSignal West Pico Chemiluminescent Substrate was used for detection as described above.

**Statistical Sampling.** To understand whether a relationship existed between pulsing in sister and parent-child cells, only cell-lineages that successfully divided into two continuous daughter cells were sampled and analyzed for pulses. In these lineages, it was not required that a pulse was present. 'Twin' pulses occurred if at least one pulse occurred in both daughter cells of each cell lineage, where a 'parent-child' pulse occurred if a pulse occurred in at least one of the daughter cells of a parent who also pulsed.

To compare these results to an expected value, the pulse frequency of daughter cell was used to create a randomized set of pulsing in each daughter cell for the same number of analyzed lineages as found in the final data set. Each trial involved randomization of daughter cell pulsing, and a subsequent twin pulse frequency calculation. This was done 50000 times, and the resulting distribution of twin



pulses was plotted as a histogram in figure 2.7.

For parent-child pulses, expected value distributions were created by randomizing both whether a parent pulsed, and whether at least one child pulsed, using measured pulse frequencies in each of these populations. As in the sister-cell analysis, 50000 trials were performed.

**Quantitative Analysis.** Quantitative movie analysis used custom image analysis code in MATLAB, similar to that previously described (Rosenfeld et al., 2005). Briefly, we segmented fluorescence images of the  $P_{trpE}$ -mCherry constitutive reporter using edge detection to identify individual cells. Segmented cells were tracked semi-automatically from frame to frame on the basis of position and orientation. Fluorescence was defined as the sum of pixel intensities within the area of the cell. Calculation of promoter activity, and analysis of pulse statistics, were carried out using custom MATLAB code, described below.

**Promoter Activity Definition.** Promoter activity is defined as the rate of protein production. We extract this quantity from time-lapse data by considering the production, degradation, photobleaching, and dilution rates of the fluorescent protein. Fluorescent protein production occurs at a rate  $P(t)$ . We combine all the degradation, dilution, and photobleaching processes into a first-order effective degradation rate constant, denoted  $\gamma$ . Thus, production rate of a Fluorescent protein,  $F$ , is given by:

$$\frac{dF(t)}{dt} = P(t) - \gamma F(t)$$

To solve for  $P(t)$  requires differentiating the total fluorescence  $F(t)$ , but this process is sensitive to cell segmentation errors. To circumvent this problem, we rewrite the cell's total fluorescence  $F(t)$  in terms of its mean fluorescence,  $M(t)$  multiplied by its area,  $A(t)$ :

$$F(t) = A(t)M(t)$$

The area is equal to the width  $W(t)$  of the cell multiplied by its length  $L(t)$ . As the width of *B. subtilis* cells are effectively constant, we can rewrite this equation as:

$$F(t) = L(t)M(t)$$

Where we suppress the constant width value  $W_o$ . Replacing  $F(t)$  in promoter activity definition with this term, and using the differentiation chain rule we obtain:

$$\tilde{P} = \frac{P(t)}{L(t)} = (\mu(t) + \gamma)M(t) + \frac{dM(t)}{dt}$$

Where we define  $\mu(t) = \frac{dL}{dt}$  as the cell's instantaneous growth rate.  $\tilde{P} = \frac{P}{L}$  can be interpreted as the production rate per chromosomal equivalent, allowing comparison of production rate throughout all points in the cell cycle. To avoid unphysical negative values of promoter activity due to bleaching of fluorescent proteins during the movie, we set  $\gamma=0.05$  for all movies analyzed in this work. Promoter activity depends only on the mean cell fluorescence and length which are continuous values that are relatively independent of the exact segmentation of the cell. Nevertheless, small changes in cell segmentation from frame to frame still occur, which can affect length and mean fluorescence measurements. Length and mean fluorescence signals were therefore smoothed using a standard first order locally weighted algorithm (the MATLAB smooth function with Lowess algorithm).

Colony promoter activity, as calculated in figure 2.3 and 2.18, is defined as the amount of protein produced per unit colony area. Unlike in single cells, here the relative impact of potential segmentation errors is strongly reduced by averaging over the entire colony. We defined colony promoter activity as:

$$\tilde{P}_{colony} = \frac{1}{A(t)} \frac{dF_{tot}(t)}{dt}$$

Here,  $A(t)$  represents total colony area in pixels, and  $F_{tot}$  is integrated fluorescence over the entire colony.

**Calculation of pulse statistics.** We characterized the amplitude, duration and frequency of the pulses using custom MATLAB software. Peak locations were found by locating the local maxima of the traces of  $P_{sigB}$ -YFP promoter activity. We defined the start and end of the pulse by locating the local minima surrounding the peak. The pulse amplitude and duration were obtained by calculating

the pulse height and half-maximum width, respectively. Pulse frequency was defined as the number of pulses per hour. To prevent erroneous detection of non-pulse fluctuations in the traces, we imposed two criteria for pulse detection: First, we rejected pulses below a minimum amplitude cutoff. Second, we rejected pulses which contributed less than thirty percent of total gene expression over their duration, i.e. pulses that were relatively small compared to the basal expression rates.

**The full  $\sigma^B$  network has energy and environmental stress inputs.** In wild-type *B. subtilis*, RsbV can be dephosphorylated by two distinct pathways. Energy stresses activate through RsbP and its co-regulator RsbQ, while under environmental stresses use RsbU and its co-regulator RsbT (Hecker et al., 2007). For both systems, dephosphorylated RsbV then binds RsbW, releasing  $\sigma^B$  to activate downstream target genes, including regulating its own operon.

The environmental stress pathway contains additional regulatory components that do not control the response in energy stress. In particular, a  $\sim 1.8$  Mda supramolecular complex, called the stressosome (Marles-Wright et al., 2008), regulates activation of  $\sigma^B$  in response to diverse stresses including ethanol, acid, heat, and osmotic stress, by controlling the activity of the RsbU phosphatase. Structurally, the stressosome is composed of several units of RsbR and RsbS, which control the availability of the kinase, RsbT, the co-activator of RsbU. Interestingly, the activation of RsbU is controlled through another partner switching mechanism (Yang et al., 1996). In the resting (no stress) state, RsbS is found unphosphorylated and complexed to RsbR and RsbT in the stressosome. Stress increases the kinase activity of RsbT, driving the phosphorylation of RsbS, an event that correlates with the release of RsbT from the stressosome. How RsbT kinase activity increases is unknown, but RsbR may mediate an increase in activity (Gaidenko et al., 1999). Once released, RsbT is free to interact with RsbU and activate it.

In addition to upstream components that are unique to the environmental stress pathway, the activation of  $\sigma^B$  results in additional expression of an environmental specific regulator, the phosphatase RsbX. RsbX acts upon the stressosome to dephosphorylate RsbS and RsbR (Chen et al., 2004), counteracting the self-activation of RsbT and blocking further activation from the environmental stress pathway. In this study we focus on the energy stress pathway, and work in a background in which the environmental stress pathway sensor, *rsbU*, is removed to avoid cross-talk between pathways.

Therefore, while  $rsbX$  is present in the wild-type operon, we have omitted it for simplicity in the circuit diagram (figure 2.1B).

**Pulse generation does not appear to involve excitability.** We note that the wild-type system does not appear to behave like a classical excitable system (Lindner et al., 2004). In such systems, threshold-crossing fluctuations generate stereotyped pulses. The amplitude of such pulses are relatively independent of the characteristics of the triggering fluctuation, leading to a unimodal distribution of pulse amplitudes. In contrast, the wild-type  $\sigma^B$  system exhibits a monotonically decreasing distribution of pulse amplitudes for each MPA condition (figure 2.1H). This characteristic is reproduced in the model (figure 2.21).

### Minimal model of $\sigma^B$ network

The gene regulatory network controlling  $\sigma^B$  is depicted in figure 2.1. For mathematical modeling, we simplified this network, concentrating on the minimal set of regulatory components required to explain both the experiments in figure 2.3 and, more generally, FM pulse generation. The purpose of this model is to demonstrate the effects observed, and not to model in detail the dynamics of the network. Here we combine the functions of RsbV and  $\sigma^B$  into a generalized activator, denoted A. Like RsbV, A is active in its unphosphorylated form, and inactive when phosphorylated ( $A^P$ ). A phosphatase, functionally analogous to RsbQP and RsbTU complexes is denoted P. An RsbW-like Kinase, K, phosphorylates A. A activates itself and its inhibitor, K via a transcriptional autoregulatory positive feedback loop.

We assume Michaelis-Menten kinetics for the phosphorylation and dephosphorylation reactions. We also assume linear degradation and transcription rates. These assumptions result in the following continuous ordinary differential equations for the network. Note that phosphatase production rates are taken to be constant for any particular condition but were varied to analyze frequency modulation.

$$\frac{dA}{dt} = trans - phos + dephos - k_d A \quad (2.1)$$

$$\frac{dA^P}{dt} = phos + dephos - k_d A^P \quad (2.2)$$

$$\frac{dK}{dt} = trans - k_d K \quad (2.3)$$

Where:  $trans = t_a A + t_i$  is the transcription rate for both  $A$  and  $K$ ,  $dephos = \frac{b_{dp} P A^P}{k_{dp} + A^P}$  is the rate of dephosphorylation, and  $phos = \frac{b_p K A}{k_p + A}$  is the rate of phosphorylation of  $A$ .

In order to generate the observed ultrasensitivity, both phosphorylation and dephosphorylation reactions are assumed to operate in the saturated regimes. Although this matches well to the experimental data (see figures 2.3, 2.4, 2.21, 2.24), we note that we do not rule out other sources of cooperativity, such as through the partner switching mechanism, or cooperative effects of protein binding (Delumeau et al., 2002).

For analysis of the effects of noise in phosphatase expression,  $P$  was replaced by a fluctuating time-series of phosphatase levels,  $P(t)$  (see below). In equations (2.1) and (2.3), the transcription rates of  $A$  and  $K$  have been assumed exactly equal without loss of generality. This is because the dephosphorylation and phosphorylation rates of  $A$  are not controlled solely by the concentrations of  $P$  and  $K$ , but rather by  $b_{dp}P$  and  $b_pK$ , respectively. Thus, changes in the relative transcription rates of the two proteins can be effectively accomplished by corresponding variation of  $b_{dp}$  and/or  $b_p$ . The transcription rate  $trans$  is assumed to consist of two terms,  $t_i$ , a basal component representing leakiness from the promoter, and  $t_a A$ , representing the autoregulatory feedback due to  $A$ .

Table 2.2: Modeling parameters

Parameter	Parameter Description	Value
$t_i$	Basal transcription rate	0.005 $\mu\text{M}/\text{min}$
$t_a$	Autoregulatory (induced) transcription rate due to $A$ feedback	0.025 $\text{min}^{-1}$
$k_{dp}$	$A^P$ concentration (Michaelis constant) for half maximal dephosphorylation	0.1 $\mu\text{M}$
$k_p$	$A$ concentration (Michaelis constant) for half maximal dephosphorylation	0.1 $\mu\text{M}$
$b_p$	Rate constant for phosphorylation	0.125 $\text{min}^{-1}$
$b_{dp}$	Rate constant for dephosphorylation	0.065 $\text{min}^{-1}$

**Open Loop Model, no noise (figure 2.3).** In the open loop model we modified the  $trans$  term to remove the transcriptional feedback, i.e. we set  $trans = t_i$ . This parameter  $t_i$  was then modulated to allow different protocols of operon induction. For each simulated operon level the system equations were numerically integrated in MATLAB for 300 minutes using the built in ode45 solver. As in the

experimental system, we assumed a constant phosphatase level ( $P=0.9 \mu\text{M}$ ). For these simulations,  $t_i$  was initially set to zero and then switched to varying constant levels at 120 minutes, corresponding to the experimental operon induction conditions used in figure 2.3C.

**Closed Loop Model, with noise (figure 2.4).** To simulate noisy phosphatase expression in the closed loop model, we replaced the constant phosphatase level,  $P$ , with a time-varying phosphatase concentration,  $P(t)$ .  $P(t)$  was pre-computed through a gamma distributed Ornstein-Uhlenbeck process (Barndorff-Nielsen and Shephard, 2001). Thus, it exhibited both a gamma distribution of concentrations (Taniguchi et al., 2010; Friedman et al., 2006; Raj et al., 2006), and an exponential auto-correlation function, with a correlation time roughly the order of the cell-cycle duration (Rosenfeld et al., 2005). We chose a gamma distributed Ornstein-Uhlenbeck process, rather than a standard Ornstein-Uhlenbeck process as used in previous work (Suel et al., 2006), as there is strong evidence gene expression is gamma distributed in many systems (Taniguchi et al., 2010; Friedman et al., 2006; Raj et al., 2006), and because it permits independent modulation of burst size and frequency. The equations were numerically simulated using ode2, a fixed-step, 2nd order Euler method solver. Discrete step sizes of 0.1 minutes were taken, to assure that the sampling rate was much faster than the timescale of the noise or of the pulses.

We modulated the burst size of the gamma distributed phosphatase in order to examine how phosphatase levels affect pulsing (figure 2.4). For each phosphatase level, we performed 250 simulations, each lasting 20,000 (simulated time), and used these data to compute pulse statistics. We calculated the pulse duration, amplitude, and frequency by examining the local maxima and minima of the simulated traces, using the same method as we used to determine pulse statistics from the experimental data.

## Chapter 3

# Rate of Environmental Change Determines Stress Response Specificity in Bacteria

### 3.1 Introduction

Cells use diverse signaling systems to respond and adapt to changing environmental conditions<sup>1</sup>. The quantitative input-output characteristics of these systems differ (Cai et al., 2008; Shoval et al., 2010; Mettetal et al., 2008; Levine et al., 2012). For example, the *E. coli* osmoresponse output tracks its input, while the chemotaxis response exhibits perfect adaptation, reverting to a set level regardless of the absolute level of ligands in the environment (Kawaji et al., 1979; Alon et al., 1999). Rate-responsiveness, or the ability for cells to sense the rate change of stress, is also a general property common to signaling systems (Shimizu et al., 2010; Nisamedtinov et al., 2008; Stone and Nicolas, 1995). In this scenario, the output of the system is dependent on the rate of change of the input signal (figure 3.1A). However, it is unclear whether cells use rate information to regulate cellular responses. Are there instances where cells need to sense the rate of incoming signals to respond appropriately? If so, how might this regulation might be achieved?

Cells also face a regulatory decision when it comes to responding to stress. Many organisms contain a pathway that responds to multiple stresses and regulates a diverse set of genes, which may cross-protect the cell against other stresses (Weber et al., 2005; Nannapaneni et al., 2012; Sadeh et al., 2011; Richter et al., 2010; Batchelor et al., 2009). This “general stress response” contrasts with cellular

---

<sup>1</sup>This chapter will be published in its entirety with authors J.W. Young and J.C.W. Locke as co-first authors, with equal contribution. This chapter is a preliminary draft of the manuscript.

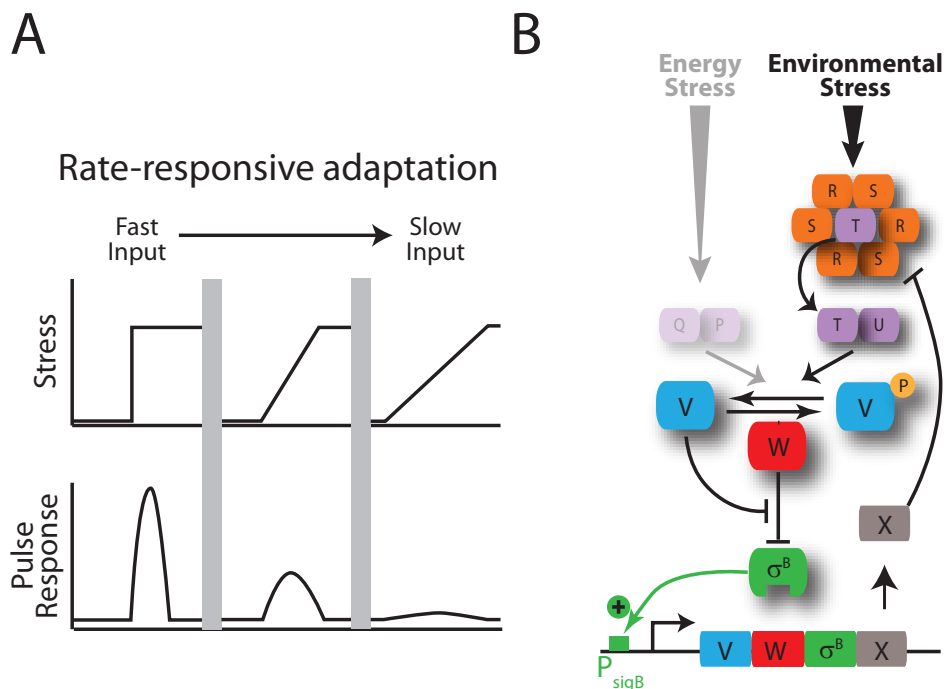


Figure 3.1: Schematic of a rate-responsive adaptive output. (A) As the stress rate decreases from a step to graded exposure, the magnitude of the adaptive response decreases. (B) Schematic of  $\sigma^B$  environmental interactions. Environmental stress is transduced by the stressosome (orange), which controls the availability of the kinase, RsbT (purple), the co-activator of RsbU. Active RsbU dephosphorylates RsbV (blue), which can bind RsbW (red), releasing  $\sigma^B$  (green) to activate target genes including its own operon. Activation of  $\sigma^B$  results in additional expression of an environmental specific regulator, the phosphatase RsbX (grey). RsbX acts upon the stressosome to counteract the self-activation of RsbT. The transducer of energy stress RsbQP is shown greyed out, to indicate its deletion in strains used for this paper.

systems that respond more specifically to stress and regulate few targets (Allenby et al., 2005; Noriega et al., 2010; Zheng et al., 1998). The decision to respond broadly or specifically is critical and must be made correctly. Unnecessary activation of stress response genes can place a burden on cell growth machinery, reducing cell proliferation and wasting valuable resources. Insufficient stress response may allow a loss of macromolecule stability, and at the very worst, may compromise cell membranes leading to cell lysis and death. Insufficient stress response may also fail to prepare the cell for multiple stresses. For example, in some native environments, the arrival of one stress quickly may frequently be coincident with several other stresses - i.e., the adage of “when it rains it pours.” In this situation then, the cell may require general stress responses to anticipate these dooms-day scenarios.

In diverse gram-positive bacteria, the general stress response is mediated by the alternative sigma factor,  $\sigma^B$ , which regulates a broad range of operons responsible for protecting the cell against many different types of stress (Hecker et al., 2007; Haldenwang and Losick, 1979). Here we use a combination



of mathematical modeling and quantitative single cell time-lapse analysis to show that  $\sigma^B$  responds to environmental stress in a rate-responsive manner: Stresses presented suddenly activate  $\sigma^B$  much more strongly than the same level of stress presented more gradually. Furthermore, in this system, rate-responsiveness provides a key capability to cells, by allowing them to control the specificity or generality of their response to a given stress. Fast increases broadly activate the full repertoire of stress response pathways, while slower increases in stress allow the cell to respond more selectively to the specific stresses it encounters. In this way, cells could anticipate other stresses that are likely to accompany a sudden change in any one stress, and cross-protect only when necessary.

The dynamic response of  $\sigma^B$  to environmental stress is qualitatively different from its response to energy stress (Locke et al., 2011). In that case,  $\sigma^B$  is activated in a series of sustained stochastic pulses, whose frequency is modulated by levels of energy stress. How does the system implement two very different dynamic responses in response to distinct classes of stress? The  $\sigma^B$  network transduces signals using a core partner-switching system between RsbV, RsbW, and  $\sigma^B$  and multiple feedback loop on  $\sigma^B$ 's own operon (Dufour et al., 1996; Brody et al., 2001; Wise and Price, 1995). The environmental pathway adds two additional features to this circuit: First, it is activated by the stressosome, a large 1.8 MDa multi-protein complex that controls the input phosphatase RsbU (Marles-Wright et al., 2008). And second, it includes another negative feedback loop provided by RsbX, a phosphatase that down-regulates activation by the stressosome (Eymann et al., 2011) (figure 3.1B). In contrast to Igoshin et al. (2007) reports on RsbX function, our computation model predicted that the RsbX feedback loop is not required for the transient activation of  $\sigma^B$  from environmental stress, but rather adjusts the sensitivity of the network to stress and modulates the shape of the rate-response curve. This prediction was verified in a strain where the RsbX feedback was removed.

## 3.2 Results

**Activation of  $\sigma^B$  by sudden environmental stresses produces a single amplitude modulated pulse.** In order to focus on the environmental response, we constructed a  $\sigma^B$  fluorescent reporter strain in which the energy stress inputs were blocked by deletion of the corresponding sensor, rsbQP (figure 3.1B). To avoid inadvertent stimulation of the pathway by stray light, we also deleted the

blue-light sensor *ytaA*. Upon addition of ethanol, a well-known activator of the environmental pathway (Boylan et al., 1993),  $\sigma^B$  promoter activity exhibited a single pulse (figure 3.2A, SI movie), peaking at 50 minutes after the addition and then falling to levels close to pre-stress levels (SI movie). This behavior was homogeneous across individual cells (figure 3.5) and was qualitatively similar across all levels of ethanol tested, up to 2% ethanol. Thus, up to intermediate levels of stress, the environmental pathway responds with near exact adaptation. This response was similar under solid phase and liquid growth. Critically, the amplitude of the pulse increased with increasing ethanol concentration (figure 3.2B) while the duration, or adaptation time, of the response was nearly constant across conditions tested (figure 3.2C), showing that the response to environmental stress is pulse amplitude modulated (PAM).

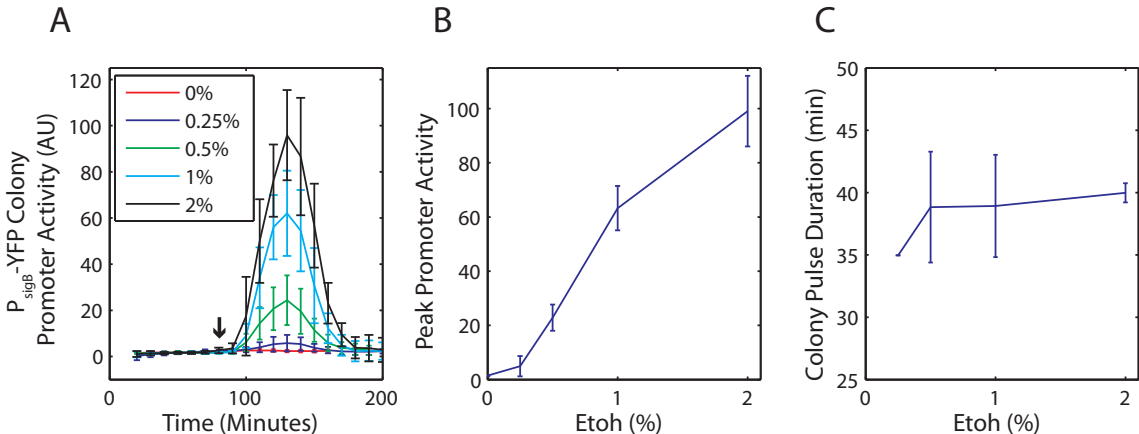


Figure 3.2: Activation of the environmental pathway results in a single pulse that is amplitude modulated. (A) When exposed to ethanol, strain JJB761 exhibits a single pulse of activity as measured from a  $P_{sigB}$ -yfp promoter reporter. Ethanol was added to each condition at 80 minutes (black arrow). Each curve represents the time-lapse response from 2 independent colonies over 2 days ( $n_{total} = 4$ ). Error bars represent standard deviation for each condition and time-point. (B-C) Peak amplitude of the environmental stress shows the magnitude of the response increases with increasing ethanol, whereas the duration of the response remains nearly constant. Error bars represent standard deviation.

**Mathematical modeling captures PAM the response of  $\sigma^B$ .** In previous work, we developed a model of  $\sigma^B$  activation by energy stresses (Locke et al., 2011). In order to adapt this model to environmental stresses (see Minimal model of  $\sigma^B$  network in Methods), we added two additional regulatory layers: First, we included a stressosome component, which sequesters a pool of phosphatase and activates it upon stress to dephosphorylate RsbV and thereby activate  $\sigma^B$ . Second, we included *rsbX*, the last gene in the  $\sigma^B$  operon, which acts upon the stressosome to remove input phosphatase and thereby down-regulate  $\sigma^B$  activity. In the model, increasing environmental stress levels yielded

corresponding increased amounts of input phosphatase from the stressosome. The model recapitulated the single pulse dynamics of the system and the increasing response amplitude to increasing ethanol concentration.

**RsbX feedback is not necessary for the adaptive response.** RsbX is a phosphatase that acts as a negative regulator of  $\sigma^B$  activity by acting upon the stressosome. Its expression is driven from the  $\sigma^B$  operon, which contains a binding site for  $\sigma^B$ . Thus, RsbX closes a negative feedback loop that only acts upon the environmental pathway. Modeling suggested that adaptation could result from the RsbW negative feedback loop alone, in contrast to previous results that suggested rsbX feedback was necessary (Igoshin et al., 2007). To test this, we engineered a feedback independent strain (-FB<sub>rsbX</sub>) where endogenous rsbX feedback (+FB<sub>rsbX</sub>) was replaced by an IPTG-inducible copy (figure 3.3A). Consistent with previous reports, removing induction of RsbX caused a rapid induction of  $\sigma^B$  that strongly affected cell growth. However, when RsbX was induced to levels that produced similar  $\sigma^B$  activity as the +FB<sub>rsbX</sub> strain, the transient nature of  $\sigma^B$  activation was strikingly similar (figure 3.6). Thus, the absence of RsbX feedback loop does not affect the dynamics of environmental  $\sigma^B$  activation, under the conditions tested.

**RsbX feedback linearizes the dose-response curve.** Modeling suggested that RsbX feedback could linearize the dose response curve, increasing the range of stress concentrations which could be distinguished by  $\sigma^B$  activity. When  $\sigma^B$  activity was measured after the addition of various ethanol concentrations, at a variety of RsbX induction levels, we find substantial differences between the +FB<sub>rsbX</sub> and the -FB<sub>rsbX</sub> strains (figure 3.3B). At low induction levels (10  $\mu$ M IPTG),  $\sigma^B$  activity is more easily induced compared to the +FB<sub>rsbX</sub> strain, suggesting that a minimal amount of RsbX is necessary to avoid extreme sensitivity to stress. At moderate and higher levels of induction ( $\geq 30$   $\mu$ M IPTG), the -FB<sub>rsbX</sub> strain exhibits a more sigmoidal dose response curve compared to that of the +FB<sub>rsbX</sub> strain, where activity is suppressed at low stress (see 0.5% ethanol) and is higher at greater ethanol concentrations. Also consistent with other functions of negative feedback (Nevozhay et al., 2009), the +FB<sub>rsbX</sub> strain displayed lower expression noise (as measured by CV) compared to the -FB<sub>rsbX</sub> strain at equivalent mean levels of gene expression (figure 3.7).

**Mathematical modeling predicts that activation of  $\sigma^B$  by environmental stresses is rate-**

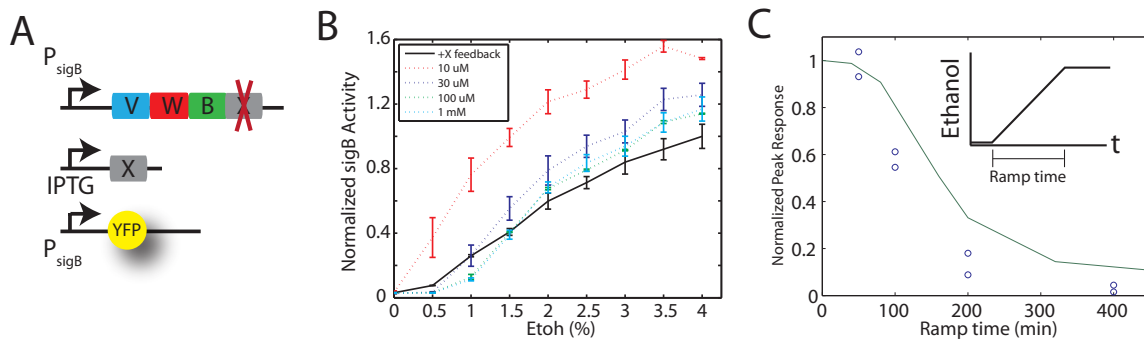


Figure 3.3: The  $\sigma^B$  response is dependent on stress-rate. RsbX feedback linearizes  $\sigma^B$  dose response curve to ethanol. The wild-type *rsbX* gene was deleted and replaced with  $P_{hyperspank}$ -*rsbX*, an IPTG controllable construct to create a RsbX feedback independent strain (A). This strain required active induction of RsbX in order to suppress  $\sigma^B$  activity. Strains were grown in SMM, either without IPTG (JJB761, + $FB_{rsbX}$ ), or with concentrations of IPTG indicated (JJB836, - $FB_{rsbX}$ ) and were exposed to different concentrations of ethanol (0 - 4%). Near the peak of activation (30 minutes of exposure)  $\sigma^B$  activity was measured using a  $P_{sigB}$ -yfp reporter via microscope snapshots. (B) Negative feedback linearizes the  $\sigma^B$  dose response curve. Across concentrations of IPTG that give comparable  $P_{sigB}$ -yfp activation (30-1000  $\mu$ M) to the +feedback strain, the dose response curve is more non-linear (cf. blue, dark-blue, green colored lines to black), where responses to low and high levels of ethanol are suppressed and elevated, respectively, when compared to the +feedback strain. (C) Strain JJB761 was exposed to different ramps (inset) of ethanol exposure. Peak  $\sigma^B$  activity decreases dramatically as ramp times increase, consistent with model results (green), showing that  $\sigma^B$  environmental stress is rate-responsive.

**responsive.** Once phosphorylated, the stressosome releases co-activator RsbT, which can then bind RsbU and activate its phosphorylation capabilities. The stressosome thus allows phosphatase changes to occur quickly through enzymatic phosphorylation in order to activate the core  $\sigma^B$  circuit. This reaction is much faster than the negative feedback from RsbW, which requires full transcription and translation. If phosphatase release is proportional to stress input, a major prediction of the model is that the activation of  $\sigma^B$  should be sensitive to how quickly the stress is applied, in addition to the magnitude of stress (figure 3.8).

We tested whether  $\sigma^B$  activation was rate-responsive using a microfluidic device to deliver 2% ethanol to cells either quickly, or gradually, to 2% (figure 3.3C, inset). When colony promoter activity (Locke et al., 2011) was compared at different ramp times, generating a rate-response curve, we observed a decreasing sigmoidal curve consistent with model predictions (figure 3.3C). This decreased  $\sigma^B$  activity in response to gradual stress was not specific to ethanol, but applied to other stresses and analytic methods (figure 3.9).

**$\sigma^B$ -independent regulation may provide rate-independent gene regulation.** The previous

results suggest that the cell uses  $\sigma^B$  inputs to provide rate-responsive regulation to target promoters. However, genes regulated by  $\sigma^B$  can be combinatorially regulated, which may allow rate-independent regulation through other cellular regulators that are sensitive to the absolute magnitude of stress, rather than its rate of increase. These regulators may also regulate genes that do not contain  $\sigma^B$  binding sites. Thus, the prediction is that slow stress would preferentially activate mixed or  $\sigma^B$ -independent targets whereas genes containing only  $\sigma^B$  regulation would activate more strongly with fast stress compared to slow stress (figure 3.4A).

**OpuE is a mixed  $\sigma^B$  target that shows rate-independence.** To test this model, we examined the response of OpuE, a transporter involved in responding to osmotic stress, by constructing a promoter-fusion reporter expressing yfp. OpuE’s promoter contains  $\sigma^B$  and  $\sigma^A$  binding sites that are both involved in activation of the gene (Spiegelhalter and Bremer, 1998). In response to a sudden osmotic shock of 0.4 M NaCl, OpuE mean reporter levels rapidly increase, then approach steady-state values that are similar to values when osmotic stress is applied over a linear gradient of 400 min (figure 3.11). In contrast,  $\sigma^B$  activation was much more limited in the gradual stress condition. Activation of OpuE did not require  $\sigma^B$ , as a  $\sigma^B$  knockout still permitted OpuE expression. Thus, OpuE is an example of a stress response gene that shows relative rate-independence.

**Rate-responsive genes are highly likely  $\sigma^B$  targets.** We were interested in knowing whether OpuE represents one of many rate-independent stress genes that activate under osmotic shock conditions. To this end, we applied salt stress to cells over a 400 minute timeframe, or instantly. We extracted cell RNA and compared relative expression between the two conditions using RNA-seq (figure 3.4B). Our model of rate-dependent regulation predicted that we would find a set of genes that would be rate-responsive (ie,  $\sigma^B$  targets), and a set of genes that would show rate-independence. We find the expression data supports this idea. Several genes prefer to upregulate under instant-salt stress compared to graded-salt stress (right of figure 3.4B dashed line), and another set of genes upregulate under both conditions (near or to left of dashed line). Moreover, many of the most rate-responsive genes were predicted  $\sigma^B$  targets (Nannapaneni et al., 2012), suggesting that the principle factor conferring salt rate-sensitivity is  $\sigma^B$ .

**$\sigma^B$  target function stratifies with rate-sensitivity.** Interestingly, several  $\sigma^B$  targets were found

to be upregulated more similarly between fast and slow stress, suggesting rate-independence. These genes represent a set of salt response targets that can be induced specifically, without simultaneous activation of the entire  $\sigma^B$  regulon. We were interested in how the function of these genes compare with rate-sensitive genes. We find that rate-independence correlates with genes known to be involved in membrane function, whereas the most rate responsive genes were more likely to be classified as general stress response genes (figure 3.4C). This is consistent with the functional response to osmotic stress. Membrane transporters maintain intracellular osmolarity by moving solutes across the cell wall. Cells may need these functions independent of how the salt stress was applied, so regulation of these genes may be more sensitive to the absolute magnitude of salt stress, rather than the rate of stress exposure.

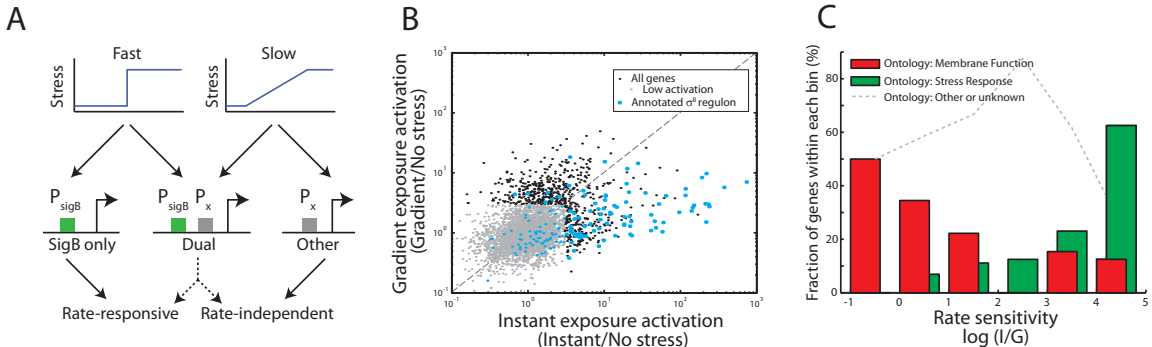


Figure 3.4: RNA-seq reveals two functional classes of  $\sigma^B$  targets. (A) Model of rate-responsive regulation of downstream stress targets. Rate-responsive genes would principally contain  $\sigma^B$  only sites ( $P_{sigB}$ ) whereas other types of regulation ( $P_x$ ) could show rate-independence. Co-regulated targets could show either type of response, depending on the promoter regulation logic. (B) RNA from cells exposed to salt under fast, slow, and no stress conditions was submitted for RNA-seq. We focused our attention from all genes (grey) to targets upregulated under salt conditions (black) and putative  $\sigma^B$  targets (blue) (Nannapaneni et al., 2012). Genes showing activation similar in both conditions (dashed line) are more rate-independent than genes away from this diagonal. Consistent with previous experiments, we find that nearly all genes highly activated under fast salt exposure are part of the  $\sigma^B$  regulon. (C)  $\sigma^B$  associated genes (blue from (B)) have two functional categories that are separated by stress rate sensitivity. ‘Membrane associated’ genes (red), such as salt and other small molecule transporters are frequently not rate-sensitive, while ‘Stress response’ genes are very sensitive to stress rate.

### 3.3 Discussion

In summary, we have shown that the cell uses rate-responsiveness to separate functional classes of genes. This property of rate-sensitivity is almost exclusively a feature of the  $\sigma^B$  regulon, which

generates this property simply by the addition of fast phosphatase input, provided by the stressosome.

The stressosome provides a crucial role in coordinating the response to environmental stress. The PAM response resulting from stress results from the large, rapid release of phosphatase that the stressosome provides. Moreover, in order for  $\sigma^B$  to activate to fast stresses and provide protection for other stresses, an element is required that integrates the environment and activates  $\sigma^B$  quickly enough to surpass the negative feedback provide by kinase, *rsbW*. The stressosome's role in integrating stresses had been discussed previously, but the present work suggests that an important additional role is its ability to rapidly release a strong bolus of phosphatase to activate the system.

The activation of the  $\sigma^B$  regulon is a drastic response to stress, activating at least 150 genes (Nannapaneni et al., 2012), many relating to protecting the cell from different physical insults. Thus, while a single stress may activate  $\sigma^B$ , the response demands an all-hands approach, preparing the cell for an onslaught of possible stresses. This type of response may be adaptive, as the sudden arrival of stress may coincide with the arrival of other insults. This type of response is not without cost though, as strong  $\sigma^B$  activation is a potent inhibitor of growth. The cell would do well then, to have mechanisms that allow separate activation of specific stress response genes when cross-protection is not necessary. The  $\sigma^B$  circuit serves this role. As a rate detector it enables broad stress response in rapidly deteriorating conditions while permitting specific responses under slower stress. Intriguingly, the cell has integrated effector and rate-response systems in one circuit. Another scenario could have had these functions distinct, where a separate rate detecting module permitted  $\sigma^B$  activation in sudden stress, and prevented it under gradual stress.

Interestingly, in contrast to previous modeling, *rsbX* feedback was not required for the adaptive response to environmental stress, provoking the question of what role *rsbX* provides. *RsbX* feedback linearizes the dose-response to stress, which is thought to also linearize the rate-response curve. Thus, the feedback helps to differentiate different stress magnitudes and stress rates, increasing the input dynamic range of the response. It is intriguing to ask whether the cell selects upon one response over the other. Does cell survival depend more on linearizing dose-response, or rate-response?

A general feature of stress responses, from prokaryotes to eukaryotes, is their ability to respond broadly to many stresses and provide cross-tolerance when exposed to a single stress.  $\sigma^B$  and  $\sigma^S$

control the general stress response in *B. subtilis* and *E. coli* respectively, while Msn2/4 and the HSP family controls the stress response in *S. cerevisiae* and higher eukaryotes. It will be interesting to see if these systems are rate-responsive, and more functionally, use this rate-responsiveness to separate gene regulatory states.



### 3.4 Supplemental Figures

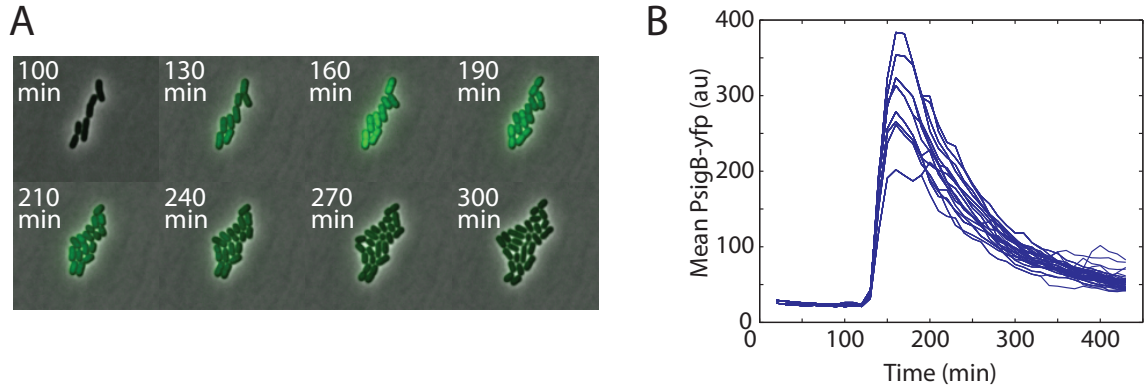


Figure 3.5:  $\sigma^B$  activation in response to environmental stress is relatively homogenous. (A) Filmstrip of  $\sigma^B$  activation when exposed to 2% ethanol, showing a single pulse in all cells. (B) Single-lineage traces of the movie in (A) showing mean  $P_{sigB-yfp}$  activity. While variation in amplitude exists, the dynamics of each lineage is extremely similar. Compare this response with that of the single cell response in Chapter 2.

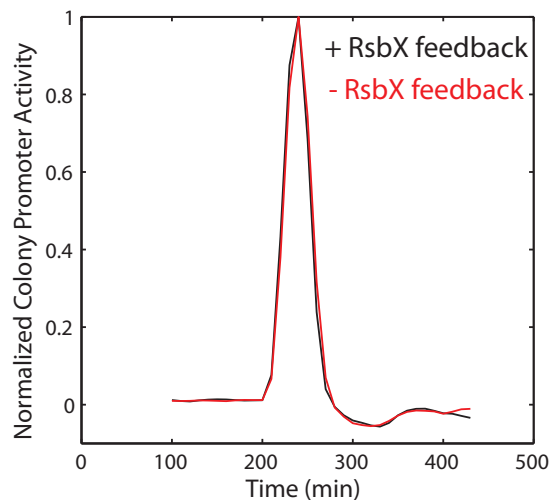


Figure 3.6: RsbX feedback is not necessary for adaptive response to environmental stress. Strains were grown in SMM with 1mM IPTG (JJB836,-RsbX feedback) or without (JJB761,+RsbX feedback), in a microfluidic environment. At  $t=200$  min SMM + 2% ethanol was added and  $P_{sigB-yfp}$  activity was measured. When comparing peak normalized colony promoter activity, the feedback independent strain (-FB<sub>rsbX</sub>) exhibits near identical dynamics compared to that of the +RsbX feedback strain (+FB<sub>rsbX</sub>).

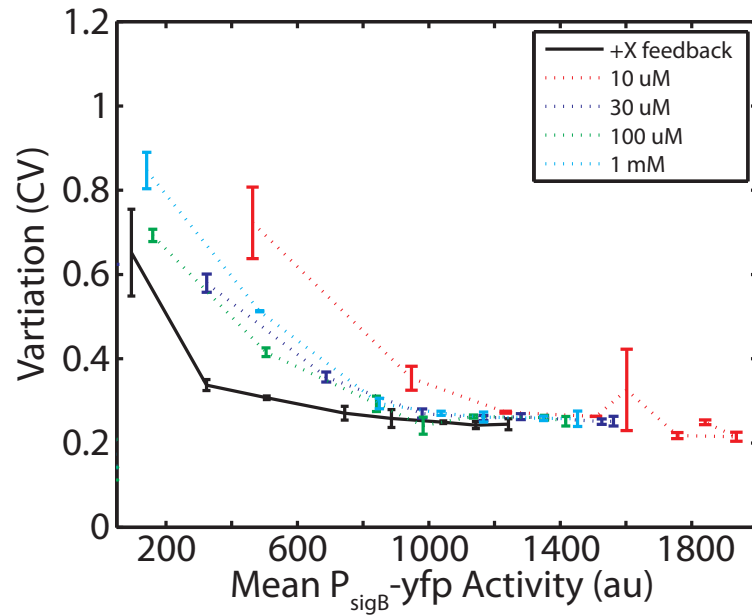


Figure 3.7: RsbX feedback reduces expression noise. Strains were grown in SMM, either without IPTG (JJB761, + RsbX feedback), or with concentrations of IPTG indicated (JJB836, - RsbX feedback) and were exposed to different concentrations of ethanol (0 - 4%). Near the peak of activation (30 minutes of exposure)  $\sigma^B$  activity was measured using a  $P_{sigB}$ -yfp reporter via microscope snapshots. At nearly all levels of  $\sigma^B$  activation, the presence of the RsbX feedback loop reduces noise, as measured by CV, compared to the feedback independent strain.

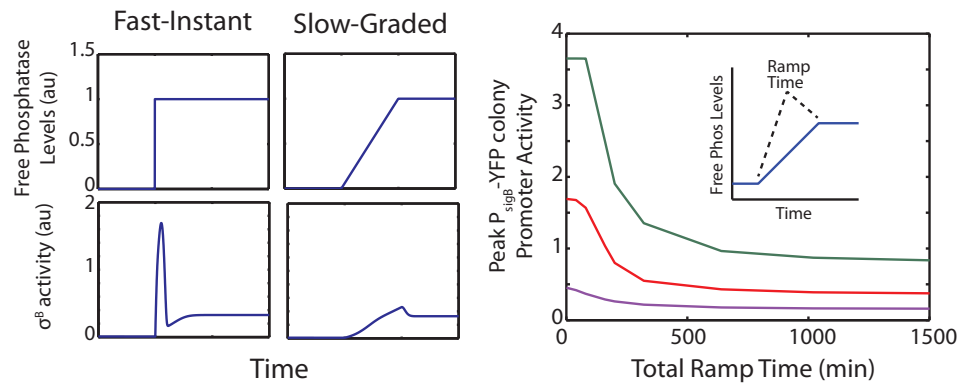


Figure 3.8: The  $\sigma^B$  response is dependent on rate of phosphatase release. (A) A minimal model incorporating the stressosome and the rsbX feedback loop predicted that  $\sigma^B$  activity is highly dependent on the rate of phosphatase release. (B) Predicted rate response curves have shapes that are relatively independent of different final concentrations of free phosphatase (purple, red, green).

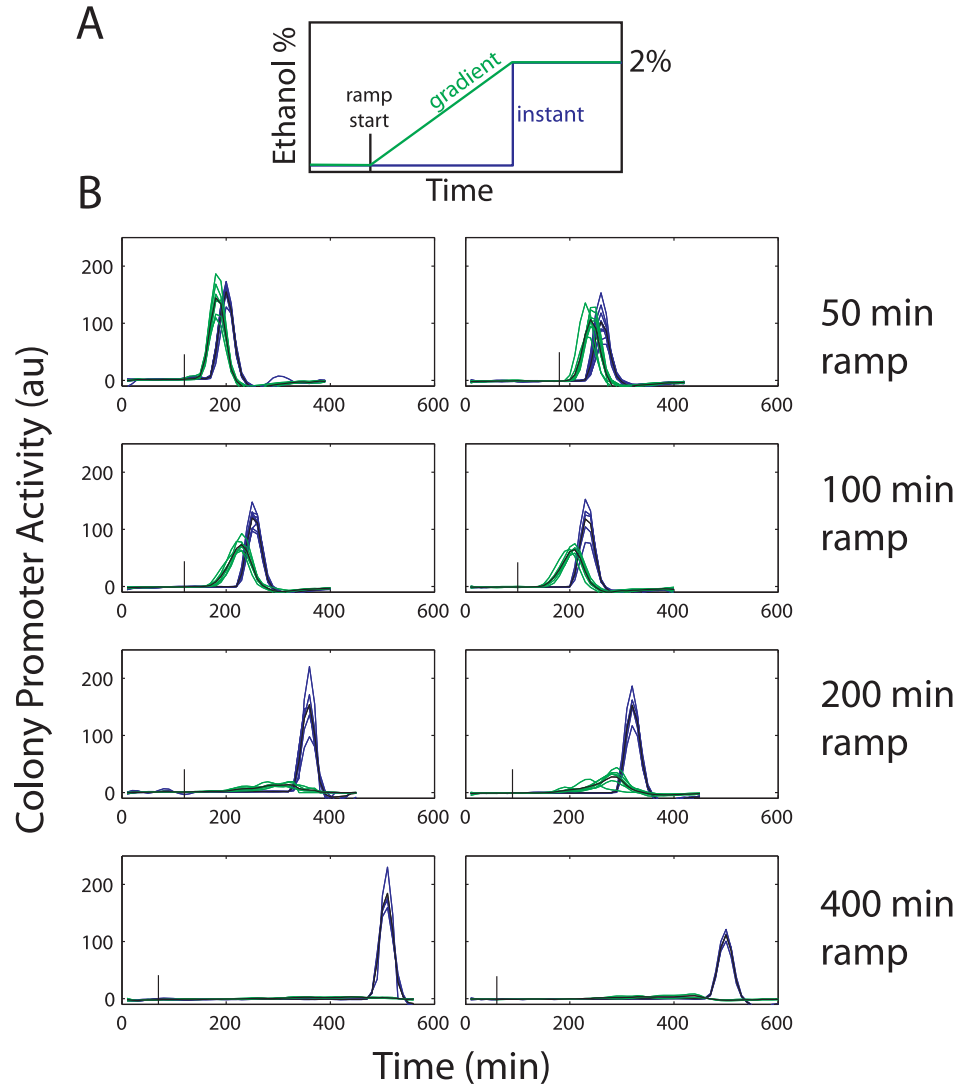


Figure 3.9: Individual  $P_{sigB}$ -yfp colony promoter activity traces under different stress rates. (A) Schematic of rate-response experiment. JJB761 was grown using SMM in a microfluidic environment. After some equilibration time, a linear increasing ramp of ethanol was started (indicated by black line) until the concentration reached 2%. In parallel, cells were exposed to a step to 2% ethanol at the end of the ramp. This was performed for data normalization. (B) Individual colony promoter activity traces for gradient (green) and instant (blue) stress conditions. Each separate plot represents a single experiment. For a single day the mean response of all gradient stress colonies was averaged and peak response was normalized to the peak of instant stress colonies, in order to generate data for the rate-response figure (figure 3.3C).

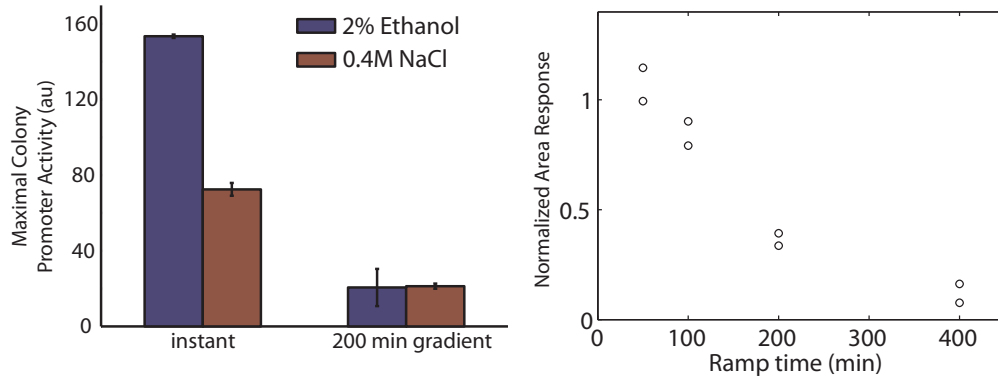


Figure 3.10:  $\sigma^B$  shows stress rate sensitivity in other conditions and using different analytical methods. (A) Strain JJB761 was exposed to either a fast stress or a 200 minute gradient using 2% ethanol or 0.4M NaCl, both known to activate  $\sigma^B$  strongly. Error bars represent standard deviation across two days of experiments. (B) Promoter activity integral shows similar rate sensitivity compared to peak amplitude measurements. The mean area under the curve for cells exposed to gradient stress was normalized to the mean area of the instant stress control, for each data point (single experiment).

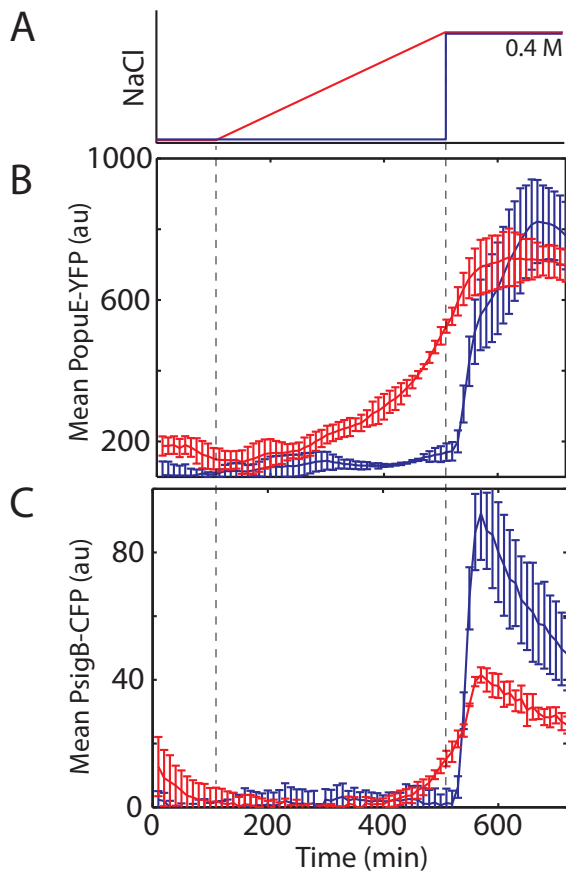


Figure 3.11: OpuE shows rate-independent steady-state expression that is rate-independent. Strain JJB848 reports on *opuE* and  $\sigma^B$  activity using a YFP and CFP reporter, respectively. (A) When exposed to fast or slow (400 min ramp) salt stress (0.4M) mean *opuE* activity (B) reaches similar steady-state levels when compared to  $\sigma^B$  activity in the same strain (C). Error bars represent standard deviation for each condition and time point.

### 3.5 Methods

**Microscopy.** All data were acquired using a CoolSnap HQ2 attached to a Nikon inverted TI-E microscope, equipped with the Nikon Perfect Focus System (PFS) hardware autofocus module. Molecular Devices commercial software (Metamorph 7.5.6.0) controlled microscope, camera, motorized stage (ASI instruments), and epifluorescent and brightfield shutters (Sutter Instruments). Epi-illumination was provided by a 300 W Xenon light source (LambdaLS, Sutter instruments) connected via a liquid light guide into the illuminator of the scope. Phase contrast illumination was provided by a halogen bulb to allow verification of cell focus and cell shape. Temperature control was achieved using an enclosed microscope chamber (Nikon) attached to a temperature sensitive heat exchanger set to 37°C. All experiments used a Phase 100x Plan Apo (NA 1.4) objective. Chroma filter sets used were as follows: #41027 (mCh), #41028 (YFP), and #31044v2 (CFP). The interval between consecutive imaging was 10 minutes.

**Sample preparation.** For agarose movies, samples were prepared using similar protocols as described in Young et al. (2012), with the following adaptations. For the ethanol experiments showing the environmental PAM response, cells were spotted on SMM agarose pads (without ethanol) and allowed to outgrow for approximately 2 hours, before the start of imaging. When ethanol was to be added, 4  $\mu$ L of ethanol solution was added to the top of the agarose pad, then immediately a small, glass-topped cap was placed around each individual pad to prevent ethanol evaporation.

**Microfluidics.** Cells were grown using the Cellasic ONIX microfluidic perfusion system with bacterial plate (#B04A). Cells were loaded onto the plate at an approximate OD of 0.001 using the automated Cellasic loading protocol. The settings for loading pressure were between 4-6.5 psi, and loading times were between 2-4 seconds. This often loaded cells at a very low density, suitable for time-lapse imaging and quantitative analysis. Cell growth and responses to stress were similar between pad and microfluidic conditions. To create a linear gradient of increasing stress, pressures across the microfluidic manifold were changed in 20 discrete steps from no stress to maximum stress. The appropriate pressures necessary to generate a linear gradient were calibrated from fluorescein dye measurements.

## Growth Conditions

**Media.** SMM is derived from Spizizens minimal media (Spizizen, 1958), which uses 0.5% glucose as the carbon source and tryptophan (50 $\mu$ g/mL) as an amino-acid supplement. Ethanol and NaCl were dissolved in SMM and diluted to working concentrations depending on whether the experiment was in pad or liquid conditions. IPTG was dissolved in H<sub>2</sub>O and diluted 1000 fold into working concentrations.

### Ethanol experiments

Cells were grown from glycerol stocks in SMM to mid-log (OD 0.3-0.8), then diluted back into SMM to an OD of 0.01. After regrowing to OD 0.1 at 37°C, cells were then spotted on SMM 1.5% low melt agarose pads. After allowing cells to equilibrate after 2-3 hours, time-lapse acquisition was started. Ethanol was added to pads as described above.

### Rate-responsive measurements

Cells were grown from glycerol stocks in SMM to mid-log, and then diluted back into SMM to an OD of 0.01. After regrowth to OD 0.1 at 37°C, cells were loaded into the microfluidic plate using all four chambers using the protocol described above. After 2 hours of outgrowth, time-lapse imaging was started. For each plate, two chambers were exposed to fast stress using a step in stress, while the other two chambers were exposed to slow stress using a 20-step gradient as described above. For ethanol experiments, the final ethanol concentration was 2%, while for osmotic experiments the final NaCl concentration was 0.4 M.

### Dose-response measurements

In the *rsbX* feedback-independent strain (JJB837), the expression of *rsbX* is controlled by the amount of IPTG in the culture. The absence of *rsbX* results in uncontrolled activation of  $\sigma^B$ , which causes cell toxicity and halts cell growth. In order to maintain minimal  $\sigma^B$  activity, JJB837 was grown from glycerol stocks with 1mM IPTG to mid-log. Cells were then washed with several exchanges of SMM without IPTG, and the resulting culture was diluted to 0.01 with varying levels of IPTG (10, 30, 100, 1000  $\mu$ M) Upon regrowth to OD 0.1 in SMM, culture volume was split and ethanol was added to varying final concentrations (0, 0.5, 1, 1.5, 2, 2.5, 3, 3.5, and 4%). After 30 minutes of ethanol

exposure, cells were spotted on PBS 1.5% agarose pads and imaged. The time between spotting of pads and imaging was kept to a minimum, with the entire process taking 15-20 minutes for each sample. Consistent with this principle, the dose-response curves for each strain/IPTG concentration was measured independently of each other in order to minimize sample preparation times for each sample. Snapshots were analyzed using custom MATLAB software.

## RNA-seq

**Growth conditions.** Cells were grown ON as described above to mid-log. Cells were diluted back to OD 0.001 into 3 conditions (fast-stress, slow-stress, and no-stress) with 2 replicates and allowed to grow at 37°C for one hour. In the slow stress conditions, salt solution was added every 20 minutes for 20 steps (400 minute ramp), in order to closely mimic the microfluidic experiments. Upon the addition of the last step, salt was added to the fast-stress conditions to same final salt concentration (0.36 M NaCl). After 10 minutes, samples were then prepared for RNA extraction.

**Library Preparation.** RNA from ~2mL of culture was extracted using the Qiagen RNeasy Protect Bacteria Mini Kit (#74524), using 5 mg/mL lysozyme for cell lysis. 10 ng of RNA was used subsequently for RNA-Seq library creation using the Epicentre ScriptSeq v2 RNA-Seq Library Preparation Kit (#SSV21106). Using this kit requires additional materials as described in the protocol. For the cDNA purification step, the Qiagen MinElute PCR Purification kits was used, and for the final library purification, the Agencourt AMPure XP System (Beckman Coulter) was used. Each sample was uniquely labeled with the Epicentres ScriptSeq Index PCR Primers. The completed libraries were submitted to the Caltech Sequencing Core facility (Pasadena, CA, USA). Libraries were sequenced with 50bp reads using the standard Solexa (Illumina) protocol and pipeline.

**Data Analysis.** Illumina raw data provided by the GERALD (Illumina) software package were aligned to a FASTA file containing the *B.subtilis* genome using the Maq short read aligning program (Wellcome Trust Sanger Institute, Hinxton, UK). Maq-aligned reads were converted into a .BAR file using the Cisgenome software (Stanford University, Stanford, CA, USA) (Ji et al., 2008). Total reads for each gene and further calculations were performed using MATLAB<sup>2</sup>.

---

<sup>2</sup>Adam Rosenthal was a critical contributor in preparing RNA-seq data into useable form

## Quantitative Analysis

Quantitative movie analysis used custom image analysis code in MATLAB, described in Young et al. (2012). Calculation of promoter activity is similar to that described in Locke et al. (2011).

### Minimal model of $\sigma^B$ network

This preliminary model builds on the previous model of the  $\sigma^B$  circuit (see Chapter 2), with the addition of the stressosome and the RsbX negative feedback loop.

We simplify the stressosome, assuming that it can exist in two states, the active state  $S^P$ , and the inactive state  $S$ .  $S^P$  acts as the input phosphatase to  $A^P$ . The rate of phosphorylation of  $S^P$  is controlled by the level of external stress,  $E$ , and the rate of dephosphorylation of  $S$  is controlled by the level of RsbX,  $X$ .

As in the previous model (See Chapter 2), we assume Michaelis-Menten kinetics for the phosphorylation and dephosphorylation reactions. We also assume linear degradation and transcription rates.

$$\frac{dA}{dt} = trans - phos + dephos - k_d A \quad (3.1)$$

$$\frac{dA^P}{dt} = phos + dephos - k_d A^P \quad (3.2)$$

$$\frac{dK}{dt} = trans - k_d K \quad (3.3)$$

$$\frac{dS}{dt} = transS - phosS + dephosS - k_d S \quad (3.4)$$

$$\frac{dS^P}{dt} = phosS + dephosS - k_d S^P \quad (3.5)$$

$$\frac{dX}{dt} = trans - k_d X \quad (3.6)$$

Where:  $trans = t_a A + t_i$  is the transcription rate for  $A$ ,  $K$ , and  $X$ ,  $transS = t_s$  is the transcription rate for  $S$ ,  $dephos = \frac{b_{dp} S^P A^P}{k_{dp} + A^P}$  is the rate of dephosphorylation of  $A^P$ ,  $phos = \frac{b_p K A}{k_p + A}$  is the rate of phosphorylation of  $A$ ,  $dephosS = \frac{b_{dps} X S^P}{k_{dps} + S^P}$  is the rate of dephosphorylation of  $A^P$ , and  $phos = \frac{b_{ps} E S}{k_{ps} + S}$  is the rate of phosphorylation of  $S$ .



## Chapter 4

# Transplanting a Non-native Sigma Factor Circuit

### 4.1 Introduction

Perhaps nothing quite conjures up the image of advanced medical science, than the idea of transplantation<sup>1</sup>. The ability to take a complex organ from one host and place it into another requires comprehensive knowledge of anatomy, precise surgical skill in handling, connecting, and caring for the organ, and a delicate sense in managing dangerous immunosuppressants after surgery. The history of transplantation is filled with many pioneering physicians that experimented heavily, and until relatively recently, were quite unsuccessful. Presently, one could say that we are in a golden age for transplantation with our growing knowledge of immunology, our expanding list of targeted medications, and computerized algorithms for matching donors.

The golden age of functional genetic circuits transplantation has not quite arrived. We are not talking about simply moving one enzyme to another non-native organism, or trying to replace one part of a circuit or pathway with a protein from some homologous organism, although this is not without challenges as well. We are discussing taking a whole circuit from one organism and putting it in another and having it function more or less similarly. Successful examples of this approach are hard to find.

The  $\sigma^B$  circuit has a complex behavior (FM pulsing), a relatively simple architecture, and an organized genetic unit that offers an interesting challenge to transplant into a naive organism. Besides

---

<sup>1</sup>This chapter is in it's infancy and was never fully realized into much more. Much of this work was contributed by Zachary Sun, a UCLA MSTP student who rotated in the lab.

the challenge, transplantation allows direct testing of how much the circuit behavior depends on its original cellular context. Consider the key components of the  $\sigma^B$  circuit described in chapters 2 and 3. The phosphoswitch underlying the circuit works without additional cellular components, except ATP. However, the mixed-feedback loop, and the output from  $\sigma^B$ , requires successful recruitment of the host RNA polymerase. Even if appropriate binding occurs, questions remain. Would the binding affinity be sufficient to generate large numbers of RNA polymerase complexes? Would  $\sigma^B$  binding to DNA promote robust transcription? Previous studies have shown that  $\sigma^B$  can function in *Escherichia coli*, but to what extent and how much native regulation could be preserved was not established (Scott et al., 1999).

In this chapter, we present preliminary efforts in moving the  $\sigma^B$  network of *B. subtilis* to *E. coli*. While both are well developed model organisms, they are quite different in evolutionary and lifestyle domains. *E. coli* is a gram-negative organism adapted for life inside a host, while *B. subtilis* is a gram-positive organism suited for life in the dirt. *E. coli* does not contain a homologous sigma factor to  $\sigma^B$  and thus presents a good organism to receive the  $\sigma^B$  circuit with minimal risk in activating endogenous genes.

The idea of minimal cross activation also provided a good platform to test our understanding of the  $\sigma^B$  circuit.  $\sigma^B$  currently represents the only known FM pulse-regulated signal transduction system in bacteria. Transplanting the  $\sigma^B$  circuit into a naive system would (a) establish the sufficiency of the core module for FM-encoding, (b) enable analysis of the  $\sigma^B$  system without the complications that result from activation of its endogenous target genes, and (c) provide a compact FM encoding circuit that could be used in synthetic biology applications.

## 4.2 Results

**Transplant Design.** As shown in figure 4.1, the  $\sigma^B$  circuit was moved into *E. coli* using a three plasmid based design. One plasmid contained the same  $\sigma^B$  reporter used in *B. subtilis*, in which YFP is under the control of the  $P_{sigB}$  promoter. The second plasmid contained the phosphatase/co-activator pair *rsbT* and *rsbU-cfp*, expressed from an IPTG inducible promoter. The third plasmid contained the core operon *rsbVWB* expressed from several possible promoters, included promoters containing

a single  $\sigma^A$  site, a single  $\sigma^B$  site, or containing both a  $\sigma^A$  and  $\sigma^B$  site. In the *B. subtilis* system, the *rsbVWB* operon is mainly controlled via a  $\sigma^B$  binding site that lies within 50 bp of *rsbV*, but is presumed that low levels of expression may be contributed by a  $\sigma^A$  site that appears nearly 2500 bp upstream. In the synthetic system, the  $\sigma^A$  site was separated by the  $\sigma^B$  site by a 350 bp spacer, composed of a partial fragment of the *rsbR* gene.

This first design strategy offered a simple method for modular circuit construction. Just as in the native system, the phosphatase input was separated from the core network expression, allowing independent tuning of these constructs. The design was remarkably similar to our rewired circuit in Chapter 2, where we showed that the frequency of pulsing could be manually tuned simply by controlling phosphatase expression. One major question was how much of *rsbVWB* endogenous promoter regulation was required for activation and pulsing behavior. A separate plasmid containing the operon allowed several promoters driving *rsbVWB* to be tested. While it was formally possible to include the native  $P_{sigA}$  site expressing *rsbVWB*, doing so would have included the core stressosome genes *rsbRSTU*, greatly increasing the complexity of the design.

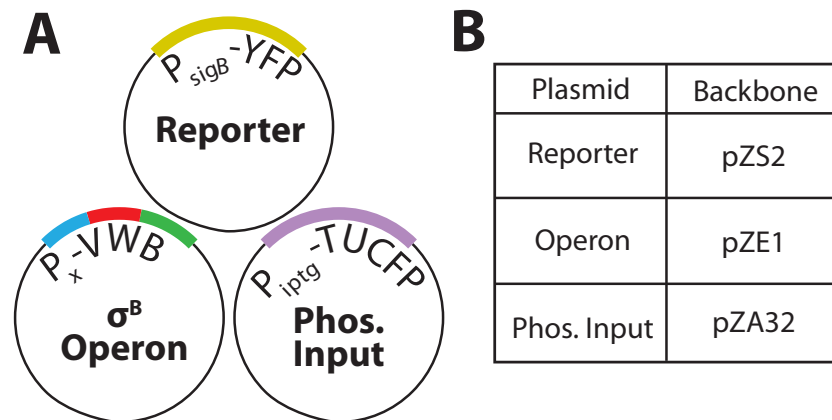


Figure 4.1: Schematic of three plasmid transplant system. (A) Three different promoters were used in front of the *VWB* operon, where  $P_x$  was either  $P_{sigA}$ ,  $P_{sigB}$ , or  $P_{sigA sigB}$ . The plasmid backbones were derived from Lutz and Bujard (1997), whose plasmid coding scheme is used to describe the plasmids in (B).

Activation of  $\sigma^B$  occurred with  $\sigma^A$  and  $\sigma^B$  promoter architecture only. Addition of IPTG resulted in strong upregulation of *rsbTU-cfp*, but only induced expression of the  $P_{sigB}$ -*yfp* reporter with the combinatorial  $\sigma^A$  and  $\sigma^B$  binding site driving the expression of *rsbVWB*. Little to no induction of the reporter was seen in these  $\sigma^A$ -only or  $\sigma^B$ -only promoters (figure 4.2). Reporter expression in the

$P_{sigAsigB}$ -VWB strain was extremely sensitive to IPTG levels, suggesting that the ultrasensitivity found with the phosphoswitch in *B. subtilis* could be retained in *E. coli*.  $\sigma^B$  activation dynamics showed sustained activity. In time-lapse movies where the  $P_{sigAsigB}$ -VWB strain was induced with IPTG,  $\sigma^B$  showed activation upon addition of IPTG, but did not show pulsing similar to *B. subtilis*.

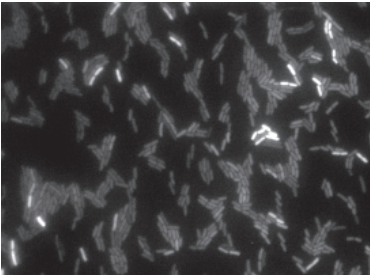
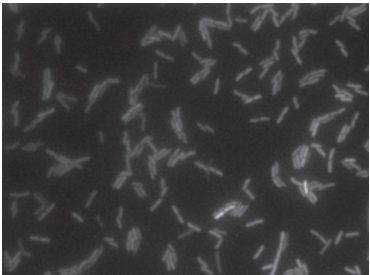
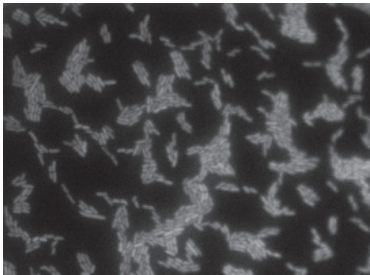
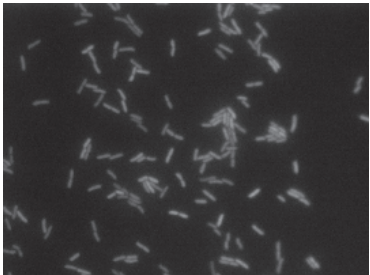
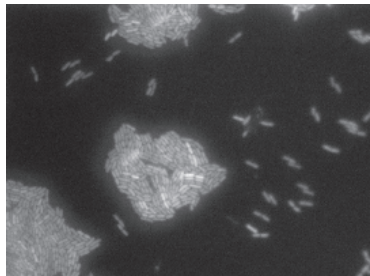
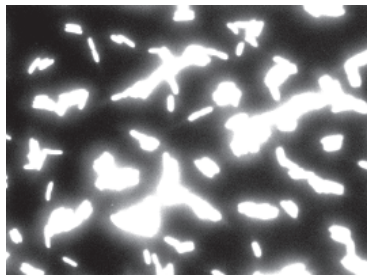
VWB Promoter Structure	pZA32-TU-CFP induction	
	0 mM IPTG	1 mM IPTG
<b>PsigA</b>		
<b>PsigB</b>		
<b>PsigAsigB</b>		

Figure 4.2: Activation of  $P_{sigB}$ -yfp reporter only occurs with  $P_{sigAsigB}$  controlling the expression of VWB. Images were acquired after inducing TU-cfp with IPTG for approximately 1 hour.

### 4.3 Conclusions

Initial attempts at regulating  $\sigma^B$  activity in *E. coli* were successful. Minimal  $\sigma^B$  activity could be detected without phosphatase induction, which suggested the interaction between  $\sigma^B$  and anti-sigma factor rsbW is intact. Moreover, it suggests a stoichiometric excess of rsbW compared to  $\sigma^B$ . This did not have to be the case, considering the ribosomal binding sites prior to rsbW and  $\sigma^B$  are not well defined, and may express to different ratios in *E. coli*. Activation could be achieved, as rsbTU-cfp induction robustly activated P<sub>sigB</sub>-yfp expression among all cells. This activation appeared to have minimal effects on *E. coli* physiology, as growth, as measured by OD changes, was minimally different in the induced and uninduced case. Somewhat surprisingly, the P<sub>sigA</sub>-VWB construct displayed no induction with phosphatase, suggesting that kinase levels may be expressed to dominant levels in this case.

The  $\sigma^B$  pulsing behavior was not observed in initial movies of P<sub>sigAsigB</sub>-VWB strain, which could be explained by several technical issues. One, IPTG induction levels could require optimization. Initial IPTG concentrations were similar to optimal concentrations in liquid conditions. However, solid-phase growth conditions used for pad-based movies can result in changes to induction strength. Thus it is possible that pulsing could be observed simply by exploring lower IPTG concentrations in pad conditions.

The balance between constitutive activation of the VWB operon, provided by P<sub>sigA</sub>, may need to be balanced with feedback from P<sub>sigB</sub>. The initial construct of P<sub>sigAsigB</sub> was developed partly because of its ease of cloning. It may be prudent to explore different spacing between P<sub>sigA</sub> and P<sub>sigB</sub>. In addition, it may be important to overall expression levels of the operon. The pZE plasmid contains a ColE1 origin of replication and confers an estimated copy number of 15-30 in a cell. It may be critical to reduce over copy numbers in order to observe pulsing behavior. This can be achieved by integrating these constructs into the genome of *E. coli*, using a variety of methods.

In the future,  $\sigma^B$  transplantation could ultimately provide a platform for novel synthetic biology tools. Adaptations can be made to the constructs to include the stressosome, which if successful, would allow specific gene regulation in response to several small molecules, including organics such as ethanol and butanol. Considering these chemicals are important targets for fuels made from metabolic

engineering, response systems designed to sense these chemicals may provide an important tool to increase cell viability and fuel yield.

## 4.4 Methods

Strains were constructed via standard molecular cloning techniques. *Bacillus* DNA was used from PB2, a standard lab strain and fluorescent proteins were cloned from Cox et al. (2010) into Dh5 $\alpha$ Z1, a cloning strain that contains a genomic cassette that overexpresses transcriptional regulators lacI and TetR. All three plasmids were transformed into MG1655Z1, which was the background used for assays. For snapshots, cells were grown in LB + carbenicillin + kanamycin + chloramphenicol and induced with 0 or 1 mM IPTG for 1 hour and imaged. For movies, cells were grown on MGC pads (M9 minimal medium + 1% glycerol + 0.01% casamino acids + 0.15  $\mu$ g/mL biotin + 1.5  $\mu$ M thiamine) with various IPTG concentrations. Imaging was performed as described in previous chapters, with minor adaptations.

# Chapter 5

## Conclusions

The richness and biological diversity of signaling dynamics is an emerging theme in current research. Complex behavior has been appreciated in a number of systems including p53 and NF $\kappa$ B activation in mammalian cells, Crz1 localization dynamics in yeast, and activation of sporulation and competence pathways in bacteria. We have added to this body of research by characterizing the response of a critical and well-conserved sigma factor in *B. subtilis*,  $\sigma^B$ .

In chapter 1, we revealed that, unexpectedly,  $\sigma^B$  activates under energy stress conditions with pulses. These pulses were sustained and irregular, reflective of the underlying stochastic process that drove them. We comprehensively dissected the  $\sigma^B$  circuit, finding that pulse initiation involved an ultrasensitive switch formed by the phosphatase/kinase proteins central to the core signaling system. The shape of the pulse, ie the amplification and termination, is a function of  $\sigma^B$  autoregulation of its operon, which contains a combination of positive and negative feedback loops. Finally we were able to show that pulse frequency modulation was an intrinsic function of the system, not a property of any one specific component involved in sensing energy stress.

In chapter 2, we found that  $\sigma^B$  activates when exposed to environmental stress in a profoundly different way than that of energy stress. Activation is strong, amplitude modulated and produces a single pulse that is nearly homogenous among cells. We find that pulse amplitude is strongly dependent on the rate of stress exposure, which suggests a general method of the cell to separate broad ( $\sigma^B$  dependent) versus specific ( $\sigma^B$  independent) stress responses. Whole genome expression data supports this hypothesis, and shows gene function is stratified by rate-sensitivity.

In chapter 3, we shared preliminary work in reconstituting the core  $\sigma^B$  signaling system in *E.coli*,

an organism that lacks an analogous sigma factor. Amazingly, we were able to show controlled, robust, and specific activation of a  $P_{sigB}$ -yfp reporter without obvious detrimental physiological effects. We were not able to pursue the project much further, but it remains an intriguing follow up story that combines fundamental understanding of sigma factor signaling and synthetic biology.

## 5.1 Future Directions

I find it amazing that single small signaling network can generate a number of diverse and novel dynamics. Naturally, several questions are raised from this work that one might ask and address if given infinite time.

Regarding the environmental activation of  $\sigma^B$ , additional work is necessary to understand the interaction of the stressosome and the core  $\sigma^B$  signaling module. While we have a quantitative model that captures many of the important features of environmental activation, it may be worthwhile to understand which assumptions of the model require refinement. For example, can we understand the relationship between stress and release of the environmental coactivator, RsbT, which is sequestered by the stressosome? Since RsbT is an intermediate and a transcriptional reporter cannot be made, other possible techniques such as FRET or FCS may have to be used. Other basic questions, such as the number of stressosomes and their variation inside the cell may suggest whether environmental activation is sensitive to these variations, or whether other mechanisms exist that buffer the response.

Measuring the quantitative relationship and network components in the  $\sigma^B$  network can be at times challenging. Strong activation of the  $\sigma^B$  is itself toxic to the cell, presumably because of the combined effect of expressing large amount of stress response genes. During our experiments we had to focus on making certain measurements were taken in proper activation ranges to avoid measurement errors cause by physiological toxicity or some other non-system effect. In a perfect world, we would have been able to measure the response of  $\sigma^B$ , disconnected from its endogenous regulation, except for the  $\sigma^B$  operon, which is critical to its response. Thus, a mutant  $\sigma^B$  target combined with a promoter that was specific for this mutant sigma factor would have been ideal.

A separate strategy involves optimizing the  $\sigma^B$  circuitry in *E. coli*. We presented some work towards this end, and it would be interesting if other key players involved in  $\sigma^B$  signaling, such as the



stressosome, could be appropriately incorporated into this organism.

How general are the  $\sigma^B$  dynamics? The structure of signaling in other alternative sigma factors is similar, in that many sigma factors are controlled and sequestered by anti-sigma factors. It would be prudent to see how activation dynamics occur in these other systems, in *B. subtilis* and other species. Such work is ongoing in our lab presently, and will undoubtedly be a part of another thesis. Stay tuned...

# Bibliography

- M. Acar, A. Becskei, and A. van Oudenaarden. Enhancement of cellular memory by reducing stochastic transitions. *Nature*, 435(7039):228–32, 2005.
- N. E. Allenby, N. O’Connor, Z. Pragai, A. C. Ward, A. Wipat, and C. R. Harwood. Genome-wide transcriptional analysis of the phosphate starvation stimulon of bacillus subtilis. *J Bacteriol*, 187(23):8063–80, 2005.
- U. Alon, M. G. Surette, N. Barkai, and S. Leibler. Robustness in bacterial chemotaxis. *Nature*, 397(6715):168–71., 1999.
- S. Alper, L. Duncan, and R. Losick. An adenosine nucleotide switch controlling the activity of a cell type-specific transcription factor in b. subtilis. *Cell*, 77(2):195–205, 1994.
- O.E. Barndorff-Nielsen and N. Shephard. Non-gaussian ou based models and some of their uses in financial econometrics. *Journal of the Royal Statistical Society, B(Statistical Methodology)*, 63:167–241, 2001.
- E. Batchelor, A. Loewer, and G. Lahav. The ups and downs of p53: understanding protein dynamics in single cells. *Nature reviews. Cancer*, 9(5):371–7, 2009.
- S. A. Boylan, A. R. Redfield, M. S. Brody, and C. W. Price. Stress-induced activation of the sigma b transcription factor of bacillus subtilis. *J Bacteriol*, 175(24):7931–7, 1993.
- M. S. Brody, K. Vijay, and C. W. Price. Catalytic function of an alpha/beta hydrolase is required for energy stress activation of the sigma(b) transcription factor in bacillus subtilis. *J Bacteriol*, 183(21):6422–8, 2001.
- A. Burgess-Cassler, J. J. Johansen, D. A. Santek, J. R. Ide, and N. C. Kendrick. Computerized quantitative analysis of coomassie-blue-stained serum proteins separated by two-dimensional electrophoresis. *Clin Chem*, 35(12):2297–304, 1989.

- L. Cai, C. K. Dalal, and M. B. Elowitz. Frequency-modulated nuclear localization bursts coordinate gene regulation. *Nature*, 455(7212):485–90, 2008.
- M. Chalfie, Y. Tu, G. Euskirchen, W. W. Ward, and D. C. Prasher. Green fluorescent protein as a marker for gene expression. *Science*, 263(5148):802–5, 1994.
- C. C. Chen, M. D. Yudkin, and O. Delumeau. Phosphorylation and rsbx-dependent dephosphorylation of rsbr in the rsbr-rsbs complex of bacillus subtilis. *J Bacteriol*, 186(20):6830–6, 2004.
- Z. Cheng, F. Liu, X.P. Zhang, and W. Wang. Reversible phosphorylation subserves robust circadian rhythms by creating a switch in inactivating the positive element. *Biophysical journal*, 97(11):2867–2875, 2009.
- 3rd Cox, R. S., M.J. Dunlop, and M.B. Elowitz. A synthetic three-color scaffold for monitoring genetic regulation and noise. *J Biol Eng.*, Jul 21:4–10, 2010.
- O. Delumeau, R. J. Lewis, and M. D. Yudkin. Protein-protein interactions that regulate the energy stress activation of sigma(b) in bacillus subtilis. *J Bacteriol*, 184(20):5583–9, 2002.
- A. Dufour and W. G. Haldenwang. Interactions between a bacillus subtilis anti-sigma factor (rsbw) and its antagonist (rsbv). *J Bacteriol*, 176(7):1813–20, 1994.
- A. Dufour, U. Voelker, A. Voelker, and W. G. Haldenwang. Relative levels and fractionation properties of bacillus subtilis sigma(b) and its regulators during balanced growth and stress. *J Bacteriol*, 178(13):3701–9 sigma, 1996.
- A. Eldar, V. K. Chary, P. Xenopoulos, M. E. Fontes, O. C. Loson, J. Dworkin, P. J. Piggot, and M. B. Elowitz. Partial penetrance facilitates developmental evolution in bacteria. *Nature*, 460(7254):510–4, 2009.
- M. B. Elowitz and S. Leibler. A synthetic oscillatory network of transcriptional regulators. *Nature*, 403(6767):335–8., 2000.
- C. Eymann, S. Schulz, K. Gronau, D. Becher, M. Hecker, and C. W. Price. In vivo phosphorylation patterns of key stressosome proteins define a second feedback loop that limits activation of bacillus subtilis sigmab. *Mol Microbiol*, 80(3):798–810, 2011.
- N. Friedman, L. Cai, and X. S. Xie. Linking stochastic dynamics to population distribution: an analytical framework of gene expression. *Phys Rev Lett*, 97(16):168302, 2006.

- T. A. Gaidenko, X. Yang, Y. M. Lee, and C. W. Price. Threonine phosphorylation of modulator protein rsbr governs its ability to regulate a serine kinase in the environmental stress signaling pathway of bacillus subtilis. *J Mol Biol*, 288(1):29–39, 1999.
- A. Goldbeter and Jr. Koshland, D. E. An amplified sensitivity arising from covalent modification in biological systems. *Proc Natl Acad Sci U S A*, 78(11):6840–4, 1981.
- T. M. Gruber and C. A. Gross. Multiple sigma subunits and the partitioning of bacterial transcription space. *Annu Rev Microbiol*, 57:441–66, 2003.
- W. G. Haldenwang and R. Losick. A modified rna polymerase transcribes a cloned gene under sporulation control in bacillus subtilis. *Nature*, 282(5736):256–60, 1979.
- M. Hecker and U. Volker. Non-specific, general and multiple stress resistance of growth-restricted bacillus subtilis cells by the expression of the sigmab regulon. *Mol Microbiol*, 29(5):1129–36, 1998.
- M. Hecker, J. Pane-Farre, and U. Volker. Sigb-dependent general stress response in bacillus subtilis and related gram-positive bacteria. *Annu Rev Microbiol*, 61:215–36, 2007.
- O. A. Igoshin, M. S. Brody, C. W. Price, and M. A. Savageau. Distinctive topologies of partner-switching signaling networks correlate with their physiological roles. *J Mol Biol*, 369(5):1333–52, 2007.
- N. Ivanova, R. Dobrin, R. Lu, I. Kotenko, J. Levorse, C. DeCoste, X. Schafer, Y. Lun, and I.R. Lemischka. Dissecting self-renewal in stem cells with rna interference. *Nature*, 442(7102):533–538, 2006.
- H. Ji, H. Jiang, W. Ma, D. S. Johnson, R. M. Myers, and W. H. Wong. An integrated software system for analyzing chip-chip and chip-seq data. *Nat Biotechnol*, 26(11):1293–300, 2008.
- H. Kawaji, T. Mizuno, and S. Mizushima. Influence of molecular size and osmolarity of sugars and dextrans on the synthesis of outer membrane proteins o-8 and o-9 of escherichia coli k-12. *J Bacteriol*, 140(3):843–7, 1979.
- M. J. Kazmierczak, S. C. Mithoe, K. J. Boor, and M. Wiedmann. Listeria monocytogenes sigma b regulates stress response and virulence functions. *J Bacteriol*, 185(19):5722–34, 2003.
- E. Kussell and S. Leibler. Phenotypic diversity, population growth, and information in fluctuating environments. *Science*, 309(5743):2075–8, 2005.

- J.H. Levine, M.E. Fontes, J. Dworkin, and M.B. Elowitz. Pulsed feedback defers cellular differentiation. *PLoS biology*, 10(1):e1001252, 2012.
- B. Lindner, J. Garcia-Ojalvo, A. Neiman, and L. Schimansky-Geier. Effects of noise in excitable systems. *PHYSICS REPORTS- REVIEW SECTION OF PHYSICS LETTERS*, 392(6):321–424, 2004.
- J. C. Locke and M. B. Elowitz. Using movies to analyse gene circuit dynamics in single cells. *Nat Rev Microbiol*, 7(5):383–92, 2009.
- J. C. Locke, J. W. Young, M. Fontes, M. J. Hernandez Jimenez, and M. B. Elowitz. Stochastic pulse regulation in bacterial stress response. *Science*, 334(6054):366–9, 2011.
- Y.H. Loh, Q. Wu, J.L. Chew, V.B. Vega, W. Zhang, X. Chen, G. Bourque, J. George, B. Leong, J. Liu, et al. The oct4 and nanog transcription network regulates pluripotency in mouse embryonic stem cells. *Nature genetics*, 38(4):431–440, 2006.
- U. Lorenz, C. Huttinger, T. Schafer, W. Ziebuhr, A. Thiede, J. Hacker, S. Engelmann, M. Hecker, and K. Ohlsen. The alternative sigma factor sigma b of staphylococcus aureus modulates virulence in experimental central venous catheter-related infections. *Microbes Infect*, 10(3):217–23, 2008.
- R. Losick and C. Desplan. Stochasticity and cell fate. *Science*, 320(5872):65–8, 2008.
- R. Lutz and H. Bujard. Independent and tight regulation of transcriptional units in escherichia coli via the lacr/o, the tetr/o and arac/i1-i2 regulatory elements. *Nucleic Acids Res*, 25(6):1203–10., 1997.
- J. Marles-Wright, T. Grant, O. Delumeau, G. van Duinen, S. J. Firbank, P. J. Lewis, J. W. Murray, J. A. Newman, M. B. Quin, P. R. Race, A. Rohou, W. Tichelaar, M. van Heel, and R. J. Lewis. Molecular architecture of the "stressosome," a signal integration and transduction hub. *Science*, 322(5898):92–6, 2008.
- G.J. Melen, S. Levy, N. Barkai, and B.Z. Shilo. Threshold responses to morphogen gradients by zero-order ultrasensitivity. *Molecular systems biology*, 1(1), 2005.
- J. T. Mettetal, D. Muzzey, C. Gomez-Urbe, and A. van Oudenaarden. The frequency dependence of osmo-adaptation in saccharomyces cerevisiae. *Science*, 319(5862):482–4, 2008.
- P. Nannapaneni, F. Hertwig, M. Depke, M. Hecker, U. Mader, U. Volker, L. Steil, and S. A. van Hijum.

- Defining the structure of the general stress regulon of bacillus subtilis using targeted microarray analysis and random forest classification. *Microbiology*, 158(Pt 3):696–707, 2012.
- D. Nevozhay, R.M. Adams, K.F. Murphy, K. Josić, and G. Balázsi. Negative autoregulation linearizes the dose–response and suppresses the heterogeneity of gene expression. *Proceedings of the National Academy of Sciences*, 106(13):5123, 2009.
- H. Nikaïdo. Multidrug resistance in bacteria. *Annual review of biochemistry*, 78:119, 2009.
- I. Nisamedtinov, G. G. Lindsey, R. Karreman, K. Orumets, M. Koplmaa, K. Kevvai, and T. Paalme. The response of the yeast *saccharomyces cerevisiae* to sudden vs. gradual changes in environmental stress monitored by expression of the stress response protein hsp12p. *FEMS Yeast Res*, 8(6):829–38, 2008.
- C. E. Noriega, H. Y. Lin, L. L. Chen, S. B. Williams, and V. Stewart. Asymmetric cross-regulation between the nitrate-responsive narx-narl and narq-narp two-component regulatory systems from *escherichia coli* k-12. *Mol Microbiol*, 75(2):394–412, 2010.
- P. H. O’Farrell. High resolution two-dimensional electrophoresis of proteins. *J Biol Chem*, 250(10):4007–21, 1975.
- S. Osterberg, T. Del Peso-Santos, and V. Shingler. Regulation of alternative sigma factor use. *Annual review of microbiology*, 2011.
- A. Raj and A. van Oudenaarden. Nature, nurture, or chance: stochastic gene expression and its consequences. *Cell*, 135(2):216–26, 2008.
- A. Raj, C. S. Peskin, D. Tranchina, D. Y. Vargas, and S. Tyagi. Stochastic mrna synthesis in mammalian cells. *PLoS Biol*, 4(10):e309, 2006.
- J. C. Ray and O. A. Igoshin. Adaptable functionality of transcriptional feedback in bacterial two-component systems. *PLoS Comput Biol*, 6(2):e1000676, 2010.
- K. Richter, M. Haslbeck, and J. Buchner. The heat shock response: life on the verge of death. *Mol Cell*, 40(2):253–66, 2010.
- N. Rosenfeld, J. W. Young, U. Alon, P. S. Swain, and M. B. Elowitz. Gene regulation at the single-cell level. *Science*, 307(5717):1962–5, 2005.
- A. Sadeh, N. Movshovich, M. Volokh, L. Gheber, and A. Aharoni. Fine-tuning of the msn2/4-mediated

- yeast stress responses as revealed by systematic deletion of *msn2/4* partners. *Mol Biol Cell*, 22(17):3127–38, 2011.
- T. Schweder, A. Kolyschkow, U. Volker, and M. Hecker. Analysis of the expression and function of the sigma<sub>b</sub>-dependent general stress regulon of *Bacillus subtilis* during slow growth. *Arch Microbiol*, 171(6):439–43, 1999.
- J. M. Scott, N. Smirnova, and W. G. Haldenwang. A *Bacillus*-specific factor is needed to trigger the stress-activated phosphatase/kinase cascade of sigma<sub>b</sub> induction. *Biochem Biophys Res Commun*, 257(1):106–10, 1999.
- T. S. Shimizu, Y. Tu, and H. C. Berg. A modular gradient-sensing network for chemotaxis in *Escherichia coli* revealed by responses to time-varying stimuli. *Mol Syst Biol*, 6:382, 2010.
- O. Shimomura, F. H. Johnson, and Y. Saiga. Extraction, purification and properties of aequorin, a bioluminescent protein from the luminous hydromedusa, *Aequorea*. *J Cell Comp Physiol*, 59:223–39, 1962.
- O. Shoval, L. Goentoro, Y. Hart, A. Mayo, E. Sontag, and U. Alon. Fold-change detection and scalar symmetry of sensory input fields. *Proc Natl Acad Sci U S A*, 107(36):15995–6000, 2010.
- F. Spiegelhalter and E. Bremer. Osmoregulation of the *opuE* proline transport gene from *Bacillus subtilis*: contributions of the sigma<sub>a</sub>- and sigma<sub>b</sub>-dependent stress-responsive promoters. *Mol Microbiol*, 29(1):285–96, 1998.
- J. Spizizen. Transformation of biochemically deficient strains of *Bacillus subtilis* by deoxyribonucleate. *Proc Natl Acad Sci U S A*, 44(10):1072–8, 1958.
- M. Steinmetz and R. Richter. Plasmids designed to alter the antibiotic resistance expressed by insertion mutations in *Bacillus subtilis*, through in vivo recombination. *Gene*, 142(1):79–83, 1994.
- P. J. Stone and M. E. Nicolas. Comparison of sudden heat stress with gradual exposure to high temperature during grain filling in two wheat varieties differing in heat tolerance .1. grain growth. *Australian Journal of Plant Physiology*, 22(6):935–944, 1995.
- G. M. Suel, J. Garcia-Ojalvo, L. M. Liberman, and M. B. Elowitz. An excitable gene regulatory circuit induces transient cellular differentiation. *Nature*, 440(7083):545–50, 2006.
- G. M. Suel, R. P. Kulkarni, J. Dworkin, J. Garcia-Ojalvo, and M. B. Elowitz. Tunability and noise

- dependence in differentiation dynamics. *Science*, 315(5819):1716–9, 2007.
- Y. Taniguchi, P. J. Choi, G. W. Li, H. Chen, M. Babu, J. Hearn, A. Emili, and X. S. Xie. Quantifying *e. coli* proteome and transcriptome with single-molecule sensitivity in single cells. *Science*, 329(5991):533–8, 2010.
- H. Weber, T. Polen, J. Heuveling, V. F. Wendisch, and R. Hengge. Genome-wide analysis of the general stress response network in *escherichia coli*: sigmas-dependent genes, promoters, and sigma factor selectivity. *J Bacteriol*, 187(5):1591–603, 2005.
- A. A. Wise and C. W. Price. Four additional genes in the sigb operon of *bacillus subtilis* that control activity of the general stress factor sigma b in response to environmental signals. *J Bacteriol*, 177(1):123–33, 1995.
- X. Yang, C. M. Kang, M. S. Brody, and C. W. Price. Opposing pairs of serine protein kinases and phosphatases transmit signals of environmental stress to activate a bacterial transcription factor. *Genes Dev*, 10(18):2265–75, 1996.
- J. W. Young, J. C. Locke, A. Altinok, N. Rosenfeld, T. Bacarian, P. S. Swain, E. Mjolsness, and M. B. Elowitz. Measuring single-cell gene expression dynamics in bacteria using fluorescence time-lapse microscopy. *Nat Protoc*, 7(1):80–8, 2012.
- S. Zhang and W. G. Haldenwang. Contributions of atp, gtp, and redox state to nutritional stress activation of the *bacillus subtilis* sigmab transcription factor. *J Bacteriol*, 187(22):7554–60, 2005.
- M. Zheng, F. Aslund, and G. Storz. Activation of the oxyr transcription factor by reversible disulfide bond formation. *Science*, 279(5357):1718–21, 1998.